Time-linear scaling nonequilibrium Green's function theory for quantum transport

R. Tuovinen[*1], **Y. Pavlyukh** [2], **E. Perfetto** [3,4], **G. Stefanucci** [3,4]

1. Department of Physics, Nanoscience Center, P.O. Box 35, 40014 University of Jyväskylä, Finland

2. Department of Theoretical Physics, Faculty of Fundamental Problems of Technology, Wrocław University of Science and Technology, 50-370 Wrocław, Poland

3. Dipartimento di Fisica, Università di Roma Tor Vergata, Via della Ricerca Scientifica 1, 00133 Rome, Italy

4. NFN, Sezione di Roma Tor Vergata, Via della Ricerca Scientifica 1, 00133 Rome, Italy

We present a time-linear scaling method for open and correlated quantum systems. The method inherits from many-body theory [1] the possibility of selecting the most relevant scattering processes, thereby paving the way for real-time characterizations of correlated ultrafast phenomena in quantum transport [2]. The open system dynamics is described in terms of an embedding correlator from which the transient current can be calculated via the Meir-Wingreen formula [3]. We efficiently implement the method through a combination with recent time-linear schemes for closed systems [4]. Electron-electron and electron-phonon interactions can be treated on equal footing while preserving all fundametal conservation laws. We employ the method by studying transport of correlated electron-hole pairs in semiconductors [5].

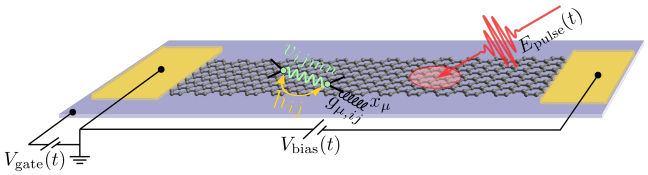

Fig. 1: Illustration of a quantum transport set up. A nanoribbon (system) is contacted to left and right electrodes and lies over a gate (electronic reservoirs). Electron-electron and electron-phonon interactions are confined to the nanoribbon, which can be possibly excited by a laser pulse.

References

[1] G. Stefanucci and R. van Leeuwen, Nonequilibrium Many-Body Theory of Quantum Systems: A Modern Introduction (Cambridge University Press, 2013).
[2] M. Ridley, N. W. Talarico, D. Karlsson, N. Lo Gullo, and R. Tuovinen, J. Phys. A: Math. Theor. **55** 273001 (2022).
[3] Y. Meir and N. S. Wingreen, Phys. Rev. Lett. **68**, 2512 (1992).
[4] N. Schlünzen, J.-P. Joost, and M. Bonitz, Phys. Rev. Lett. **124** (2020) 076601.
[5] R. Tuovinen, Y. Pavlyukh, E. Perfetto, and G. Stefanucci, arXiv:2211.15635 (2022).

[*]Corresponding author: riku.m.s.tuovinen@jyu.fi

Nonlinear σ model for disordered systems with spin-orbit coupling

P. Virtanen[*1], **F.S. Bergeret,** [2,3,4] **I.V. Tokatly** [3,5,6,7]

1. Department of Physics and Nanoscience Center, University of Jyväskylä, P.O. Box 35 (YFL), FI-40014 University of Jyväskylä, Finland
2. Centro de Física de Materiales (CFM-MPC) Centro Mixto CSIC-UPV/EHU, E-20018 Donostia-San Sebastián, Spain
3. Donostia International Physics Center (DIPC), 20018 Donostia–San Sebastián, Spain
4. Institut für Theoretische Physik und Astrophysik, Universität Würzburg, 97074 Würzburg, Germany
5. Nano-Bio Spectroscopy Group, Departamento de Polímeros y Materiales Avanzados: Física, Química y Tecnología, Universidad del País Vasco (UPV/EHU), 20018 Donostia-San Sebastián, Spain
6. ITMO University, Department of Physics and Engineering, Saint-Petersburg 197101, Russia
7. IKERBASQUE, Basque Foundation for Science, 48011 Bilbao, Spain

The intrinsic spin-Hall effect is a magnetoelectric coupling between spin and charge degrees of freedom, which arises from a geometric property of the electron bands caused by the spin-orbit coupling (SOC). The spin-charge interconversion is the basis of the spin-Hall magnetoresistance, the Edelstein, and spin-galvanic effects, observed in a wide variety of systems.

We derive [1] the nonlinear σ model to describe diffusive transport in normal metals and superconductors with intrinsic spin-orbit coupling. The SOC is described via an SU(2) gauge field, and we expand the model to the fourth order in gradients to find the leading field-strength contribution. This contribution generates the spin-charge coupling that is responsible for the spin-Hall effect. We derive the corresponding kinetic equation describing the diffusive spin-charge dynamics in superconducting systems. As an example, we apply the obtained equations to describe the anomalous supercurrent in dirty Rashba superconductors. The same model can also describe effects due to extrinsic spin-orbit coupling generated by spin-orbit impurity scattering. [2] The results suggest that the spin-current swapping and the spin-Hall effect exhaust the possible bulk magnetoelectric effects generated by weak SOC in the low-energy phenomenological theory of diffusion modes.

References

[1] P. Virtanen, F.S. Bergeret, I.V. Tokatly, Phys. Rev. B **105**, 224517 (2022)
[2] P. Virtanen, F.S. Bergeret, I.V. Tokatly, Phys. Rev. B **104**, 064515 (2021)

[*]Corresponding author: pauli.t.virtanen@jyu.fi

Lee-Yang theory of Quantum Phase Transitions with Quantum Network States

Pascal M. Vecsei[*1], **Jose L. Lado** [1], **Christian Flindt** [1]
1. Department of Applied Physics, Aalto University, 00076 Aalto, Finland

Predicting the phase diagram of interacting quantum many-body systems is one of the key open problems in quantum physics. A variety of quantum many-body systems, ranging from unconventional superconductors to spin liquids, exhibit complex competing phases whose theoretical description has been the focus of intense efforts. Here, we show that variational approaches towards quantum states can be combined with a Lee-Yang theory of quantum phase transitions[1] to predict the critical point of a strongly-correlated spin system. Firstly, we demonstrate that an approach based on matrix product states (MPS) allows us to map out the phase diagram in the temperature-field plane of the transverse field Ising model in two dimensions[2]. Secondly, we show the applicability of a methodology combining neural network quantum states with Lee-Yang theory for quantum phase transitions in the transverse-field Ising model on different lattice geometries in one, two, and three dimensions, at vanishing temperature[3]. We find that Lee-Yang theory with neural-network quantum states provides faithful predictions of the critical field for different lattices and dimensionalities, consistent with large-scale quantum many-body methods. Our results provide a starting point for determining the phase diagram of more complex quantum systems such as frustrated Heisenberg and Hubbard models.

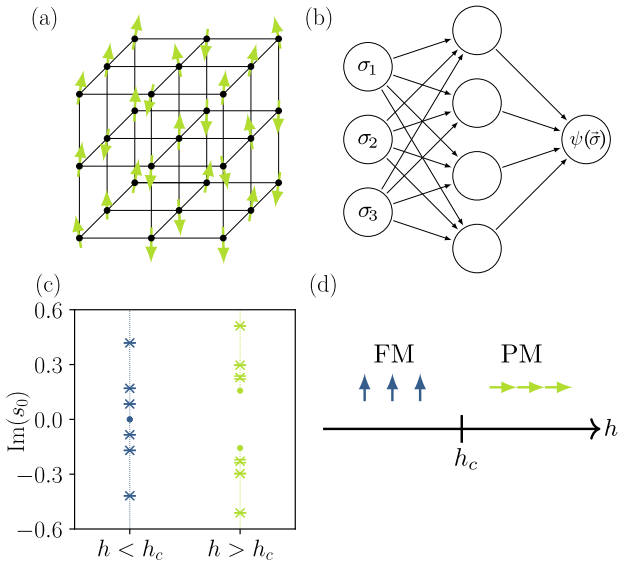

Fig. 1: Neural-network approach to quantum phase transitions. (a) Cubic Ising lattice of interacting spins in a transverse magnetic field, here a system of size $3 \times 3 \times 3$. (b) A neural network takes a configuration of the spins, encoded in the vector $\vec{\sigma} = (\sigma_1, ..., \sigma_N)$, and outputs the corresponding value of the wave function, $\psi_{\vec{\theta}}(\vec{\sigma}) = \langle \vec{\sigma} | \psi \rangle$, which depends on the variational parameters in $\vec{\theta}$. (c) From the fluctuations of the magnetization, we extract the zeros of the moment generating function of the magnetization and investigate their motion in the complex plane as we increase the system size. (d) Above the critical field, $h > h_c$, the zeros remain complex in the thermodynamic limit, and the system is in the paramagnetic phase (PM). At $h = h_c$, the zeros reach the real-axis, signaling a quantum phase transition. For $h < h_c$, the system is in the ferromagnetic phase (FM) with finite magnetization.

References

[1] T. Kist, J. L. Lado, C. Flindt (2021), Phys. Rev. Research 3, 033206
[2] P. M. Vecsei, J. L. Lado, C. Flindt (2022), Phys. Rev. B 106, 054402
[3] P. M. Vecsei, C. Flindt, J. L. Lado (2023), arXiv preprint, arXiv:2301.09923

[*]Corresponding author: pascal.vecsei@aalto.fi

Signatures of many-body localization of quasiparticles in a flat band superconductor

Koushik Swaminathan[*1], **Paula Tadros**[2], **Sebastiano Peotta**[†1]
1. Department of Applied Physics, Aalto University School of Science, FI-00076 Aalto, Finland
2. Department of Physics and Astronomy, University of Turku, FI-20014 Turku, Finland

We construct a class of exact eigenstates of the Hamiltonian obtained by projecting the Hubbard interaction term onto the flat band subspace of a generic lattice model. These exact eigenstates are many-body states in which an arbitrary number of localized fermionic particles coexist with a sea of mobile Cooper pairs with zero momentum. By considering the dice lattice as an example, we provide evidence that these exact eigenstates are in fact manifestation of local integrals of motions of the projected Hamiltonian. In particular the spin and particle densities retain memory of the initial state for a very long time, if localized unpaired particles are present at the beginning of the time evolution. This shows that many-body localization of quasiparticles and superfluidity can coexist even in generic two-dimensional lattice models with flat bands, for which it is not known how to construct local conserved quantities. Our results open new perspectives on the old condensed matter problem of the interplay between superconductivity and localization.

References

[1] K. Swaminathan, P. Tadros, S. Peotta, article in preparation.

[*]Corresponding author: koushik.swaminathan@aalto.fi
[†]Corresponding author: sebastiano.peotta@aalto.fi

Hamiltonian learning of quantum dots in a minimal Kitaev chain with conditional GANs

Rouven Koch[*,1], David van Driel[2], Jose L. Lado[1], Eliska Greplova[3]
[1] *Department of Applied Physics, Aalto University, 00076 Aalto, Espoo, Finland*
[2] *QuTech and Kavli Institute of NanoScience, Delft University of Technology, 2600 GA Delft, The Netherlands*
[3] *Kavli Institute of Nanoscience, Delft University of Technology, NL-2600 GA Delft, The Netherlands*

Knowledge of the underlying Hamiltonian in quantum devices is key for tuning and controlling experimental quantum systems. Here we demonstrate an adversarial machine learning framework capable of Hamiltonian learning of a quantum dot chain from noisy experimental measurements [1]. In particular, we train a convolutional conditional generative adversarial network (Conv-cGAN) with simulated data of the differential conductances based on a Kitaev chain model [2]. The trained model is able to predict the parameters determining the sweet spot conditions of the two-quantum-dot system at which the predicted mid-gap bound state emerge. The Conv-cGAN model gives us a fast and numerically efficient way to explore the phase diagram describing the transition between elastic co-tunning and Andreev reflection regimes and thus is suitable to assist the sweet-spot tuning of the Kitaev chains.

We verify the theoretical predictions of the model by applying in on experimental measured conductance obtained from two spin-polarized quantum dots coupled by superconductor-semiconductor hybrid [3]. We obtain good accuracy in the predictions of the experimental parameter across the phase diagram. The application of our methodology to experimental measurements in an InSb nanowire shows promising results in extracting Hamiltonians from measurements, potentially supporting the hard task of tuning quantum-dot systems into distinct Hamiltonian regimes. Our work constitutes a stepping stone towards fast reliable parameter prediction for tuning Kitaev chain and for efficiently sweet-spot tuning in the larger topological chains.

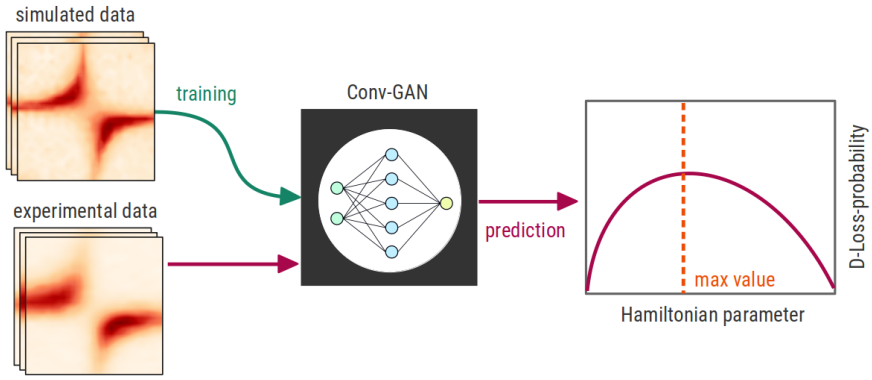

References

[1] R. Koch, D. v. Driel, J. L. Lado, E. Greplova, “Adversarial Hamiltonian learning of quantum dots in a minimal Kitaev chain”, *in preparation* (2023).
[2] Leijnse, Martin, and Karsten Flensberg. "Parity qubits and poor man's Majorana bound states in double quantum dots." Physical Review B 86.13 (2012): 134528.
[3] Dvir, Tom, et al. "Realization of a minimal Kitaev chain in coupled quantum dots." arXiv preprint arXiv:2206.08045 (2022).

[*]Corresponding author: rouven.koch@aalto.fi

Suppression of non-equilibrium quasiparticle transport in flat band superconductors

Ville Pyykkönen[*1], **Sebastiano Peotta** [1], **Päivi Törmä**[†1],
1. Department of Applied Physics, Aalto University School of Science, FI-00076 Aalto, Finland

In this talk I will discuss our recent study of non-equilibrium transport through a superconducting flat-band lattice in a two-terminal setup using the Schwinger-Keldysh method. We find that quasiparticle transport is suppressed and coherent pair transport dominates. For superconducting leads, the AC supercurrent overcomes the DC current which relies on multiple Andreev reflections. With normal-normal and normal-superconducting leads, the Andreev reflection and normal currents vanish. Flat band superconductivity is thus promising not only for high critical temperatures but also for suppressing unwanted quasiparticle processes.

References

[1] Suppression of non-equilibrium quasiparticle transport in flat band superconductors, Ville A. J. Pyykkönen, Sebastiano Peotta, Päivi Törmä, arXiv:2211.09483

[*]Corresponding author: ville.pyykkonen@aalto.fi
[†]Corresponding author: paivi.torma@aalto.fi

Transitions in vortex skyrmion structures in superfluid ^{3}He-A

Riku Rantanen[*1], **Vladimir Eltsov** [1]
1. Department of Applied Physics, Aalto University, Finland

Helium-3 becomes superfluid at millikelvin temperatures. The helium atoms form Cooper pairs in a p-wave spin-triplet state, and the internal structure of these pairs supports multiple distinct superfluid phases. In the chiral A phase, the orbital angular momentum of all Cooper pairs is aligned along a unit vector $\hat{\mathbf{l}}$. The spatial distribution (texture) of the $\hat{\mathbf{l}}$ vectors is determined by multiple competing interactions from flow, magnetic fields, and boundaries. The $\hat{\mathbf{l}}$ texture is directly linked to the superflow through the Mermin-Ho relation. This link separates ^{3}He-A from most other superfluids, because it allows quantized vortices to be continuous structures without suppressing the superfluid state. We present numerical calculations of these vortex structures with a focus on skyrmions, objects where $\hat{\mathbf{l}}$ rotates to cover every possible direction on the unit sphere. The $\hat{\mathbf{l}}$ vector also determines the locations of two nodes in the energy spectrum of Bogoliubov quasiparticles in ^{3}He-A. Near these nodes the quasiparticles act like Weyl fermions. Spatial variation of $\hat{\mathbf{l}}$ creates a synthetic electromagnetic field for the Weyl fermions, with features of quantum electrodynamics. One such feature – the zero-charge effect – is predicted to change the structure of continuous vortices at low temperatures [1], and we present numerical calculations of these structures in rotating ^{3}He-A.

Continuous single quantum vortices, called merons, are typically not observed in bulk ^{3}He-A. The most common vortices observed in experiments are two types of skyrmion structures: a bound pair of merons called the double-quantum vortex (DQV), and the vortex sheet (VS), which is a chain of merons. Our calculations demonstrate the process of DQVs merging to VS and the opposite process of emitting DQVs from VS. The transition from vortices to sheets has been observed in experiments [2]. We have found that the possibility of vortex merging is related to the axial superflow along the vortex cores and the chirality of ^{3}He-A.

In quantum electrodynamics, the zero-charge effect is connected to a logarithmically divergent term in the action of the electromagnetic field. Analogously, the synthetic electromagnetic field in ^{3}He-A is predicted to result in the logarithmic divergence of one of the energy terms in the $T \to 0$ limit [1]. We have performed numerical calculations of the vortex structures in this limit and found a transition in the VS from a uniform vorticity state to one where the vorticity is distributed in tubes around the circular merons [3]. The transition temperature depends on the vortex density of the system. A similar transition is found for the double-quantum vortex, and the formation of vorticity tubes is in line with the earlier prediction [1]. We have calculated the response of those structures in nuclear magnetic resonance measurements, which could be used to observe the transition.

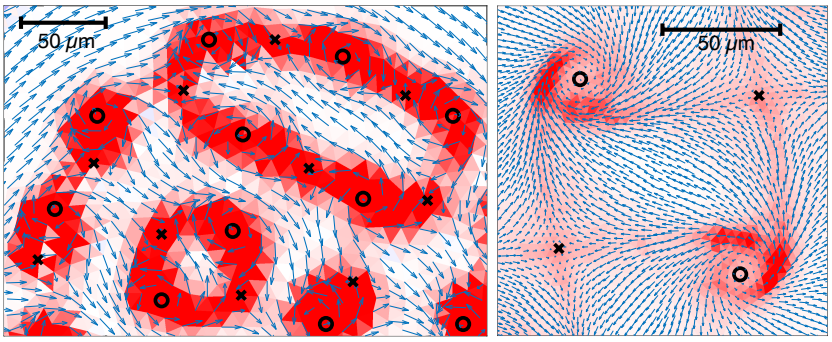

Fig. 1: Vortex skyrmion structures in rotating ^{3}He-A calculated for realistic experimental geometry. Arrows show the direction of $\hat{\mathbf{l}}$ and color represents vorticity. Circles and crosses mark the centers of circular and hyperbolic merons, respectively. *(Left)* Mixture of DQVs (blobs of vorticity connecting two merons) and VS (extended structure with multiple merons) after some DQVs merge to VS on increase of the angular velocity. *(Right)* Vorticity is spread into tubes around the circular merons in the zero-charge regime.

References

[1] G.E. Volovik, JETP Lett. **47**, 55 (1988).
[2] V.B. Eltsov *et al.*, Phys. Rev. Lett. **88**, 065301 (2002).
[3] R. Rantanen, V.B. Eltsov, arXiv:2301.05558 [cond-mat.other].

[*]Corresponding author: riku.s.rantanen@aalto.fi

Topological spin excitations in non-Hermitian spin chains with a generalized kernel polynomial algorithm

Guangze Chen[1], **Fei Song**[2], **Jose L. Lado** [1]
1. Department of Applied Physics, Aalto University, 02150 Espoo, Finland
2. Institute for Advanced Study, Tsinghua University, Beijing, 100084, China

Non-Hermitian (NH) Hamiltonians have risen as a rich framework to describe the post-selected quantum dynamics of open quantum systems[1][2][3]. NH Hamiltonians have been found to host a variety of phenomena lacking a counterpart in Hermitian systems, including the unique topological properties[4]. Recently, the generalization of NH topology as well as other interesting aspects of NH physics to NH many-body systems have attracted much interest. Despite the intense interest in the study of NH many-body physics, efficient numerical tools are lacking. In particular, the computation of local spectral functions of many-body excitations allow revealing many-body topological modes[5], and therefore would be of key interest to address topological interacting NH many-body models.

Here[6], we put forward a numerical approach to compute spectral functions of a non-Hermitian many-body Hamiltonian based on the kernel polynomial method and the matrix-product state formalism. Focusing on a topologically non-trivial NH spin chain (Fig. 1), we show that the local spectral functions computed with our algorithm reveal the topological spin excitations, faithfully reflecting the non-trivial topology. We further show that the algorithm works in the presence of the non-Hermitian skin effect, a regime commonly discussed for NH systems. Our results put forward a new method to efficiently compute spectral functions of non-Hermitian many-body systems of large sizes beyond the capability of exact diagonalization, and makes an essential step towards the critical open problem of addressing non-trivial topology in non-Hermitian many-body systems.

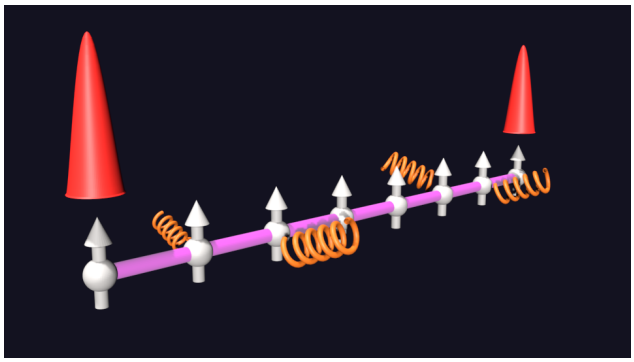

Fig. 1: Sketch of the non-Hermitian may-body spin chain model we study. With a spatially-dependent dissipation (orange curves), a topologically non-trivial regime can be achieved and topological boundary excitations appear (the red peaks).

References

[1] H. Breuer and F. Petruccione, The theory of Open Quantum Systems (Oxford University Press, 2002)
[2] E. J. Bergholtz, J. C. Budich, and F. K. Kunst, Rev. Mod. Phys. **93** 015005 (2021)
[3] Y. Ashida, Z. Gong, and M. Ueda, Advances in Physics **69** 249 (2020)
[4] K. Kawabata, K. Shiozaki, M. Ueda, and M. Sato, Phys. Rev. X **9** 041015 (2019)
[5] J. L. Lado and O. Zilberberg, Phys. Rev. Research **1** 033009 (2019)
[6] G. Chen, F. Song and J. L. Lado, arxiv:2208.06425

Neutron-rich refractory nuclei studied via precision mass measurements at JYFLTRAP

M. Hukkanen[*1,2], **A. Kankainen** [1], **P. Ascher** [2], **M. Bender** [3], **T. Eronen** [1], **Z. Ge** [4], **M. Gerbaux** [2], **S. Grévy** [2], **A. Husson**[†2], **D.A. Nesterenko** [1], **A. de Roubin** [5], **W. Ryssens** [6], **M. Stryjczyk** [1], **A.P. Weaver** [7] **and the I261 experiment collaboration**

1. University of Jyvaskyla, Department of Physics, Accelerator Laboratory, Finland
2. LP2i Bordeaux, Université de Bordeaux, France
3. Université de Lyon, Université Claude Bernard Lyon 1, France
4. GSI Helmholtzzentrum für Schwerionenforschung GmbH, Darmstadt, Germany
5. KU Leuven, Instituut voor Kern- en Stralingsfysica, Leuven, Belgium.
6. Institut d'Astronomie et d'Astrophysique, Université Libre de Bruxelles, Belgium
7. TRIUMF, Vancouver, British Columbia, Canada

Neutron-rich refractory nuclei in the vicinity of mass number A $\approx$ 100 exhibit complex nuclear structures and rapid changes in the shape of the nuclei [1]. Some of the nuclei in this region are predicted to have a triaxial shape [2] and many have low-lying isomeric states. If the isomeric states are unresolved, this could cause a shift in the measured mass value or the measured mass value could be assigned to a wrong state. The shape changes of the nucleus can be studied for example through observing the trend exhibited by two-neutron separation energies. Aside from revealing shape evolution, precise mass values of the neutron-rich elements far from stability are required for simulations of the rapid neutron capture process, in short the r-process [3], which is one of the main processes that are responsible for the heavy-element abundances beyond iron.

The JYFLTRAP double Penning trap mass spectrometer [4], located at the Ion Guide Isotope Separator On-Line (IGISOL) facility of the Accelerator Laboratory of the University of Jyväskylä, was used to perform high-precision mass measurements on neutron-rich yttrium (Z = 39) to rhodium (Z = 45) nuclei [5]. These neutron-rich refractory nuclei were produced in proton-induced fission on a natural uranium target, mass-separated based on the mass-to-charge ratio and prepared with a radio-frequency quadrupole (RFQ) cooler-buncher before performing high-precision mass measurements with the JYLFTRAP Penning trap.

The Phase-Imaging Ion-Cyclotron-Resonance (PI-ICR) technique [6][7] was used to separate and measure the masses of the ground states and low-lying isomeric states in neutron-rich odd-odd $^{110-118}$ Rh and ^{115}Ru isotopes. The masses of the most exotic nuclei in the isotopic chains from yttrium and rhodium were measured utilizing the Time-Of-Flight Ion-Cyclotron-Resonance (TOF-ICR) technique [8]. In total eight masses were measured for the first time and the precision of several literature values were significantly improved. The measured masses and their differences were compared in detail to the predictions of the global mass model BSkG1 [2]. In this contribution the results of the measurement campaign and their implications on nuclear structure in this mass region will be presented.

References

[1] U. Hager et al., Phys. Rev. Lett. **96** 042504 (2006)
[2] G. Scamps et al., Eur. Phys. J. A **57** 333 (2021)
[3] E.M. Burbidge et al., Rev. Mod. Phys. **29** 547 (1957)
[4] T. Eronen et al., Eur. Phys. J. A **48** 46 (2012)
[5] M. Hukkanen et al., Phys. Rev. C. **107** 014306 (2023)
[6] S. Eliseev et al., Phys. Rev. Lett. **110** 082501 (2013)
[7] D.A Nesterenko et al., Eur. Phys. J. A **54** 154 (2018)
[8] M. König et al., Int. J. Mass Spectrom. Ion Process. **142** 95 (1995)

[*]Corresponding author: marjut.h.hukkanen@jyu.fi
[†]Present: Aix Marseille Univ, CNRS, PIIM, Marseille, France

Double-beta decay Q-value measurement of ^{104}Ru with the JYFLTRAP Penning trap

J. K. A. Ruotsalainen*, **T. Eronen, A. Kankainen, M. Mougeot, A. Jaries, V. Virtanen, A. Raggio**
Accelerator Laboratory, Department of Physics, University of Jyväskylä,
P.O. Box 35 (YFL), FI-40014 University of Jyväskylä, Finland

In a double-beta decay of an atomic nucleus two protons transform into neutrons or vice versa, while simultaneously releasing two (anti-)electrons and two (anti-)neutrinos. The energy released in the decay is called the Q-value of the decay, which is divided between the particles as kinetic energy. While a double-beta decay releasing two neutrinos has been observed, a neutrinoless double-beta decay has been proposed as an alternative branch. This decay would require the neutrino to be a Majorana particle (i.e. its own antiparticle) which is not permitted by the Standard Model of particle physics. Confirming its existence is currently a major goal in neutrino physics experiments [1].

In the search for the neutrinoless double-beta decay, a precise Q-value of the decay is required. Firstly, the Q-value is used to calculate the partial half-life of the decay branch, which indicates the feasibility of observing the decay in a given isotope, as the half-lives are on the order of $\geq 10^{25}$ a [1]. Secondly, the decay can be detected by measuring the kinetic energy of the two electrons, as the sum of the energies is constant. The Q-value is thus used to locate the sum signal from background noise [1,2]. Currently, the most precise method of determining the decay Q-value is by measuring the atomic mass difference of the mother and daughter nuclides.

In our recent measurement at the Ion Guide Isotope Separator On-Line (IGISOL) facility [3] in the University of Jyväskylä, the JYFLTRAP Penning trap [4] was used to determine the Q-value of the ^{104}Ru double-beta decay by measuring the mass difference between the mother ^{104}Ru and daughter ^{104}Pd ions using the PI-ICR measurement technique [5,6]. The obtained Q-value is in agreement with the currently accepted value of 1299.4(27) keV [7], but is over 20 times more precise. In addition, the well-known double electron-capture Q-value of ^{102}Pd was measured and found to be in agreement with the literature value [7]. The ^{104}Ru Q-value will soon be used to determine the suitability of this isotope for experiments searching for the existence of neutrinoless double-beta decay and the mass of the neutrino [1,2]. In my contribution, I will present the measurement setup and technique, and initial results of the measurement.

References

[1] M. J. Dolinski et. al, Annu. Rev. Nucl. Part. Sci. **69** 219 (2019)
[2] F. T. Avignone et. al, Rev. Mod. Phys. **80** 481 (2008)
[3] I. Moore et. al, Nucl. Instrum. Methods Phys. Res. B **317** 208 (2013)
[4] T. Eronen et. al, Eur. Phys. J. A. **48** 46 (2012)
[5] S. Eliseev et. al, Phys. Rev. Lett. **110** 082501 (2013)
[6] D. A. Nesterenko et. al, Eur. Phys. J. A. **57** 302 (2021)
[7] M. Wang et. al, Chinese Phys. C **45** 030003 (2021)

*Corresponding author: jouni.k.a.ruotsalainen@jyu.fi

Study of Fission Fragment Mass & Energy distribution in Pre-Actinide Region

Meghashree Cheralu House, on behalf of the CORSET collaboration

In the sub-lead region, the fission fragment shell properties are dominated by the ridges and valleys in the potential energy surface leading from the saddle to the scission point. These structures result from shell corrections and vanish with increasing excitation energy. The asymmetric fission of mercury nuclei, initially observed in the low-energy region [1,2,3], was later supported by the theory of doubly magic shell configuration of the fragments [4]. In recent years, several experiments investigated the asymmetric behaviour of Hg nuclei showing the influence of shell effects on the asymmetric fission process [5]. Spherical shells are generally more stable towards asymmetric fission than deformed nuclei. It has been observed that, unlike other mercury isotopes, the three odd ^{181,183,185}Hg nuclei have highly deformed charged radii attributed to quadrupole and monopole momentum [6]. Thus, one may expect ^{183}Hg to show more asymmetry in fission fragments' mass-energy distribution than ^{182}Hg.

Our experiments with the CORSET [7] setup investigated the asymmetric nature of several isotopes in the pre-actinide region. The ^{36}Ar and ^{40}Ca beams of various energies have been projected on ^{142}Nd ^{144,154}Sm and ^{142,143}Nd targets leading to the formation of the ^{178}Pt, ^{180,182,183,190}Hg compound nuclei, respectively. We have investigated mass and energy distributions of fragments and fission characteristics of the oblate ^{182} Hg ($\beta_2 = 0.147$) and prolate ^{183}Hg ($\beta_2 = 0.313$) nuclei formed in the ^{40}Ca+^{142,143}Nd reaction. Observing their β_2 value, we conclude that ^{182}Hg is less deformed than ^{183}Hg. Therefore, we expected to get a higher asymmetry for ^{183}Hg. Instead, we didn't observe any large variations in the mass-energy distribution between ^{182}Hg and ^{183}Hg at any of the measured energies. This puzzling outcome requires a thorough revaluation of the influence of shell structure, charge radii deformation and factors associated with the potential energy surface that are responsible for fission in the Hg region.

1. M.G.Itkis et al., Sov. J. Nucl. Phys. 52, 601 (1990).
2. M.G.Itkis et al., Sov. J. Nucl. Phys. 53, 757 (1991).
3. R.Vandenbosch and J.R.Huizenga, Nuclear Fission, Academic Press, New York, (1973).
4. A.N.Andreyev et al., Phys. Rev. Lett. 105, 252502 (2010).
5. E.Prasad et al., Phys.Rev. C 91, 064605 (2015).
6. B.A.Marsh et al., Nature Phys. V.14. P.1163 (2018)
7. E.M.Kozulin et al., Instruments and Experimental Techniques V.51 No.1 (2008).

My Abstract for Physics Days 2023

Photo-assisted negative ion production in caesium sputter negative ion source

A. Hossain,[1,a)] O. Tarvainen,[2] M. Reponen,[1] R. Kronholm,[1] J. Julin,[1] T. Kalvas,[1] V. Toivanen,[1] M. Kivekäs,[1] and M. Laitinen[1]

[1)]*Accelerator Laboratory, Department of Physics, University of Jyväskylä, FI-40014 Jyväskylä, Finland*

[2)]*STFC ISIS Pulsed Spallation Neutron and Muon Facility, Rutherford Appleton Laboratory, Harwell, OX11 0QX, UK*

(Dated: 25 January 2023)

The negative ion formation in the caesium sputter ion sources occurs on the surface of a cathode containing the ionized material. The cathode is covered by a thin layer of Caesium (Cs), which lowers the work function of the surface enhancing the negative ion formation. Vogel recently introduced a hypothesis that the negative ion current can be enhanced by exposing the cathode to a laser beam resonantly exciting neutral caesium atoms to electronic states, acting as a catalyst for negative ion production via so-called ion pair production[1]. Recent experiments at the JYFL-ACCLAB have revealed that the photo-assisted production of negative ions can be provoked by any external laser with the photon energy exceeding a certain threshold, which questioned the resonant ion pair production hypothesis[2]. Furthermore, the laser-assisted production of negative ions of oxygen (O^-) as well as aluminium (Al^-) was observed with the off-resonance diode lasers[3]. Recently, we demonstrated[4] that the beam current enhancement depends on the applied laser power and ion source conditions, where the beam current enhancement of more than a factor of 2 was reported with 80 mW laser output power at the cathode. In the recent experiment with 15 W laser, we observed that the beam current enhancement factor up to 9 could be obtained under the Cs-depleted operation mode (Unpublished, in review).

In this presentation, we present the overview of our existing results and the corresponding qualitative model for the laser-assisted beam current enhancement mechanism. Our future plans include testing the method with other, high-performance, caesium sputter ion sources to develop a "turn-key" laser booster for SNICS sources.

REFERENCES

[1]J. S. Vogel, "Lasis: The laser assisted sputter ion source," Nuclear Instruments and Methods in Physics Research Section B: Beam Interactions with Materials and Atoms **438**, 89–95 (2019).

[2]O. Tarvainen, R. Kronholm, M. Laitinen, M. Reponen, J. Julin, V. Toivanen, M. Napari, M. Marttinen, D. Faircloth, H. Koivisto, and T. Sajavaara, "Experimental evidence on photo-assisted O^- ion production from Al_2O_3 cathode in cesium sputter negative ion source," Journal of Applied Physics **128**, 094903 (2020).

[3]O. Tarvainen, R. Kronholm, M. Laitinen, M. Reponen, J. Julin, V. Toivanen, M. Napari, M. Marttinen, T. Kalvas, D. Faircloth, H. Koivisto, and T. Sajavaara, "Photo-assisted O^- and Al^- production with a cesium sputter ion source," AIP Conference Proceedings **2373**, 020001 (2021).

[4]A. Hossain, O. Tarvainen, M. Reponen, R. Kronholm, J. Julin, T. Kalvas, V. Toivanen, M. Kivekäs, and M. Laitinen, "Photo-enhanced o-, h- and br- ion production in caesium sputter negative ion source—no evidence for resonant ion pair production," Journal of Physics D: Applied Physics **55**, 445202 (2022).

[a)]Electronic mail: akbar.a.hossain@jyu.fi

High-precision Solar pp neutrino Measurement with SERAPPIS

Timo Enqvist[*1], **Kai Loo**[†1], **Wladyslaw H. Trzaska**[‡1]
1. Department of Physics, University of Jyväskylä, Finland

The Standard Solar Model predicts the flux of solar pp neutrinos emitted in the main fusion process of two protons to a deuteron (pp-I) with an uncertainty of $\pm 0.6\%$ (see, for example, [1]). The only real-time measurement of the solar pp neutrino flux has been performed by the Borexino collaboration using the high-purity, 300-ton organic liquid scintillator experiment BOREXINO with ~ 3800 m.w.e. muon shielding. The uncertainty of the pp flux measurement reported by the collaboration is $\sim 10\%$ [2].

The SERAPPIS project (SEarch for RAre PP neutrinos In Scintillator) [3] aims at a precision measurement of the solar pp neutrino flux on the level of few percent. The concept of SERAPPIS relies on a small organic liquid scintillator detector of ~ 21 m^3 (~ 18 tons) having an excellent energy resolution of $\sim 2.5\%$ at 1 MeV energy deposit, a low internal background radioactivity (especially on ^{14}C), and a sufficient shielding against the surrounding external radioactivity of gammas and neutrons.

The SERAPPIS experiment will profit from the existing infrastructure of the Jiangmen Underground Neutrino Observatory (JUNO) [4]. This includes the online monitoring of the liquid radiopurity where the pre-detector OSIRIS [5] is used during the JUNO filling phase. After completing the JUNO filling phase, OSIRIS is converted to SERAPPIS which requires some upgrades, mainly:

- the excellent photon collection efficiency (the energy resolution) will be achieved with $\sim 75\%$ PMT coverage (possibly with utilizing reflective cones),
- the current external shielding of 3 m.w.e. of water should be increased by ~ 1.25 m of water (or, equivalently, adding ~ 15 cm of steel),
- the concentration of ^{14}C isotope should be recuded by $2-3$ orders of magnitude compared with the current value, being presumably between $10^{-17}-10^{-18}$.

While the two first items of the upgrade are mostly practical, identifying liquid scintillator solvents and fluors with the concentration of the ^{14}C isotope below $\sim 10^{-18}$ is probably a more difficult task. The concentration of the ^{14}C isotope, i.e., ratio of ^{14}C : ^{12}C, in the BOREXINO experiment was $\sim 2\times 10^{-18}$, being the lowest concentration value measured. Typically, the ^{14}C concentration ranges inside a magnitude in various large-scale liquid scintillator detectors.

Based on the analysis of the ^{14}C concentration in liquid scintillators derived from deep oil and gas fields [6], values lower than 10^{-18}, even down to $\sim 5\times 10^{-21}$, are plausible provided the source is carefully chosen. The contamination from the reaction ^{14}N(n,p)^{14}C is expected to be the main source of ^{14}C also deep underground where a low but steady neutron flux is mostly created by the natural radioactivity in rock, (α, n) reactions, and spontaneous fission of ^{238}U. It has also been speculated that the higher concentration values could have been created during the liquid scintillator manufacturing, or they could have been created by the ^{14}C contamination in the fluors, or they could have been caused by a biological activity of extremophilic bacteria deep underground.

A new, small-scale liquid scintillator setup, with the aimed sensitivity to detect concentrations below 10^{-18}, is under design in the Department of Physics, University of Jyväskylä, Finland. The setup situates at the Callio Lab in the Pyhäsalmi mine, Finland, at the depth of 4000 m.w.e. It uses copper and lead shielding (completed with bricks) against γ-background from rock and polyethyene bricks against neutron background. The amount of (active) liquid scintillator is planned to be few liters. The design of the new setup is based on the counting rates and background conditions measured by the first version of the setup.

The simulation results of the SERAPPIS feasibility design [3] show that the uncertainty of the solar pp neutrino flux measurement of $\sim 3.4\%$ could be obtained using the default set of parameters: ^{14}C concentration 10^{-20}, light yield 1500 photoelectrons/MeV, measurement time 1500 days, and ^{210}Bi and ^{85}Kr internal background 0.16 decays/(day·ton). By optimizing the parameters, especially the concentration of the ^{14}C isotope and the external γ-background, the uncertainty in the solar pp neutrino flux measurement can be pushed down to $\sim 1.2\%$.

A more accurate measurement of the solar pp neutrino flux can be used to constrain the solar mixing angle θ_{12} at high precision (for electron neutrinos), where the current uncertainty (in $\sin^2\theta_{12}$) is $\sim 4\%$. Due to the low energy of the solar pp neutrinos ($Q_{pp} = 420$ keV), they experience only vacuum oscillations, and not matter effect at the center of the Sun. When combined with the sub-percent mixing-angle precision result of JUNO (for electron antineutrinos), an interesting comparison between neutrino–antineutrino symmetry in oscillations can be done. Moreover, additional energy production or energy loss mechanisms (e.g., thermal production of axions or hidden photons [7]) in the Sun can be studied together with JUNO precision results.

References

[1] A. Serenelli, Alive and well: A short review about standard solar models. Eur. Phys. J. A **52** 78 (2016)
[2] BOREXINO COLLABORATION, Neutrinos from the primary proton-proton fusion process in the Sun. Nature **512** 383 (2014); BOREXINO COLLABORATION, Comprehensive measurement of pp-chain solar neutrinos. Nature **562** 505 (2018)
[3] L. Birger *et al.*, Potential for a precision measurement of solar pp neutrinos in the Serappis experiment. Eur. Phys. J. C **82** 779 (2022)
[4] JUNO COLLABORATION, JUNO Physics and Detector. Prog. Part. Nucl. Phys. **123** (2022) 103927
[5] JUNO COLLABORATION, The design and sensitivity of JUNO's scintillator radiopurity pre-detector OSIRIS. Eur. Phys. J. C **81** 973 (2021)
[6] G. Bonvicini, N. Harris, and V. Paolone, The chemical history of ^{14}C in deep oilfields. arXiv:hep-ex/0308025v2 [8 Aug 2003]
[7] N. Vinyoles, A. Serenelli, F.L. Villante, S. Basu, J. Redondo, J. Isern, New axion and hidden photon constraints from a solar data global fit. JCAP **10** 015 (2015)

[*]Corresponding author: timo.t.enqvist@jyu.fi
[†]Corresponding author: kai.k.loo@jyu.fi
[‡]Corresponding author: wladyslaw.h.trzaska@jyu.fi

Dijet invariant mass in pp and p–Pb collisions at $\sqrt{s_{\mathrm{NN}}} = 5.02$ TeV with the ALICE detector at the LHC at CERN

Laura Huhta (for the ALICE collaboration)[*1]
1. University of Jyväskylä, Jyväskylä, Finland

At extreme density and temperature, matter undergoes a deconfinement phase transition to a quark-gluon plasma (QGP). This high-temperature region of the QCD phase diagram can be studied in ultra-relativistic heavy ion collisions. ALICE (A Large Ion Collider Experiment) is optimized to study the properties of the QGP.

High-energy partons lose their energy while traversing through the hot and dense QGP medium created in lead-lead collisions at the LHC. The high energy partons hadronize and form a collimated hadron shower, a jet, which can be measured. Properties of the QGP can be studied by performing versatile measurements of the energy loss of partons propagating through the medium.

The dijet asymmetry observed by ATLAS in 2010 [1] and dijet momentum imbalance measured by CMS in 2012 [2] clearly show that energetic dijets are modified in Pb–Pb collisions at the LHC. The strength of the ALICE experiment in jet studies comes from our capability to study low energy jets, for which the medium modifications are expected to be stronger.

The invariant mass of a dijet system is a Lorentz invariant quantity that can provide a well-motivated measure of interaction hardness in the collision. The dijet invariant mass is closely tied to the partonic center-of-mass energy $\sqrt{\hat{s}}$, which ties it to the virtuality of the event, while also making it a natural observable for theory. Our goal in the long run is to measure modifications in the invariant mass of the dijet system as a function of collision centrality down to small masses.

To better quantify modifications caused by the dense QGP medium, the measurement is performed in smaller collision systems, like in proton-proton and proton-lead collisions at the LHC. The pp collisions provide a baseline result, and the p–Pb collisions measure effects of cold nuclear matter, such as possible modifications arising from nuclear parton distributions. This is a crucial step towards the interpretation of Pb–Pb results.

We present the dijet invariant mass distribution in pp and p–Pb collisions at center-of-mass energy $\sqrt{s_{\mathrm{NN}}} = 5.02$ TeV measured by ALICE, in the mass range of $65 - 150$ GeV$/c^2$. Charged particle jets are reconstructed using the anti-k_T algorithm and a radius parameter $R = 0.4$. We have developed a new method to characterize background fluctuations of the dijet mass, which are important in the low mass region. Effects from background fluctuations are unfolded together with detector inefficiencies using a Bayesian unfolding procedure. The p–Pb data was recorded in 2016, and the pp reference data at the same collision energy in 2017. In line with earlier jet studies [3,4], there is no significant cold nuclear matter modification to be seen in the measured range within uncertainties.

References

[1] ATLAS collaboration, "Observation of a Centrality-Dependent Dijet Asymmetry in Lead-Lead Collisions at $\sqrt{s_{\mathrm{NN}}} = 2.76$ TeV with the ATLAS Detector at the LHC", Phys.Rev.Lett. 105 (2010), 252303.
[2] CMS collaboration, "Jet momentum dependence of jet quenching in PbPb collisions at $\sqrt{s_{\mathrm{NN}}} = 2.76$ TeV", Phys.Lett.B 712 (2012), 176-197.
[3] ALICE collaboration, "Measurement of charged jet production cross sections and nuclear modification in p-Pb collisions at $\sqrt{s_{\mathrm{NN}}} = 5.02$ TeV", Phys.Lett.B 749 (2015), 68-81.
[4] ATLAS collaboration, "Centrality and rapidity dependence of inclusive jet production in $\sqrt{s_{\mathrm{NN}}} = 5.02$ TeV proton-lead collisions with the ATLAS detector", Phys.Lett.B 748 (2015), 392-413.

[*]Corresponding author: laura.m.huhta@jyu.fi

ERO2.0 Modelling of medium-Z impurity sources in JET

Pyry Virtanen[*1], **Mathias Groth** [1], **Henri Kumpulainen** [1], **Juri Romazanov** [2], **Roni Mäenpää** [1]
1. Aalto University, PL 11000 00076 AALTO, Espoo, Finland
2. Forschungszentrum Jülich GmbH, Jülich, Germany

Nuclear fusion is a process in which two lighter atomic nuclei combine into a larger nuclei. This process releases energy as the created nucleus has a lower mass than the combined mass of the lighter nuclei, resulting from the reduced binding energy requirement for the coalescence of the larger nuclei. Man-made fusion is attempted in tokamaks, which utilize strong magnetic fields to confine a fusing plasma.

In this work, the transport of the medium-Z impurities nickel, iron and chromium is studied in the Joint European Torus (JET) using the ERO2.0 Monte Carlo code. These simulations were carried out to gain insight on the erosion of wall components and the release of impurities into the plasma. Generally, impurities dilute the plasma and cause radiation losses which lead to shorter confinement times resulting in reduced fusion performance.

The simulations predict that the erosion of the vessel wall occurs mainly on the low field side and that the impurities are transported from the far scrape-off layer (SOL) into the near separatrix SOL and into the core plasma. Furthermore, the impurities are predicted to be transported to the high field side of the vessel, which is consistent with observed medium-Z deposition. Comparing the ERO2.0 predictions to the measured impurity density shows that the predictions for the total nickel density are within measurement uncertainties for high-confinement mode plasma, while they overestimate the total nickel density for the low-confinement mode plasma by a factor of two to three. The working hypothesis of the discrepancies between the simulations and the measurements is the sufficiently accurate adaption of the radial gradients in the measured deuterium background plasma.

[*]Corresponding author: pyry.l.virtanen@aalto.fi

The new ALICE Fast Interaction Trigger in LHC Run 3

Andreas Molander, on behalf of the ALICE Collaboration[*1,2]
1. Helsinki Institute of Physics (HIP), University of Helsinki, P.O. Box 64, 00014, Finland
2. Department of Physics, University of Jyväskylä, P.O. Box 35, 40014, Finland

On the 5th of July 2023, the Large Hadron Collider (LHC) at CERN, Geneva, started the official data taking of the current LHC run, Run 3, after a maintenance, upgrade, and commissioning period of around three and a half years. ALICE (A Large Ion Collider Experiment) has undergone many upgrades and improvements [1], one of which is the brand-new Fast Interaction Trigger (FIT) detector [2-4]. With its Cherenkov and scintillating arrays, FIT detects particles from proton-proton and heavy-ion collisions in the forward regions of ALICE. It provides low-latency interaction triggers, precise interaction time, luminosity and background monitoring, and determination of centrality, multiplicity, and event plane [5]. Thus far, FIT has performed well in both nominal proton-proton collisions and the short Pb-Pb pilot run. FIT shows good collision time and vertex reconstruction, provides a sophisticated interaction trigger menu, and has been giving critical feedback about luminosity and background to the LHC for online beam tuning. The performance of FIT is continuously improving thanks to electronics, firmware, and software upgrades. The installation and commissioning of FIT [6], its performance during the start of Run 3, and future development and outlook for 2023 are presented.

References

[1] W. H. Trzaska, "New ALICE detectors for Run 3 and 4 at the CERN LHC", *Nuclear Instruments and Methods in Physics Research Section A: Accelerators, Spectrometers, Detectors and Associated Equipment* **958** (2020) 162116, https://doi.org/10.1016/j.nima.2019.04.070.
[2] M. Slupecki, "Fast Interaction Trigger for ALICE upgrade", *Nuclear Instruments and Methods in Physics Research Section A: Accelerators, Spectrometers, Detectors and Associated Equipment* **1039** (2022) 167021, https://doi.org/10.1016/j.nima.2022.167021.
[3] M. Slupecki, "The Fast Interaction Trigger for the ALICE Upgrade", Ph.D. thesis (2020), ISBN 978-951-39-8186-0, http://urn.fi/URN:ISBN:978-951-39-8186-0.
[4] D. Finogeev, "Fully integrated digital readout for the new Fast Interaction Trigger for the ALICE upgrade", *Nuclear Instruments and Methods in Physics Research Section A: Accelerators, Spectrometers, Detectors and Associated Equipment* **952** (2020) 161920, https://doi.org/10.1016/j.nima.2019.02.047.
[5] H. M. Rytkonen, "Event plane determination with the new ALICE FIT detector", *PoS* **ICHEP2020** (2021) 814, https://doi.org/10.22323/1.390.0814.
[6] W.H. Trzaska, *CERN EP newsletter*, 23 September 2021 https://ep-news.web.cern.ch/content/new-alice-fast-interaction-trigger.

JYVÄSKYLÄN YLIOPISTO
UNIVERSITY OF JYVÄSKYLÄ

HELSINKI INSTITUTE OF PHYSICS

ALICE

PHYSICS DAYS 2023 TAMPERE

[*]Corresponding author: andreas.molander@cern.ch

Extracting real-space correlation entropy with machine learning in Kondo impurity problems

Faluke Aikebaier[*1,2,3], **Teemu Ojanen** [2,3], **Jose L. Lado** [1]
1. Department of Applied Physics, Aalto University, 00076, Espoo, Finland
2. Computational Physics Laboratory, Physics Unit, Faculty of Engineering and Natural Sciences, Tampere University, FI-33014 Tampere, Finland
3. Helsinki Institute of Physics P.O. Box 64, FI-00014, Finland

Studying strongly correlated materials is one of the most intriguing and challenging research directions in quantum many-body physics [1]. In quantum impurity problems, strong interactions are localized in a few sites, which generate complex quantum states in a larger non-interacting part of the system [2]. Such quantum states manifest long-range spatial entanglement due to Kondo screening cloud [3]. The characterization of correlation in quantum impurity problems is of great interest, yet its measurement with real space probes has remained an open challenge [4] [5] [6]. Here we put forward a methodology [7] to extract spatially dependent correlation entropy density by means of real-space measurements. We demonstrate that a supervised machine learning approach based on the artificial neural network allows us to extract the correlation entropy density from finite local measurements. We show that the correlation entropy density can be reconstructed from a finite set of local particle and density measurements in an electronic system, a task that was considered to require knowledge of all the correlations in the system. Our methodology provides a strategy for experimentally extracting the Kondo screening cloud based on the information contained in the spatial correlation entropy density. Ultimately, our results establish a pathway toward extracting the quantum entanglement locally by combining scanning spectroscopy data and machine learning.

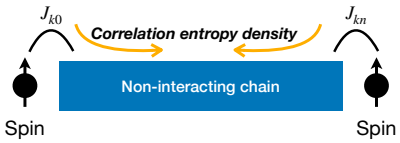

Fig. 1: Schematic structure of the impurity problem.

References

[1] Fulde, P, Springer Science & Business Media (1995)
[2] A. C. Hewson, Cambridge University Press, Cambridge, New York (1993)
[3] V. Barzykin and I. Affleck, Phys. Rev. Lett. **68**, 4959 (1996)
[4] Maxime Debertolis, Serge Florens, Phys. Rev. B. **103**, 235166 (2021)
[5] I. V. Borzenets, J. Shim, J. C. H. Chen, A. Ludwig, A. D. Wieck, S. Tarucha, H. S. Sim, and M. Yamamoto, Nature (London) **579**, 210 (2020)
[6] J. Park, S. S. B. Lee, Y. Oreg, and H.-S. Sim, How to Directly Measure a Kondo Cloud's Length, Phys. Rev. Lett. **110**, 246603 (2013)
[7] F. Aikebaier, T. Ojanen, and J. L. Lado, In preparation (2023)

[*]Corresponding author: faluke.aikebaier@aalto.fi

Curation of Big Data for Atmospheric Science Purposes

Vitus Besel[*1], **Milica Todorović** [2], **Theo Kurtén** [1], **Patrick Rinke** [3], **Hanna Vehkamäki** [1]
1. Institute for Atmospheric and Earth System Research, P.O 64, 00014 University of Helsinki
2. Dept. Mechanical and Materials Engineering, University of Turku, Turku, FI-20014, Finland
3. Department of Applied Physics, Aalto University, P.O. Box 11100, Aalto FI-00076, Finland

As cloud and aerosol interactions remain large uncertainties in current climate models[1] they are of special interest for atmospheric science. It is estimated that more than 70% of all cloud condensation nuclei origin from so-called New Particle Formation, which is the process of gaseous precursors clustering together in the atmosphere and subsequent growth into aerosol particles. After initial clustering growth is driven strongly by condensation of low volatile organic compounds (LVOC), that is molecules with saturation vapor pressures (p_{Sat}) below 10^{-6} mbar.[2] These stem from organic molecules emitted by vegetation or anthropogenic sources that are subsequently rapidly oxidized in the air.

We have created a big data set of LVOC using high-throughput computing and Density Functional Theory (DFT), and use it to train Machine Learning models to predict p_{Sat} of previously unseen LVOC. Figure 1a illustrates some sample molecules from the data.

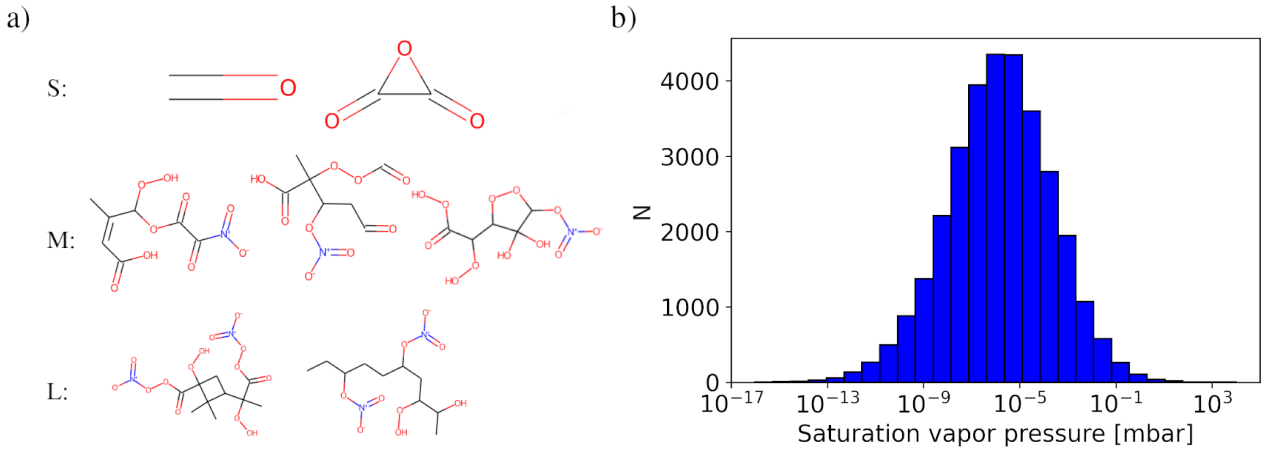

Fig. 1: a) Sample molecules from the dataset for sizes, small (s), medium (m), and large (l). b) A histogram of the p_{Sat} of the calculated data.

Initially the chemical mechanism GECKO-A provides possible LVOC molecules in the form of SMILES strings. In a first step the COSMO*conf* program finds and optimizes structures of possible conformers and provides their energies for the liquid phase on a DFT level of theory. After an additional calculation of the gas phase energies with Turbomole, COSMO*therm* calculates thermodynamical properties, such as the p_{Sat}, using the COSMO-RS model.[3] We bundled all these computations in a highly parallelised high-throughput workflow to calculate **32k** LVOC, that include over **7 Mio.** molecular conformers. See a histogram of the calculated p_{Sat} in Figure 1b.

We use the calculated p_{Sat} to train a Gaussian Process Regression (GPR) machine learning model with the Topological Fingerprint as descriptor for molecular structures. The GPR incorporates noise and outputs uncertainties for predictions on the p_{Sat}. These uncertainties and data cluster techniques allow for the active choosing of molecules to include in the training data, so-called Active Learning.

References

[1] IPCC. Summary for Policymakers , Camb. Univ. Press 3-32 (2021)
[2] Metzger, A. et al., Proc. Natl. Acad. Sci. **107** 6646 (2010)
[3] Klamt, A., Schuüürmann, G. , J. Chem. Soc., Perkin Trans. **2** 799 (1993)

*Corresponding author: vitus.besel@helsinki.fi

LUMI supercomputer update

Jussi Heikonen[*,1], **Pekka Maninen**[1], **Emmanuel Ory**[1], **Fredrik Robertsen**[1]
[1] CSC – IT Center for Science Ltd, PO Box 405, 02101, Espoo, Finland

Figure 1 LUMI supercomputer

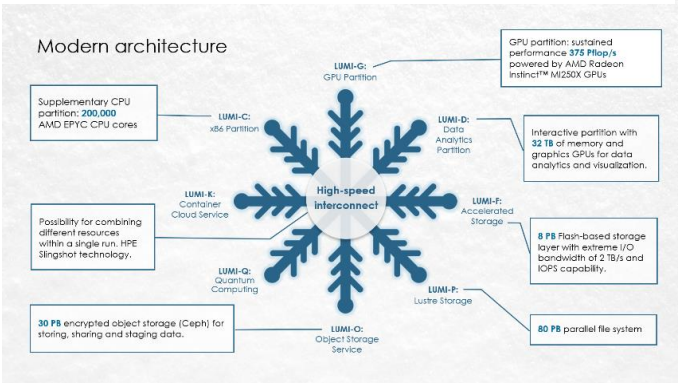

Figure 2 LUMI partitions

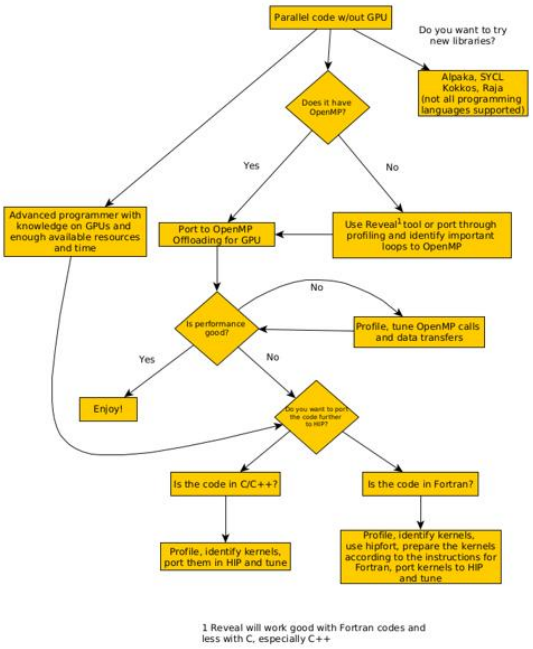

Figure 3 LUMI GPU porting

LUMI supercomputer (Figure 1), which is currently #3 on the Top500 list and the most powerful system in Europe, started full production earlier this year. LUMI is jointly funded by EuroHPC JU and a consortium of ten countries led by CSC in Finland.

In this presentation we first discuss the architecture of LUMI from the user's point of view. More precisely, we introduce the various partitions (Figure 2) that make LUMI exceptionally versatile and suitable for a wide array of applications and workflows.

To fully harness the computing power of the system, programmers must be able to utilize the AMD MI250X GPUs of the system. Accordingly, we present the available GPU programming models and paradigms together with the performance analysis tools. We will provide information on the particular strategies to apply based on the initial situation of the application the user wants to be ported and deployed on LUMI; e.g. in terms of existing code-base, programming language etc. (Figure 3, Figure 4).

Most importantly, we discuss the access and support model: There are various modes and calls for access available from both EuroHPC and the consortium countries. The support is handled by the distributed LUMI User Support Team to which all the consortium countries contribute. The consortium also runs a comprehensive training programme.

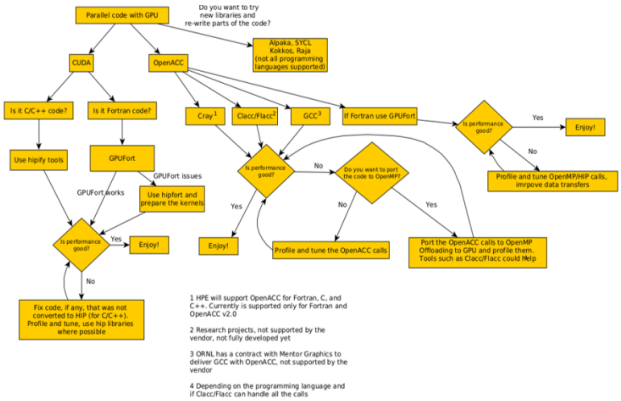

Figure 4 LUMI GPU porting

*Corresponding author: jussi.heikonen@csc.fi

Adaptive Mesh Refinement in Vlasiator

Leo Kotipalo[*1],
1. Space Physics, University of Helsinki, Gustaf Hallströmin katu 2, Helsinki, Finland

Simulating space plasma on a global scale is computationally demanding due to the system size involved. Modeling regions with variable resolution depending on physical behavior can save computational resources without compromising too much on simulation accuracy. This presentation examines adaptive mesh refinement as a method of optimizing Vlasiator, a global hybrid-Vlasov plasma simulator.

Behavior of plasma near the Earth's magnetosphere and different characteristic scales that need to be considered in simulation are introduced. Kinetic models using statistical methods and fluid methods are examined. Modeling electrons kinetically requires resolutions orders of magnitude finer than ions, so in Vlasiator ions are modeled kinetically and electrons as a fluid. This allows for lighter simulation while preserving some kinetic effects.

Mesh refinement used in Vlasiator is introduced as a method to save memory and computational work. Due to the structure of the magnetosphere, resolution isn't uniform in the simulation domain, with particularly the tail regions and magnetopause having rapid spatial changes compared to the relatively uniform solar wind. The region to refine is parametrized and static throughout a simulation run.

Adaptive mesh refinement based on the simulation data is introduced as an evolution of this method. This provides several benefits: more rigorous optimization of refinement regions, easier reparametrization for different conditions, following dynamic structures and saving computation time in initialization.

Refinement is done based on two indices measuring the spatial rate of change of relevant variables and reconnection respectively. The grid is re-refined at set intervals as the simulation runs.

Tests similar to production runs show adaptive refinement to be an efficient replacement for static refinement. Refinement parameters produce results similar to the static method, while giving somewhat different refinement regions. Performance is in line with static refinement, and refinement overhead is minor. Further avenues of development are presented, including dynamic refinement intervals.

[*]Corresponding author: leo.kotipalo@helsinki.fi

A Study of Neutron and Ion Irradiation Induced Atomic Recoil Spectra with Newly Developed Tools RMINDD and pkaESSRIM for Materials Modelling

Uttiyoarnab Saha[*,1]
[1] Nuclear Materials and Engineering Group, Department of Applied Physics,
Aalto University P.O. Box 11000 (Otakaari 1B) FI-00076

The structural materials in nuclear reactors are subjected to intense irradiation by various particles, chiefly neutrons. In materials modelling experiments such materials are tested for their different physical and mechanical properties which are of relevance towards applications in the reactor operating conditions. These experiments mainly use light charged particles and different ions in the MeV energy range. In such pursuits, often the theoretical estimations using advanced methods of computer simulation provide the first light to the discovery of materials for improved performance as well as the fundamental insights to lead the research forward. The nuclear reaction databases [1] for light radiation particles form the starting point in the estimation of numerous effects of radiation on materials. These data are also important if we want to have numerical estimates of radiation damage and compare them with an instance of irradiation experiment. We base on the evaluated nuclear data for neutrons to estimate the primary radiation damage metrics which are crucial parameters in reactor designing. Similarly, the nuclear data for particles like p, d, etc can be used to find the damage metrics due to the irradiation by these charged particles.

When an energetic particle interacts with the target material it creates primary knock-on atoms (PKAs) over a range of energy and there is a series of subsequent knock-on atoms produced which cause damage to different extents depending on the incident particle, its energy, the material and its ambient conditions. The energy spectrum of the PKAs is a vital quantity to categorize different irradiations, especially in the context of emulating the neutron radiation damage response in the structural materials of nuclear reactors. In order to study the (neutron and light charged particle) radiation-matter interaction using the nuclear data a new computation tool called RMINDD [2] is being developed. Another computation tool called pkaESSRIM to estimate the PKA energy spectra due to high energy ion-matter interactions from simulations using the SRIM-2013 software [3] has been developed so that the ion-irradiation scenarios can be effectively planned through comparison of the PKA spectra. In this presentation, the energy dissipation processes of the incident radiation in the target material will be discussed so that we can go through the paths of these new developments. We will also see how different irradiation scenarios compare in terms of the energy spectra of their PKAs. These estimations can serve necessary inputs for MD simulations of radiation cascades which are highly useful in modelling and investigating radiation-induced microstructure in materials.

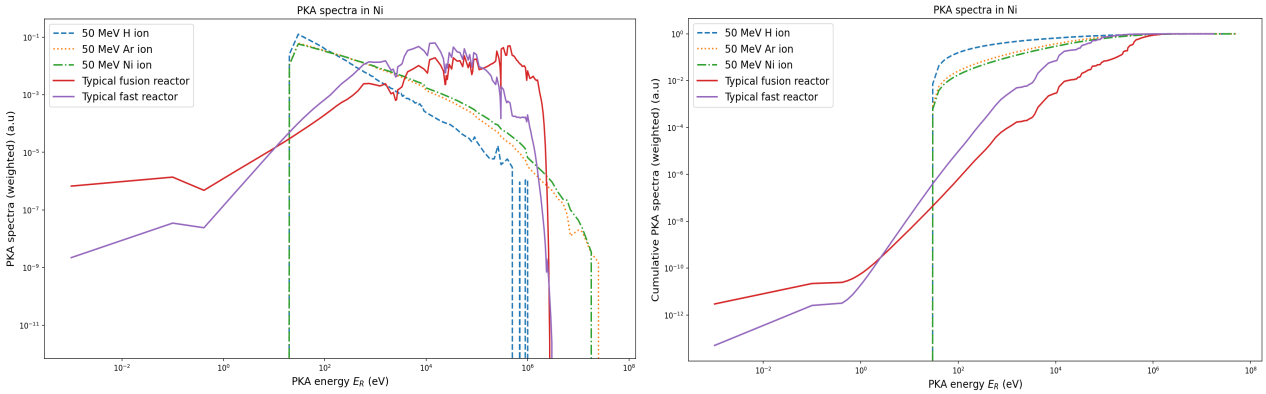

Fig 1: Energy spectra of Ni PKAs under 50 MeV H, Ar, Ni ions, typical fast and fusion neutron spectra weighted by the number of point defects: differential probability density distribution (left panel) and cumulative distribution (right panel) estimated using RMINDD, pkaESSRIM and (Quick:K-P model) SRIM-2013.

References

[1] https://www.nndc.bnl.gov/endf/.
[2] Uttiyoarnab Saha, Proceedings of the DAE Symp. on Nucl. Phys. **65**, 808 (2021).
[3] J. F. Ziegler, M. D. Ziegler, J. P. Biersack, Nucl. Instr. Meth. Phys. Res. B **268**, 1818 (2010).

[*]Corresponding author: uttiyoarnab.saha@aalto.fi

Materials discovery using natural language processing

M. Sipilä[*1], **F. Mehryary** [2], **J. Luoma** [2], **F. Ginter** [2], **S. Pyysalo** [2], **M. Todorović** [1]
1. Department of Mechanical & Materials Engineering, University of Turku
2. Department of Computing, University of Turku

In the recent decades materials research has shifted from solely experimental and theoretical research to approaches based on machine learning and materials data. One underutilized source of data in materials science is scientific text; articles, books and theses. Extraction of meaningful information from large textual datasets can be done via training large deep learning models called transformers, the state-of-the-art models in natural language processing (NLP). For the training, a method called transfer learning is used, see Figure 1a [1][2]. The aim of my research is to apply NLP to materials science scientific text data and to discover previously unknown relationships between materials, their properties and applications.

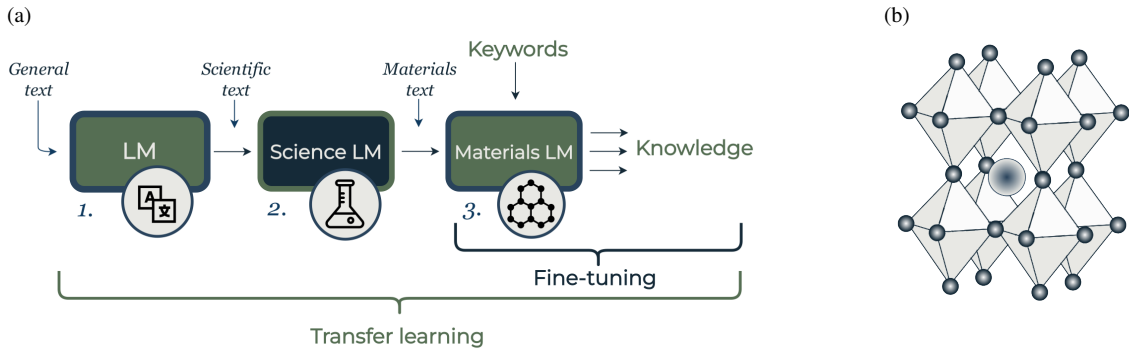

Figure 1: a) Principle of transfer learning, b) Perovskite material structure

This study focuses on the perovskite materials (Figure 1b), which are promising candidates for next generation solar cells. We have utilized the transformer-based models to automatically extract functional properties for a perovskite material of interest from scientific text data. These extracted values can then be collected into large databases, compared and analysed to understand the gaps in composition space, where new materials could be discovered. This kind of an information extraction also allows us to find underlying trends in the materials science across application domains, and discover superior materials for energy production and storage.

References

[1] Olivetti E. A., Cole J. M., Kim E. & al., Appl. Phys. Rev. **7(4)** 041317 (2020)
[2] Kononova O., He T., Huo H. & al., Iscience **24(3)** 102155 (2021)

[*]Corresponding author: matilda.m.sipila@utu.fi

Multi-Reflection Time-of-Flight Mass Separator for radioactive nuclei at the IGISOL facility

V.A. Virtanen[*,1] **T. Eronen A. Kankainen and the IGISOL group**

[1] University of Jyvaskyla, Department of Physics, Accelerator Laboratory,
P.O. Box 35(YFL), FI-40014 University of Jyvaskyla, Finland

Multi-Reflection Time-of-Flight Mass-Spectrometers (MR-ToF-MS) [1] have gained ground in radioactive beam facilities in the past 10 years, due to their comparatively fast operation cycles (~10 ms) and high mass resolution (dm/m ~ 5 ppm). This enables the separation and subsequent mass measurement of particularly short-lived and exotic radioactive nuclei. The operation of an MR-ToF-MS is based on trapping a temporally short bunches of ions (~50 ns FWHM in temporal width), which have been accelerated to an approximately the same energy. Ions with different mass-to-charge ratios are separated by their time-of-flight, as they are trapped and moving along closed paths in the device. At the Ion-Guide Isotope-Separator On-Line (IGISOL) facility [2] at the University of Jyväskylä an MR-ToF-MS has been recently commissioned and used for mass separation and measurements of exotic isobaric radioactive nuclei, as well as for selecting ions of interest for other experiments, such as decay spectroscopy. In this contribution, an overview and the recent mass measurements utilizing the IGISOL MR-ToF-MS are presented, with preliminary mass spectra of the astrophysical r-process nuclei near mass number A = 90. These measurements are relevant for understanding nuclear structure and elemental nucleosynthesis via the r-process.

References

[1] W. R. Plan, T. Dickel, and C. Scheidenberger, “Multiple-reflection time-of-flight mass spectrometry”, International Journal of Mass Spectrometry, vol. 349-350, pp. 134–144, 2013. doi: 10.1016/j.ijms.2013.06.005.

[2] I. Moore et al., “Towards commissioning the new IGISOL-4 facility”, Nuclear Instruments and Methods in Physics Research Section B: Beam Interactions with Materials and Atoms, vol. 317, pp. 208–213, 2013. doi: 10.1016/j.nimb.2013.06.036.

[*]Corresponding author: ville.a.virtanen@jyu.fi

Spectroscopy of neutron deficient actinium isotopes

Jussi Louko[*1], **Juha Uusitalo** [1], **Kalle Auranen** [1]
1. Accelerator Laboratory, Department of Physics, University of Jyväskylä, FI-40014 Jyväskylä, Finland

Prompt and delayed spectroscopy of neutron deficient actinium isotopes was performed at JYFL-ACCLAB. Recoils produced in fusion-evaporation reactions were separated from the beam and unwanted products using MARA vacuum mode recoil separator and subsequently tagged at focal plane using recoil-α decay method. In-beam γ-ray spectroscopy could then be performed for selected recoils by looking back at events seen in JUROGAM 3 spectrometer [1](Fig. 1). Possible delayed γ-rays were detected by focal plane HPGe-detectors.

Excited states in trans-lead nuclei offer an important experimental fingerprint about the onset of nuclear deformation. Past studies have shown that many nuclei in this region exhibit longer living isomers as well as shears bands [2][3]. These were also expected to be present in actiniums, but no supporting evidence was found in this experiment. However, it was confirmed that a more established phenomenon seen in the spherical and nearly spherical astatine and francium nuclei, in which the low-lying negative parity states follow the systematics of the 2^+, 4^+ and 6^+ states of the respective even-even isotone core, also applies to actiniums.

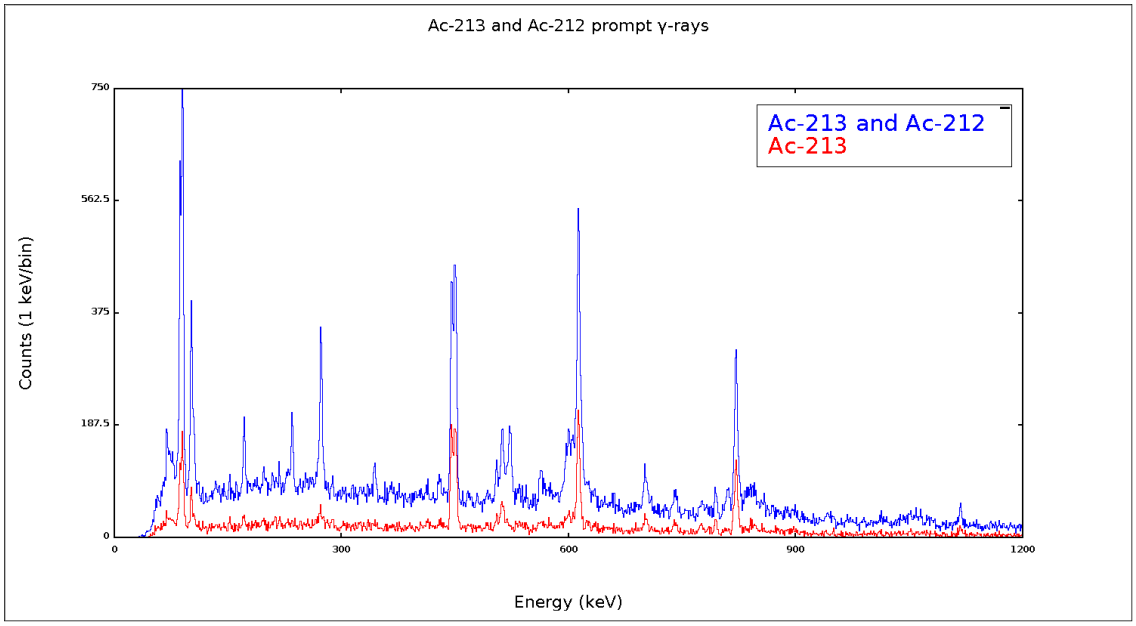

Fig. 1: Recoil-α-tagged prompt γ-rays originating from ^{213}Ac and ^{212}Ac nuclei, seen by the JUROGAM 3 spectrometer.

References

[1] J. Pakarinen et al., Eur. Phys. J. A 56, 149 (2020).
[2] G. D. Dracoulis et al., Rep. Prog. Phys. 79, 076301 (2016).
[3] R. M. Clark and A. O. Macchiavelli, Annu. Rev. Nucl. Part. Sci. 50, 1 (2000).

[*]Corresponding author: jussi.i.louko@jyu.fi

Deuterium induced defects and embrittlement behavior of a Co-free high entropy alloy

X. An[1,2*], E. Lu[1], Z. Chen[1], T. Yang[2], F. Tuomisto[1]

[1] Department of Physics, University of Helsinki, Helsinki, Finland

[2] College of Materials Science and Engineering, Hunan University, Changsha, China

Long-term exposure of structural materials to extreme hydrogen-enriched environments will lead to hydrogen embrittlement, and thus search and design of new alloys with economic and safety benefits against hydrogen embrittlement have become a top priority for the development of many engineering fields [1-2]. We have systematically investigated the hydrogen embrittlement behavior of a new cobalt-free high-entropy alloy $Fe_{27}Ni_{28}Mn_{27}Cr_{18}$ by X-ray diffraction, positron annihilation spectroscopy (PAS), thermal desorption spectrometry (TDS), backscattered electrons and tensile tests, and compared it with $Fe_{25}Co_{25}Cr_{25}Ni_{25}$ alloy. Numerous vacancies are produced in the process of electrochemical deuterium charging and the corresponding concentration is related with the solubility of deuterium atoms. $Fe_{27}Ni_{28}Mn_{27}Cr_{18}$ has much higher concentrations of deuterium and vacancies than $Fe_{25}Co_{25}Cr_{25}Ni_{25}$, which is attributed to the Mn induced severe lattice distortion and results in different variations of mechanical properties. The ultimate tensile strength (UTS) of $Fe_{27}Ni_{28}Mn_{27}Cr_{18}$ increases from 353.73 MPa to 589.50 MPa after electrochemical hydrogen charging while the elongation still remains at 74.73 %, and its deformation mechanism is dominated by dislocation proliferation. In contrast, the UTS of hydrogen charged $Fe_{25}Co_{25}Cr_{25}Ni_{25}$ decreases from 552.79 MPa to 501.53 MPa and the corresponding elongation also decreases from 74.65 % to 67.24 %, and the plastic deformation mechanism is dominated by twinning. Our work demonstrates an economic cobalt-free HEA with great resistance to hydrogen embrittlement, which would enhance the applications of HEAs in hydrogen-enriched environments [3].

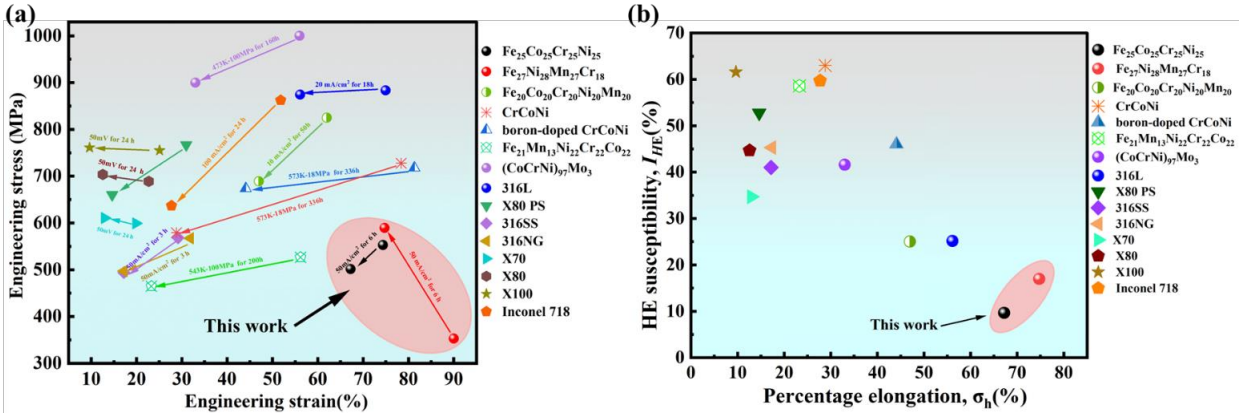

Figure 1. (a) The variations of strength and the loss of strength and strain in this work is compared with the previously reported results; (b) Comparison of the hydrogen embrittlement susceptibility of the alloys prepared in this work with those reported in previous studies.

References

[1] I.M. Robertson, P. Sofronis, K.E. Nygren, Metall Mater. Trans. B. **46** 1085 (2015).

[2] X. Li, J. Yin, X. Ren, J. Mater. Sci. Technol. **122** 20 (2022).

[3] X. An, D. Zhang, H. Zhan, T Yang, J. Alloy. Compd. **940** 168800(2023)

*Corresponding author: xudong.an@helsinki.fi

New avenues for materials research opened by operando x-ray absorption spectroscopy

Antti-Jussi Kallio[1], Nina S. Genz[2], Alexander Weiß[3], Ramon Oord[2], Rene Bes[1], Frank Krumeich[4], Anuj Pokle[5], Mikko J. Heikkilä[3], Øystein Prytz[5], Unni Olsbye[6], Mikko Ritala[3], Marianna Kemell[3], Florian Meirer[2], Bert Weckhuysen[2], Simo Huotari[1]

[1] Department of Physics, University of Helsinki
[2] Inorganic Chemistry and Catalysis group, Department of Chemistry, Utrecht University
[3] Department of Chemistry, University of Helsinki
[4] Laboratory of Inorganic Chemistry, Department of Chemistry, ETH Zurich
[5] Department of Physics, Center for Materials Science and Nanotechnology, University of Oslo
[6] Department of Chemistry, University of Oslo

Characterization of the local chemical environment and the oxidation state of an element of interest are essential tools in various disciplines, such as biology, chemistry, materials science, environmental and Earth sciences, as well as in research of our material cultural heritage. Their evolution in time is vital in chemistry to study e.g., catalysts or thin film growth under working conditions i.e., *in situ / operando*. Such *operando* x-ray tools have not been hitherto available outside large scale facilities such as synchrotrons. We have developed new laboratory-scale x-ray spectroscopy methods to study the chemistry of a) heterogeneous catalysis and b) thin films at Helsinki Center for X-ray Spectroscopy [1].

In heterogeneous catalysis, we significantly improve the understanding of the CO_2 hydrogenation catalysts by tuning the selectivity of supported mono-, bi-, and trimetallic (combinations of Ni, Fe, and Cu) nanoparticles. The study revealed the synergistic effect of metal alloy formation in the Ni, Fe, and Cu containing nanoparticles [2]. Detailed operando x-ray absorption near edge spectroscopy (XANES) of multi-elemental catalysts provided new insights into the metal-dependent differences in the reducibility and re-oxidation behavior and their influence on the catalytic performance in CO_2 hydrogenation.

For thin films grown by atomic layer deposition (ALD) we applied the x-ray absorption spectroscopy for the first time in a local laboratory environment to *in situ* chemistry of films, in this case CuI, down to 12 nm thickness [3]. This improvement in photon collection efficiency has enabled us to collect the XAS spectrum from even thin films in minutes, which was not previously thought possible using low-brilliance x-ray sources. We demonstrate the *in situ* capabilities of the local laboratory-based x-ray spectroscopy by observing the oxidation of CuI into CuO upon annealing at 240°C, with both XANES and extended x-ray absorption fine structure (EXAFS).

The research studies vastly enabled new research on inorganic chemistry and materials and created tools for novel *operando* studies on working catalysts and thin films.

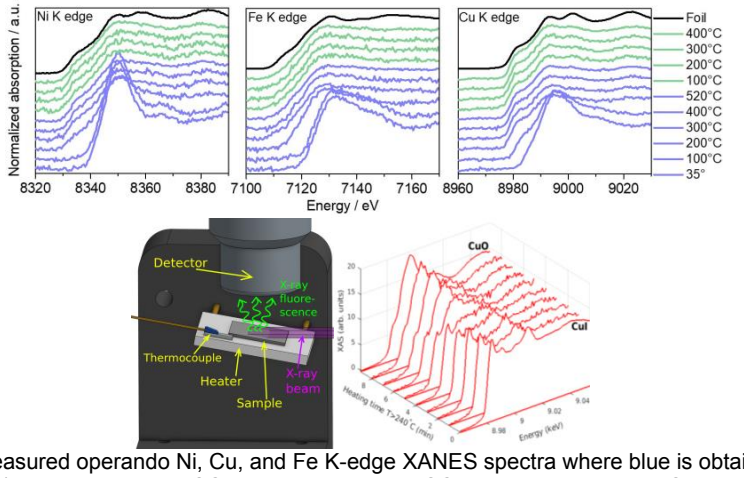

Figure 1: Above the measured operando Ni, Cu, and Fe K-edge XANES spectra where blue is obtained during reduction (H_2:He=1, 35-520ºC, 1 bar) and green during CO_2 hydrogenation (H_2:CO_2:He= 4:1:5, 100-400ºC, 1 bar). Below, CuI annealing setup on the left and obtained XANES spectra on the right.

References

[1] https://www.helsinki.fi/en/infrastructures/center-for-x-ray-spectroscopy
[2] N. S. Genz, A.-J. Kallio, R. Oord, F. Krumeich, A. Pokle, Ø. Prytz, U. Olsbye, F. Meirer, S. Huotari, B. M. Weckhuysen: Operando Laboratory-Based Multi-Edge X-ray Absorption Near Edge Spectroscopy of Solid Catalysts, *Angew. Chem. Int. Ed.* 2022, *61*, e202209334
[3] A.-J. Kallio, A. Weiß, R. Bes, M.J. Heikkilä, M. Ritala, M. Kemell, S. Huotari, Laboratory-scale X-ray absorption spectroscopy of 3d transition metals in inorganic thin films, ***Dalton Trans.***, 2022,**51**, 18593-18602

Thermally induced simultaneous reduction and crystallization of amorphous TiO_2

Lauri Palmolahti[1], Harri Ali-Löytty*[1], Markku Hannula[1], Jesse Saari[1], Weimin Wang[2], Antti Tukiainen[3], Kimmo Lahtonen[3], Mika Valden† [1],

1. Surface Science Group, Faculty of Engineering and Natural Sciences, Tampere University, Tampere, Finland
2. MAX IV laboratory, Lund University, Lund, Sweden
3. Faculty of Engineering and Natural Sciences, Tampere University, Tampere, Finland

TiO_2 is a common photocatalyst material which has been more recently applied as protective coatings on solar cells in artificial photosynthesis. The crystallinity and grain boundaries affect the chemical stability and longevity of the protective coatings. Atomic Layer Deposition (ALD) grown TiO_2 thin films are typically amorphous and have low chemical stability but post-deposition annealing treatments can induce crystallization and thus increase the chemical stability[1]. Precursor traces and Ti^{3+} defects may affect phase transition kinetics and crystallization. The type and amount of precursor traces and Ti^{3+} defects depend on the growth temperature, which allow for optimization of protective TiO_2 coating fabrication process.

In this study[2] 30 nm thick TiO_2 samples were ALD grown on Si from tetrakis(dimethylamino)titanium (TDMAT) and water precursors at 100, 150, and 200 °C. The effect of post-deposition annealing in ultra-high vacuum on chemical composition and structure was studied by XPS and XAS at the FinEstBeAMS beamline in MAX IV Laboratory. Low deposition temperature resulted more TDMAT traces but less Ti^{3+} defects. This led to a higher onset temperature for the reduction of Ti^{4+} to Ti^{3+} and crystallization that occurred simultaneously. Samples grown at 100 and 150 °C crystallized into anatase, but unexpectedly the 200 °C grown sample crystallized into nanocrystalline rutile. Nanocrystalline rutile was not susceptible to corrosion at the grain boundaries under alkaline water splitting conditions unlike microcrystalline anatase films. Thus the defect engineered nanocrystalline rutile thin film is a suitable candidate for protective coatings used in artificial photosynthesis.

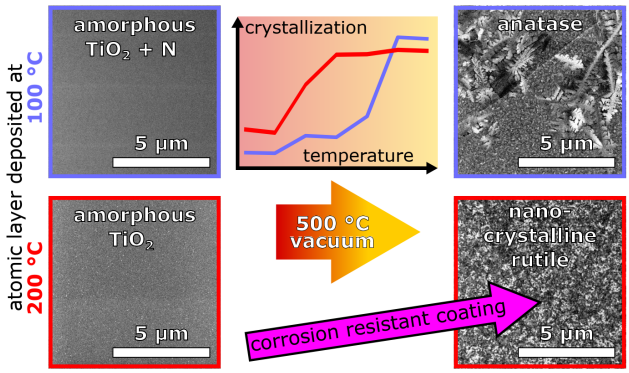

Fig. 1: Crystallization of amorphous TiO_2 samples during vacuum annealing. Reproduced from Ref [2] under CC BY 4.0 license (https://creativecommons.org/licenses/by/4.0/)

References

[1] Hannula, M., Ali-Löytty, H., Lahtonen, K., Sarlin, E., Saari, J. and Valden, M., 2018. Improved stability of atomic layer deposited amorphous TiO_2 photoelectrode coatings by thermally induced oxygen defects. Chemistry of Materials, 30(4), pp.1199-1208. https://doi.org/10.1021/acs.chemmater.7b02938

[2] Palmolahti, L., Ali-Löytty, H., Hannula, M., Saari, J., Wang, W., Tukiainen, A., Lahtonen, K. and Valden, M., 2022. Pinhole-resistant nanocrystalline rutile TiO_2 photoelectrode coatings. Acta Materialia, p.118257. https://doi.org/10.1016/j.actamat.2022.118257

*Corresponding author: harri.ali-loytty@tuni.fi
†Corresponding author: mika.valden@tuni.fi

Surface composition of size-selected aerosol particles studied *in situ* using synchrotron radiation X-ray photoelectron spectroscopy

Minna Patanen[*,1], Isaak Unger[2,3], Clara-Magdalena Saak[2,4], Geethanjali Gopakumar[2], Rebecka Lexelius[5], Olle Björneholm[2], Matthew Salter[6,7], Paul Zieger[6,7]

[1]Nano and Molecular Systems Research Unit, University of Oulu, P.O. Box 3000, 90014, Finland.
[2]Department of Physics and Astronomy, Uppsala University, Box 516, 75120 Uppsala, Sweden.
[3]Deutsches Elektronen-Synchrotron DESY, Notkestr. 85, 22763 Hamburg, Germany
[4]University of Vienna, Department of Physical Chemistry, Währinger Straße 42, 1090 Vienna, Austria.
[5]Department of Cell and Molecular Biology, Uppsala University, Box 596, 75124 Uppsala, Sweden
[6]Department of Environmental Science, Stockholm University, 10691 Stockholm, Sweden
[7]Bolin Centre for Climate Research, 10691 Stockholm, Sweden

Sea spray aerosol is a complex mixture of organic matter and inorganic salts and is one of the most numerous natural aerosols in the atmosphere. Sea spray aerosol particles are involved in various atmospheric chemical processes. They play an important role in the Earth's radiation budget, especially due their hygroscopicity and thus capacity to serve as cloud condensation nuclei. Many aerosol particle characterisation techniques probe integrated particle properties such as size and total elemental content. In contrast, the interaction of aerosol particles with their environment is often determined by their surface chemical composition. Through the use of high brilliance synchrotron radiation, we have carried out surface characterisation of size-resolved laboratory generated free flying sea spray aerosol particles [1].

Bubble bursting processes at the ocean surface eject sea spray aerosol particles to the atmosphere, where they are involved in a multitude of physical and chemical processes [2,3]. Bubble bursting produces film and jet droplets, which have their own typical size distributions and compositions [4]. Film droplets are formed when the bubble cap bursts, and they contain typically more organics and are smaller than the jet droplets produced when the bubble cavity collapses. Thus, sea spray aerosols are a complex mixture of organic matter and inorganic salts and their representation in atmospheric models is challenging. One of the key knowledge gaps in our understanding of sea spray aerosol is the chemical composition of the particle surface, important for various atmospheric chemical processes, as a function of size and bulk composition. Here, we have applied X-ray photoelectron spectroscopy (XPS) to determine the surface composition of both pure inorganic sea salt aerosols and sea salt aerosols spiked with an amino acid (phenylalanine) and a straight chain fatty acid (octanoic acid). Importantly, the use of a differential mobility analyser allowed size-selection of 150, 250 and 350 nm monodisperse aerosol particles for comparison to polydisperse aerosol particles. We observed enrichment of magnesium at the particle surfaces relative to chloride in all aerosols tested, across all particle sizes. Interestingly, the magnitude of this enrichment was dependent on the type of organic present in the solution as well as the particle size. Our results suggest that the observed enrichment in magnesium is an inorganic effect which can be either enhanced or diminished by the addition of organic substances.

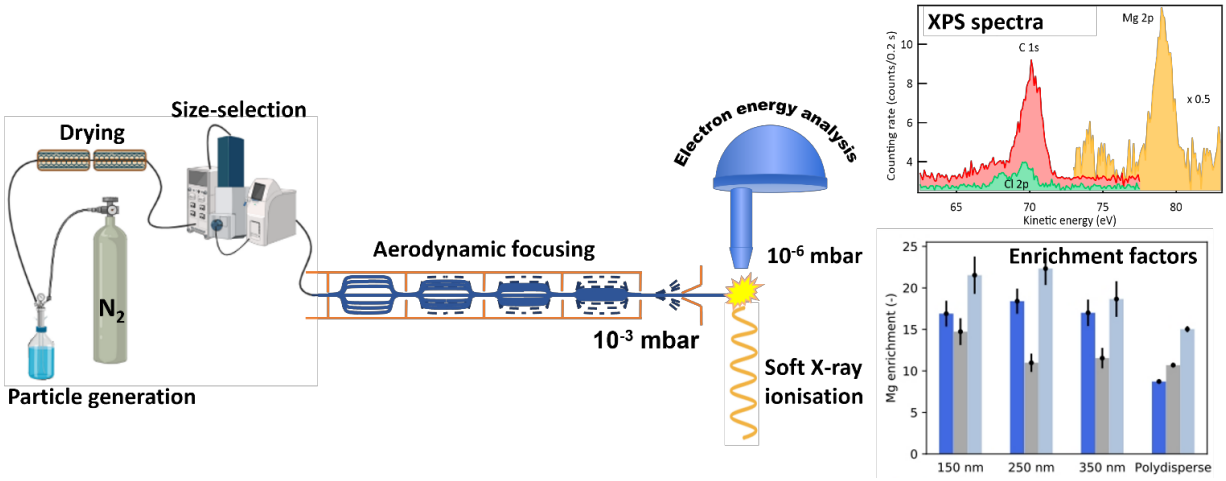

Figure 1 A schematic of the experimental setup and XPS spectra from which the relative enrichment factors are determined. In the enrichment factor histogram, blue bars refer to pure inorganic sea salt particles, and grey and light blue bars to sea salt spiked with phenylalanine and octanoic acid, respectively. Part of the graphics created with BioRender.com.

References

[1] M. Patanen, I. Unger, C.-M. Saak, G. Gopakumar, R. Lexelius, O. Björneholm, M. Salter, P. Zieger, Env. Sci. Atmosph. **2**, 1032 - 1040 (2022).
[2] A. H. Woodcock, J. Meteorol. **10**, 362–371 (1953).
[3] P. K. Quinn, D. B. Collins, V. H. Grassian, K. A. Prather and T. S. Bates, Chem. Rev. **115**, 4383–439 (2015).
[4] D. C. Blanchard, Estuaries **12**, 127–137 (1989).

[*]Corresponding author: minna.patanen@oulu.fi

Additive manufacturing of next generation ceramic fuel cells

Muhammad Imran Asghar[1], Sini Virtanen[1], Axel Savikko[1], Sanaz Zarabi[1], Buse Bilbey[1], Alpi Jokinen[1], Magnus Markkanen[1], Sami Jouttijärvi[1], Anna Maitre[1] and Peter Lund[1]

[1]New Energy Technologies Group, Department of Applied Physics, Aalto University School of Science, P. O. Box 15100, FI-00076 Aalto, Espoo, Finland.

Abstract. A continual improvement in the synthesis of ceramic nanocomposite materials have revolutionized the ceramic fuel cells with improved performance at a lower temperature (400-600°C). With the help of an optimized composition of electrolyte material, a record high ionic conductivity of 0.5 S/cm has been achieved at 550°C. Application of these promising nanomaterials in traditional three-layer fuel cells resulted in ca. 1.1 W/cm^2 at 550°C, whereas application in so called "single-layer cell configuration" resulted in ca. 0.8 W/cm^2 at 550°C. The additive manufacturing including 3D and inkjet printing has the potential to revolutionize the manufacturing of these cells since it can fabricate both the dense and porous structures with good mechanical and electrochemical properties. Inks and pastes of the nanocomposite materials have been developed with appropriate rheological properties and investigated in detail with the dynamic light scattering, viscometer, tensiometry, differential scanning calorimetry and thermal gravimetric analysis. The initial results of our 3D printed nanocomposite electrolytes are very encouraging (0.31 S/cm at 550°C) and we envision a performance of >2W/cm^2 at 550°C with the help of our robust nanocomposite materials and their fabrication through digital printing. A systematic study is conducted with the help of the state-of-art electrochemical, spectroscopic and microscopic characterization techniques to understand the mechanisms in the cells. Furthermore, effect of sintering temperature was systematically studied to optimize the cell performance. Finally, the stability of these cells is investigated to understand the degradation mechanisms in the cells.

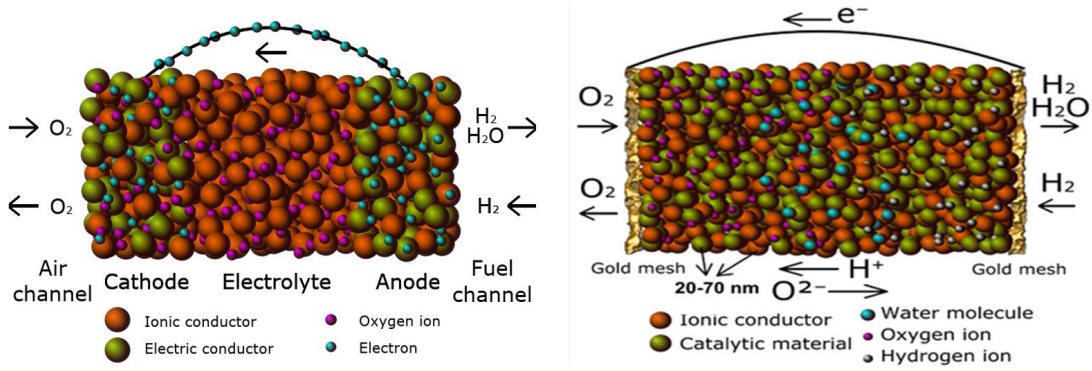

Figure 1: left) Traditional 3-layer ceramic nanocomposite fuel cell, right) Single-layer ceramic fuel cell.

Acknowledgement: This work is supported by Academy of Finland through fellowship projects granted to Dr. Asghar (Grant No. 13329016, 13 352669 and 13322738).

Review of Solid Oxide Electrolysis Cells for H_2 production

Buse Bilbey[*,1], **Muhammad Imran Asghar**[†,1], **Peter D. Lund**[1]

[1] Institute 1, University 1, Address 1
[2] New Energy Technologies Group, Department of Applied Physics, School of Science, Aalto University, P.O. BOX 15100, FI-00076 Aalto, Finland

The global energy demand is rapidly increasing and most of the energy demand is currently fulfilled by fossil fuels. That limited and not renewable energy source causes CO_2 emission by burning hydrocarbons. There are promising renewable energy sources, but the issue is the storage of the energy. Hydrogen has a crucial role as an energy carrier for energy transition [1], and is used as fuel for solid oxide fuel cell(SOFC) technologies. The electrolysis by solid oxide electrolysis cells (SOECs) is one of the green hydrogen production methods and reversible operation of SOFCs system. Green color code for H_2 production refers to water electrolysis. The H_2 and O_2 gases are produced in the SOEC system through the electrolysis processes of the water. SOECs system can also be used for CO production from the electrolysis of CO_2 and syngas ($CO+H_2$) production from the co-electrolysis of the H_2O+CO_2. The SOECs product H_2 is also a fuel for SOFCs, which is the main advantage of using the solid oxide cell (SOC) technology, the system can be used reversibly. The SOCs studies have been focusing mostly on oxide ion conductor-based electrolytes conventionally. In this review, we focused on both the oxide ion conductor solid oxide electrolysis cell (OC-SOEC) and the proton conductor solid oxide electrolysis cell (PC-SOEC) . There is no need to gas separation to produce H_2 at the PC-SOECs while gas separation is required in OC-SOECs. The working principle of the SOECs is shown in figure 1. [2] Another advantage of the PC-SOEC systems is it requires lower operation temperature than OC-SOECs. We summarize materials, fabrication methods, characterization techniques, performances of the cells, stability issues and degradation mechanism for both oxide ion conductor and proton conductor electrolysis cells in this study.

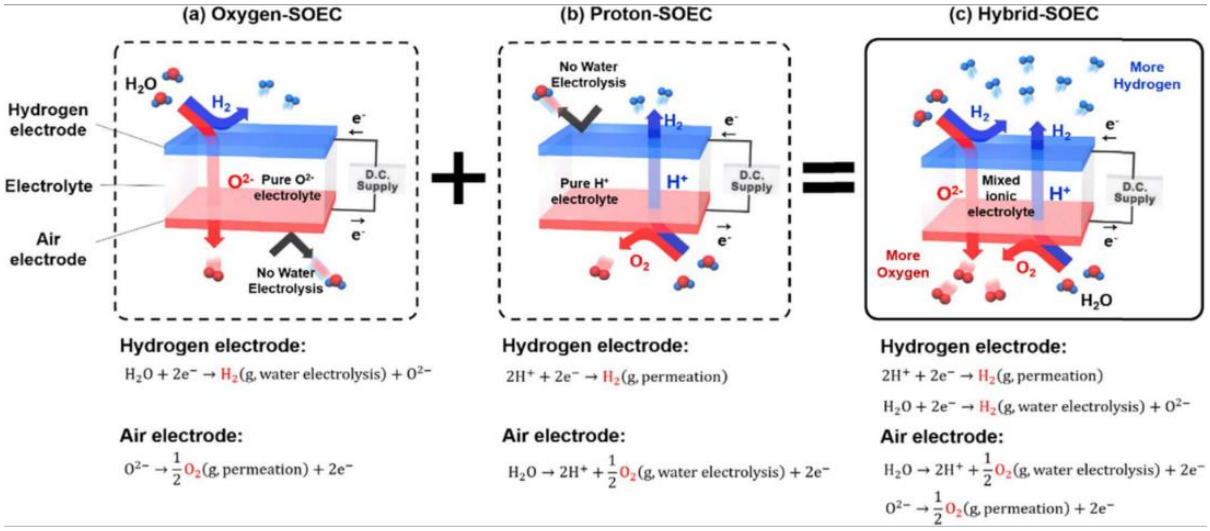

Figure 1. The working principle a) OC-SOEC, b) PC-SOEC and c) Hybrid SOEC system [2]

References

[1] E. Cetinkaya, I. Dincer, G. F. Naterer, Int. J. Hydrog. Energy. **37**(3), 181 (2012).
[2] J. Kim, S. Sengodan, S. Kim, O. Kwon, Y. Bu, G. Kim, Renewable Sustainable Energy Rev. **109**, 606 (2019).

[*]Corresponding author: bbilbey@gtu.edu.tr
[†]Corresponding author: imran.asghar@aalto.fi

Physicochemical characterisation of particle emissions from a modern heavy-duty diesel engine and three different fuels

Kimmo Korhonen[*,1], Panu Karjalainen[1], Petteri Marjanen[1], Vilhelm Berg Malmborg[2], André Olson[3], Ioannis Sadiktsis[2,4], Niina Kuittinen[1], Ukko-Ville Mäkinen[1], Axel C. Eriksson[2], Mari Honkanen[5], Joakim Pagels[2], and Topi Rönkkö[1]

[1]Aerosol Physics Laboratory, Tampere University, P.O. Box 1001, 33014, Tampere, Finland
[2]Ergonomics and Aerosol Technology, Lund University, P.O. Box 118, 22100, Lund, Sweden
[3]Division of Combustion Engines, Lund University, P.O. Box 118, 22100, Lund, Sweden
[4]Department of Materials and Environmental Chemistry, Stockholm University, Svante Arrhenius väg 16C, 10691, Stockholm, Sweden
[5]Tampere Microscopy Center, Tampere University, P.O. Box 692, 33014, Tampere, Finland

Despite ongoing fast electrification of road traffic, especially passenger vehicles, challenges still exist in heavy-duty operation where diesel is the most common engine type used. Due to these challenges, reduction of traffic-originated CO_2 emissions and mitigation of climate change requires not only technological development of diesel engines, but also replacing traditional fossil diesel with renewable options that are already available. This study focuses on physicochemical characterisation of emission particles from a modern heavy-duty diesel engine. The test engine, a Scania DC13, was operated on three different test fuels: fossil diesel, hydrotreated vegetable oil (HVO), and rapeseed methyl ester (RME). From these, the two latter ones are renewable and commonly available as neat biofuel, and in fuel blends used for reduction of net CO_2 emissions from diesel-powered vehicles. The experiments included emission sampling with and without diesel oxidation catalyst.

The instrumentation applied in the experiments comprised a variety of online and offline methods. The online measurements included particle total number concentration with a particle size magnifier, particle size distributions with a fast particle analyser and two scanning mobility particle sizer systems. Black carbon (BC) mass concentration was measured with an aethalometer, and chemical composition of particles with a soot-particle aerosol mass spectrometer (SP-AMS). The offline analyses included filter sampling measurements for organic chemical composition, reactive oxygen species, and organic carbon/elemental carbon ratio. In addition, particle imaging and elemental analyses were performed using (scanning) transmission electron microscopy together with electron dispersive spectroscopy (S/TEM-EDS).

The chemical composition from the SP-AMS measurements showed that all diesel emission particles studied were dominated by organic compounds. In a few cases, we observed higher BC emissions from HVO combustion, in comparison to the other two test fuels. According to the TEM studies, we observed that the soot particles from diesel combustion exhibit complex agglomerated morphologies (Figure 1), regardless of the test fuel used.

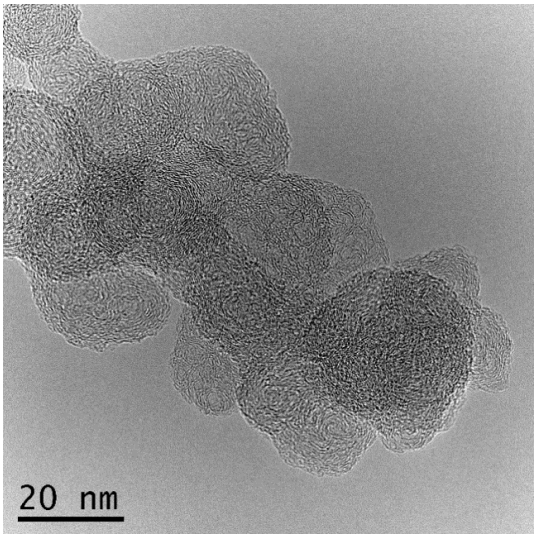

Figure 1: A TEM image of an emission soot agglomerate from RME combustion.

Acknowledgements

This study was a part of Black Carbon Footprint project, funded by Business Finland, participating companies, and municipalities involved. Funding has also been acquired from the Swedish Research Council for Sustainable Development (Formas, grant numbers: 2018-00475 and 2021-02010). The TEM work made use of Tampere Microscopy Center facilities at Tampere University.

[*]Corresponding and presenting author: Kimmo.korhonen@tuni.fi

Climate Digital Twin – a pre-exascale climate information system to support decision making

Jenni Kontkanen*[1], Mario Acosta[2], Pierre-Antoine Bretonnière[2], Miguel Castrillo[2], Paolo Davini[3], Francisco Doblas-Reyes[2,4], Barbara Früh[5], Jost von Hardenberg[6], Thomas Jung[7], Heikki Järvinen[8], Jan Keller[5], Daniel Klocke[9], Outi Sievi-Korte[1], Sami Niemelä[10], Bjorn Stevens[9], Stephan Thober[11], Pekka Manninen[1]

[1] CSC – IT Center for Science, Espoo, Finland
[2] Barcelona Supercomputing Centre, Barcelona, Spain
[3] ISAC-CNR – Institute of Atmospheric Sciences and Climate, Consiglio Nazionale delle Ricerche, Torino, Italy
[4] Institució Catalana de Recerca i Estudis Avançats, Barcelona, Spain
[5] DWD – Deutscher Wetterdienst, Offenbach Germany
[6] Politecnico di Torino, Torino, Italy
[7] Alfred Wegener Institute Helmholtz Center for Polar and Marine Research, Bremerhaven, Germany
[8] University of Helsinki. Helsinki, Finland
[9] MPI-M – Max Planck Institute for Meteorology, Hamburg, Germany
[10] Finnish Meteorological Institute, Helsinki, Finland
[11] Helmholtz Centre for Environmental Research, Leipzig, Germany

Climate change is expected to have far reaching impacts on human and natural systems during the 21st century. To support policy decisions on climate change adaptation and mitigation, there is a need for developing new types of climate information systems that can provide timely information on regional and local impacts of climate change. The European Commission's Destination Earth programme aims towards this by developing high precision digital twins (DT) of the Earth. We present here the overview of one of the two first priority DTs, Climate Change Adaptation DT. The Climate DT will encompass a pre-exascale climate information system that can be used to guide climate change adaptation efforts.

The Climate DT harnesses two different kilometer-scale Earth-system models (ESMs), ICON and IFS-FESOM/NEMO. The Climate DT introduces the idea of a generic state vector (GSV), which is evolved by the ESMs and streamed to applications. This enables the ESMs to work at an unprecedented scale (multi-decadal simulations on 5 km or finer global meshes) and thus improves the fidelity of the information the models provide as well as its relevance for the users. Use cases from different impact sectors are implemented within Climate DT as applications that operate on the streamed GSV. The Climate DT will explore five use cases which will provide information on (1) wind energy supply and demand, (2) wildfire risk and emissions (3) river flows, (4) hydrometeorological extreme events, and (5) heat stress in urban environments. Additional applications operating on the GSV include a quality assessment and uncertainty quantification framework, used for monitoring and evaluation of the GSV. The Climate DT will be deployed on two EuroHPC pre-exascale computing systems: LUMI that is currently in operation in Kajaani, Finland, and Mare Nostrum 5 that will be available during 2023 in Barcelona, Spain.

The Climate DT is developed as a joint effort of 13 European organizations led by CSC – IT Center for Science, under a contract granted by European Centre for Medium-Range Weather Forecasts (ECMWF). The Finnish scientific community has a strong representation in the team developing Climate DT – in addition to CSC leading the project, Finnish Meteorological Institute and University of Helsinki are part of the consortium delivering the Climate DT.

*Corresponding author: jenni.kontkanen@csc.fi

Creating a computational database for CO_2 to methanol conversion

Prajwal Pisal[1], Ondřej Krejčí[*,1], Patrick Rinke[1]
[1] Department of Applied Physics, School of Science, Aalto University, Espoo, Finland

The search for new and better catalysts is one of key research directions in material science, as heterogeneous catalysis is essential in conversion of CO_2 to fuel in the closed loop carbon cycle. Advanced computational tools, big data and machine learning facilitate faster searches in much larger materials space. Still, machine learning predictions depend not only on the chosen model, but also, and more crucially, on the quality and volume of available data.

In this work, we make use of an already existing infrastructure, the Open Catalysts Project that hosts the Open Catalyst Dataset (OCD) [1]. OCD contains the results of many millions of density functional theory (DFT) calculations for adsorption geometries and energies of small molecules on various types of substrates including various metal alloys and oxides. To gain better insight into CO_2 conversion, we have adjusted the OCD workflow to add new data to OCD: i) we start from new materials from the Materials Project [2], ii) identify the most stable surface facets, and iii) end with computing the adsorption energies for CO_2, reaction intermediates (H_xCO_y), and water on these materials, as it is illustrated in Figure 1. The identification of relevant surfaces is important for reducing the computational cost and filtering out data, that is not relevant for subsequent statistical analysis and machine learning predictions of the new materials. The adsorption energies are calculating with the revised Perdew-Burke-Ernzerhof (RPBE) [3] exchange correlation functional. We will present results of our tests on the OCD workflow setup, like the dependence of the energy cut-off, and the geometry creating libraries (ASE [4] and pymatgen [5]) on the surface energies and adsorption energies and geometries. The calculated CO_2 adsorption energies can be easily connected to the reactivity and thus to the reaction yield. Conversely, correlations of the water adsorption energy could help us reduce the water poisoning of the catalysts. The data created with our workflow will form the basis of our active learning loop for catalyst discovery.

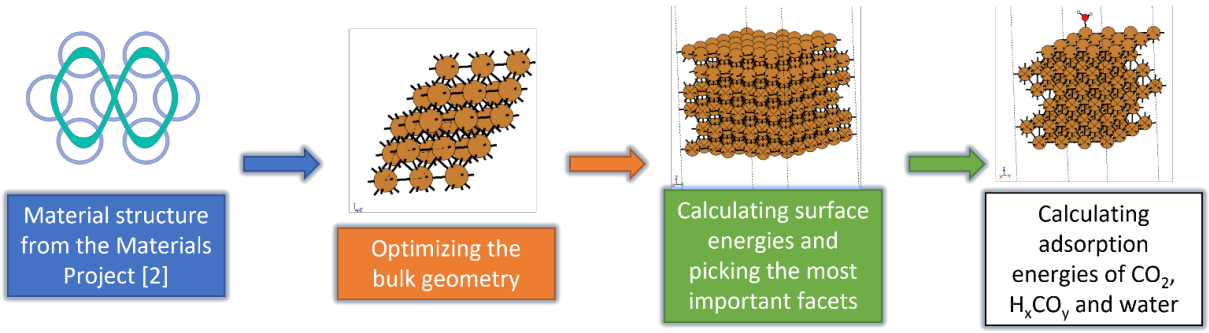

Figure 1: The current workflow used for creation of the dataset

References:

[1] L. Chanussot et al. ACS Catal. **11**, 6059-6072 (2021); R. Tran et al. arXiv 2206.08917 (2022); https://opencatalystproject.org/.
[2] https://materialsproject.org/.
[3] B. Hammer, L. B. Hansen, J. K. Nørskov, Phys. Rev. B **59**, 7413 (1999).
[4] A. H. Larsen at al. J. Phys.: Condens. Matter Vol. **29**, 273002 (2017); https://wiki.fysik.dtu.dk/ase/.
[5] R. Tran et al. Sci. Data **3**, 160080 (2016); https://pymatgen.org/.

*Corresponding author: ondrej.krejci@aalto.fi

Estimating lung deposited surface area of ambient fine particles in different urban environments in Finland

Teemu Lepistö[†,*,1], Luis M.F. Barreira[2], Henna Lintusaari[1], Jarkko V. Niemi[3], Hilkka Timonen[2], Pasi Jalava[4], Sanna Saarikoski[2], Topi Rönkkö[1]

[1]Aerosol Physics Laboratory, Faculty of Engineering and Natural Sciences, Tampere University, Tampere, 33014, Finland
[2]Atmospheric Composition Research, Finnish Meteorological Institute, Helsinki, 00101, Finland
[3]Helsinki Region Environmental Services Authority HSY, Helsinki, 00066, Finland
[4]Inhalation Toxicology Laboratory, University of Eastern Finland, Kuopio, 70211, Finland

Air pollution is one of the leading causes for premature deaths world-wide. Especially ambient fine particles have been strongly associated with the premature deaths, e.g., 10.2 million per year [1]. The health effects of fine particles are usually linked to PM2.5, which is mass concentration of particles smaller than 2.5 µm. PM2.5 is also the most commonly measured metric for fine particles even though it may not be the most ideal metric in terms of health effects. For example, the association between PM2.5 and the premature deaths depends notably on the country [2]. Also, most urban air fine particles are ultrafine (< 100 nm) and, therefore, too small to contribute to PM2.5 which emphasizes the role of larger (> 500 nm) particles that are mainly originated from regional aerosol and distant pollution sources. Furthermore, PM2.5 does not give information about particle chemistry which affects the toxicity of inhaled particles. The limitations of PM2.5 are especially relevant in Finland, where regional background air is mainly clean and, therefore, the measured PM2.5 concentrations are low. Despite the low PM2.5, local emission sources, e.g., traffic, can cause significant ultrafine particle emissions. Thus, the health effects of fine particle pollution in Finland may be underestimated as the commonly used PM2.5 ignores the effects of ultrafine particles.

In our study, we measured lung-deposited surface area (LDSA) of fine particles in different urban areas in Finland. LDSA estimates surface area of particles entering lung alveoli (Fig. 1a) where the interaction between pulmonary circulation and respiration occurs. Particles entering the alveoli can therefore end up in the blood and organs. The studied pollution sources cover traffic, residential wood combustion, airport, harbour, and industrial sites. The measurements were done in Helsinki, Raahe, and Tampere in 2019 – 2021 by utilizing Aerosol and Trace-gas Mobile Laboratory (ATMo-Lab).

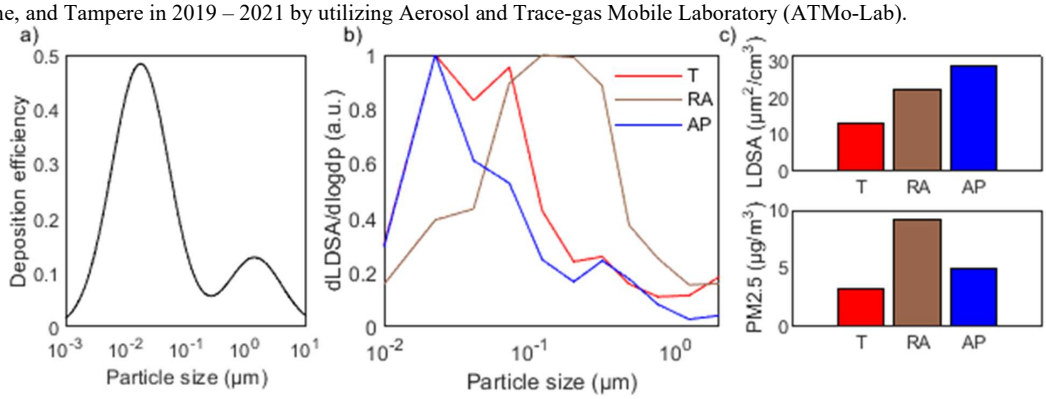

Figure 1: a) Particle deposition in the lung alveoli as a function of particle size (according to [3]), b) examples of normalized LDSA size distributions and c) average LDSA and PM2.5 concentrations near traffic (T), airport (AP) and in a residential area (RA) (according to [4]).

It was found that the characteristics and sizes of particles causing LDSA depended significantly on urban environment. Near airport, particles smaller than 50 nm dominated the LDSA, whereas, in residential areas, LDSA was mainly caused by 100 – 500 nm particles (Fig. 1b). In general, LDSA was mainly caused by ultrafine particles. The varying particle sizes affect the connection between LDSA and PM2.5, and an equal increase in PM2.5 may indicate multiple times higher LDSA in different environments. Also, high LDSA was measured near an airport where PM2.5 was notably lower than in residential site (Fig. 1c). Thus, significant fraction of total LDSA can be caused by ultrafine particles even their role in PM2.5 is almost negligible.

The results indicate major differences in the health effects caused by inhaled particles as the varying particle sizes suggest different composition and toxicity. Also, the potential health effects caused by particle lung deposition are not well seen with PM2.5 as ultrafine particles may cause significant lung exposure. Thus, local emission sources may potentially cause major health effects in Finland even though they are not well observed with the commonly measured PM2.5. In all, the results show the need to monitor ultrafine particles in various urban sites to understand the potential health effects of local pollution sources.

We acknowledge funding by TUBE (EU funded) and BC Footprint (Business Finland, companies and municipalities) projects.

References

[1] Vohra, et al. 2021. Environmental Research, 195. DOI: 10.1016/j.envres.2021.110754
[2] Li, et al. 2019. Nature, 570 (7762), pp. 437-439. DOI: 10.1038/d41586-019-01960-7
[3] ICRP 1994. Human respiratory tract model for radiological protection. Vol. 66. 24.
[4] Lepistö, et al. submitted (10/2022) to Environmental Research.

[*]Corresponding author: teemu.lepisto@tuni.fi
[†]Presenting author: teemu.lepisto@tuni.fi

Sub-23 nm particles dominate non-volatile particle number concentrations in a busy street canyon

Henna Lintusaari[*,1], Heino Kuuluvainen[1], Joonas Vanhanen[2], Harri Portin[3], Anssi Järvinen[1,4], Laura Salo[1], Jarkko V. Niemi[3], Topi Rönkkö[1]

[1] Aerosol Physics Laboratory, Physics Unit, Tampere University, Korkeakoulunkatu 3, 33720, Tampere, Finland
[2] Airmodus Oy, Erik Palménin aukio 1, 00560 Helsinki, Finland
[3] Helsinki Region Environmental Services Authority, Ilmalantori 1, 00240, Helsinki, Finland
[4] Emission Control and Sustainable Fuels, VTT Technical Research Centre of Finland, Tietotie 4C, 02150, Espoo, Finland

Urban cities are typical settings where high air pollution levels meet high population density. As one significant air quality factor, fine particulate matter ($PM_{2.5}$) has been estimated to cause 3.3 million premature deaths world-wide annually [1]. Health impacts depend on particle characteristics, including size, shape, and chemistry [2]. In contrast to larger-size particles, ultrafine particles (< 100 nm) efficiently deposit in all regions of the respiratory track and access to the blood circulation resulting in distribution throughout the body [3].

The European Union legislation limiting the number of particles (PN) emitted by vehicles follows Particle Measurement Program (PMP) protocol that takes into account only solid particles above 23 nm in size [4]. Even though sub-23 nm emission particles are in many cases known to be volatile, also non-volatile particles have been observed in this size range [5]. This has led to further study, technical development, and discussion on the feasibility to regulate PN emissions in the sub-23 nm region down to at least 10 nm. Following, EU has recently proposed size range ≥ 10 nm as a new basis for PN emission regulation in Euro 7 standard entering into force in 2025 [6]. All the same, it has been found that the size range of traffic emitted particles extends even down to 1-3 nm [7].

In this study, we extended the study of sub-23 nm particles to urban air quality monitoring in a relatively busy street canyon. We used a Condensation Particle Counter Battery (CPC Battery) to measure simultaneously the number concentration of particles larger than 1.4 nm, 3 nm, 10 nm, and 23 nm with one second time resolution for one month in May 2018. Volatile compounds were removed in the sampling line using a combination of a hot and a cold ejector diluter. Finally, we determined typical number concentrations of non-volatile particles, size ranges in which non-volatile particles are found, emission factors, and proportions of non-volatile particles in ambient air.

As a result, we found out that the non-volatile PN concentrations in all size ranges corresponded to the morning rush hour and, interestingly, typical driving hours for heavy-duty vehicles taking place after morning commuter traffic (Figure 1). Relatively examined, the concentration of non-volatile particles larger than 10 nm and larger than 3 nm were on average 2.3 and 4.6 times higher than the concentration of non-volatile particles larger than 23 nm, respectively. Thus, the number of non-volatile particles in size ranges below 23 nm clearly exceeds the number of particles larger than 23 nm.

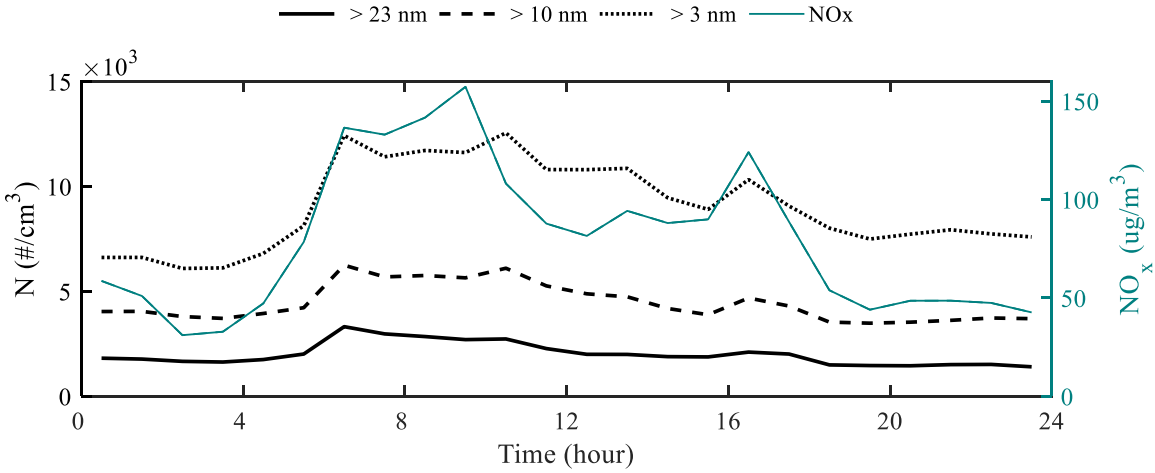

Figure 1. Diurnal variation of non-volatile particle number concentrations (N) and NOx on weekdays of the measurement period.

References

[1] J. Lelieveld, J. S. Evans, M. Fnais, D. Giannadaki, A. Pozzer, Nature 525, 367–371 (2015).
[2] C. Buzea, I. I. Pacheco, K. Robbie, Biointerphases 2, MR17-71 (2007).
[3] G. Oberdörster, E. Oberdörster, J. Oberdörster, Environ. Health Perspect. 113, 823–839 (2005).
[4] B. Giechaskiel, U. Manfredi, G. Martini, SAE Int. J. Fuels Lubr. 7(3) (2014).
[5] D. Kittelson, W. Watts, J. Johnson, Journal of Aerosol Science, 37(8), 913 – 930 (2006).
[6] European Commission, Document 52022PC0586 (2022).
[7] T. Rönkkö, et al., PNAS, 114(29), 7549-7554 (2017).

[*]Corresponding author: henna.lintusaari@tuni.fi

Feasibility study of CO_2 satellite retrievals over snow for supporting the upcoming Copernicus Anthropogenic CO_2 Monitoring Mission

Hannakaisa Lindqvist[*1], **Antti Mikkonen**[†1], **Jouni Peltoniemi** [2], **Ella Kivimäki** [1], **Rigel Kivi** [1], **Janne Hakkarainen** [1], **Maria Gritsevich** [2], **Antonio di Noia** [3], **Leif Vogel** [4], **Hartmut Boesch** [5], **Johanna Tamminen** [1], **Yasjka Meijer** [6],

1. Finnish Meteorological Institute, Helsinki, Finland
2. Finnish Geospatial Research Institute, Kirkkonummi, Finland
3. University of Leicester, Leicester, United Kingdom
4. WoePal GmbH, Trierweiler-Sirzenich, Germany
5. University of Bremen, Bremen, Germany
6. European Space Agency, Noordwijk, Netherlands

Space-based observations of greenhouse gases (GHG) are currently revolutionizing carbon cycle science and our ability to globally monitor anthropogenic GHG emissions. With the European fleet of upcoming high-priority Copernicus satellites named Anthropogenic CO_2 Monitoring Mission (CO2M), satellite observations will soon contribute to the Monitoring and Verification Support system that supports the goals of the Paris Agreement by verifying national emission reductions. This means that GHG satellite observations will directly contribute to carbon policymaking already in this decade – a significant and demanding responsibility for the entire scientific field.

In the Arctic and boreal regions, continuous monitoring can inform on the expanding anthropogenic activities and their emissions as well as the changing carbon cycle and natural carbon dioxide (CO_2) uptake in the changing climate. However, in the high latitudes there are numerous properties making observations difficult: large solar zenith angles (SZA), frequent cloud cover and snow.

Observing the carbon dioxide from a satellite is an ill-posed inverse problem. The solar radiation reflected from the Earth surface is measured by a satellite instrument and the amount of CO_2 is inferred from the attenuation. Parameters, such as other absorbing atmospheric gases, scattering from air molecules and aerosols and the reflectivity of the Earth's surface also need to be estimated.

ESA SNOWITE is a European Space Agency funded project where we carry out the first systematic and dedicated feasibility study of CO_2 retrievals over snow. We present a measurement-based snow reflectance model for use in simulated CO2M radiances and potential improvements in retrievals. In parallel, we analysed existing high-latitude retrievals of CO_2 from the Orbiting Carbon Observatory -2 (OCO-2) and identified the snow-covered satellite pixels using auxiliary snow coverage data.

The main results of the study are as follows. All the examined snow surface types had a strong forward reflecting peak, which result in an increased signal when observing the Sun's specular reflection (glint mode) compared to nadir observation mode. Simulated retrieval results established that observations in glint mode result in decreased uncertainty of XCO_2 with larger SZA over snow-covered surface. However, the glint observation mode is more susceptible for meteorological uncertainties, and the assumption of wrong snow type causes noticable biases in the XCO_2 results. The existing OCO-2 XCO_2 retrievals over snow are considerably biased, which indicates the need for more sophisticated snow modeling.

[*]Corresponding author: hannakaisa.lindqvist@fmi.fi
[†]Corresponding author: antti.mikkonen@fmi.fi

Magnetic Quincke Rollers with Tunable Single-Particle Dynamics and Collective States

R. Reyes Garza[1†], N. Kyriakopoulos[1], Z. M. Cenev[1], C. Rigoni[1], J. V. I. Timonen[1*]
[1]Department of Applied Physics, Aalto University School of Science, P.O. Box 15100, Espoo FI-02150, Finland.

Quincke rollers are electrohydrodynamically driven active particles that in recent years have attracted attention due to their complex emergent behaviour. At the Active Matter group at Aalto University, we have recently achieved to produce a system of **magnetic Quincke rollers,** and a **control mechanism based on the microparticles' anisotropic magnetic response** that does not involve control over the field that drives the self-propulsion [1]. In our approach, we apply an external magnetic field to control the direction of motion. This field is independent from the electric field that provides the energy for the active motion.

Briefly, our system consists of silica microparticles (d~21 μm) doped with iron oxide confined in a quasi-two-dimensional geometry between two parallel ITO-coated glass electrodes and suspended in an AOT-dodecane mixture. Using an external electric field, $\boldsymbol{E_o}$, perpendicular to the confining plane, the particles are set into active motion while a magnetic field, $\boldsymbol{B}$, is also being applied to the sample (Fig. 1A). The magnetic field provides the rollers with an effective magnetic dipole moment, $\boldsymbol{\mu}$. **The additional dipole-dipole interaction between the rollers leads to several new tunable collective states, such as active chains** (Fig. 1B).

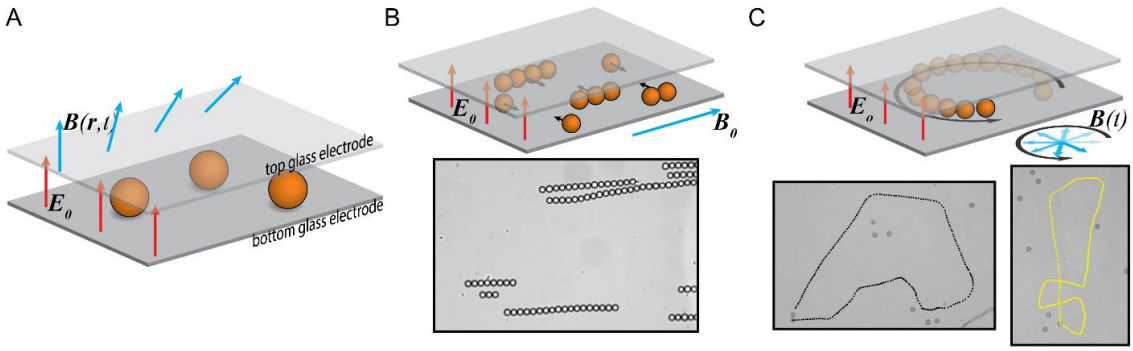

Figure 1 A) Scheme of a colloidal suspension of magnetic Quincke rollers confined between two ITO coated glass electrodes in a uniform external electric field, $\boldsymbol{E_o}$, and tunable magnetic field, $\boldsymbol{B(r,t)}$. B) Scheme and experimental snapshots of Magnetic Quincke rollers under the influence of a uniform magnetic field, $\boldsymbol{B_o}$. The magnetic dipole-dipole interaction between the particles give rise to the formation of active chains. C) Scheme and experimental snapshots of the programmable trajectory of a single magnetic Quincke roller using a uniform magnetic field with tunable orientation, $\boldsymbol{B(t)}$. In the experiment, the particle was operated to follow the contour of Aalto University´s logo.

The particles' anisotropic $\boldsymbol{\mu}$ constrains their motion through a magnetic torque, $\boldsymbol{\tau = \mu \times B}$. As thoroughly described in [1], the competition between the electrohydrodynamic active rolling and the constraining magnetic torque produces an effective rolling perpendicular to the $\boldsymbol{B}$ field lines. **We used this property to achieve control over the single-particle behavior and perform programmable trajectories** (Fig. 1C).

We highlight that this magnetic torque-based control mechanism can be, in principle, used on other types of active microparticles, provided they display magnetic properties. Thus, we foresee that **the current method can be optimized and used as a tool for basic and applied active matter research**.

References

[1] R. Reyes Garza *et al*. Magnetic Quincke Rollers with Tunable Single-Particle Dynamics and Collective States. (in preparation).

*Corresponding author: jaakko.timonen@aalto.fi
†Presenting author: ricardo.reyesgarza@aalto.fi

Controlling the collective behavior of non-magnetic microalgae using tunable magnetic traps

F. Sohrabi[†,1], C. Rigoni[1], M. Jenu[1], G. Beaune[1], N. Kyriakopoulos[1], and J. V. I Timonen[*,1]
[1]Department of Applied Physics, Aalto University

Unicellular microalga *Chlamydomonas reinhardtii* (CR) is a model system for biological active matter, as it is swimming with non-conservative dissipative forces by moving its flagella in breaststroke fashion. Larger populations of CR exhibit collective behavior that includes sets of signaling and cooperation between cells, the mechanism for which is not thoroughly understood. Investigating the interactions and function of collective behavior in microorganisms such as CR is challenging, due to their rapid movements. Therefore, confining CR could provide a mean to analyze their behavior. Here we show the possibility to confine CR using magnetic traps, by taking advantage of negative magnetophoresis. This is obtained by placing non-magnetic CR in a magnetic medium consisting of biocompatible PEG-functionalized superparamagnetic nanoparticles. Upon application of a magnetic fields on non-magnetic CR cells in a paramagnetic environment, they experience an effective force towards the decreasing magnetic potential energy. We developed near-harmonic magnetic potential energy landscapes and observed phase transitions from gas-like state to liquid-like state when the trap is strong, and studied the interaction of trapped cells. We show experimentally that magnetic manipulation is a promising technique for investigating the behavior of CR cells, that provides insight towards better understanding of their interactions with each other and controlling their collective function.

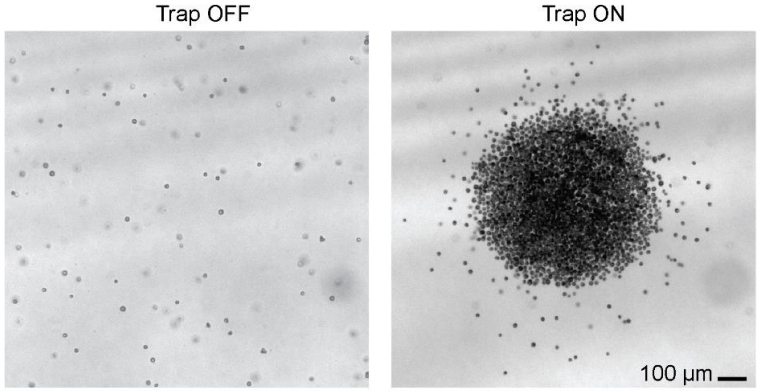

Figure 1: Example of magnetically trapped microalgae CR.

[*]Corresponding author: jaakko.timonen@aalto.fi
[†]Corresponding author: fereshteh.sohrabi@aalto.fi

Controlling polyelectrolyte interactions by ion size, shape and valency

Hossein Vahid [1,2,3], **Alberto Scacchi** [1,2,3], **Maria Sammalkorpi*** [2,3,4], **Tapio Ala-Nissila**†[1,5,6]

1. Department of Applied Physics, Aalto University, P.O. Box 11000, FI-00076 Aalto, Finland
2. Department of Chemistry and Materials Science, Aalto University, P.O. Box 16100, FI-00076 Aalto, Finland
3. Academy of Finland Center of Excellence in Life-Inspired Hybrid Materials (LIBER), Aalto University, P.O. Box 16100, FI-00076 Aalto, Finland
4. Department of Bioproducts and Biosystems, Aalto University, P.O. Box 16100, FI-00076 Aalto, Finland
5. Quantum Technology Finland Center of Excellence, Department of Applied Physics, Aalto University, P.O. Box 11000, FI-00076 Aalto, Finland
6. Interdisciplinary Centre for Mathematical Modelling and Department of Mathematical Sciences, Loughborough University, Loughborough, Leicestershire LE11 3TU, UK

Many charged macromolecules, including polyelectrolytes (PEs) such as DNA can be approximated by a model of a rigid charged rod. In aqueous solutions, the rodlike charged macromolecules are surrounded by their counterions, and often also by excess salt. Salt is a standard means of controlling interactions between charged macromolecules and their assemblies in biological and polymer materials. Experiments and theory have demonstrated that multivalent ions can induce correlations that result in an effective charge reversal of a PE, consequently an attractive interaction between like-charged PEs. However, steric effects and shape anisotropy are not straightforward to capture by purely theoretical approaches. Consequently, we consider here, by means of coarse-grained molecular dynamics simulations, the effects of ion size, shape, and (non-)Coulombic contributions, on PE interactions.

To gain a better understanding of the interactions between highly-charged PE rods in the presence of ions of different kinds, we have mapped the ion-size [1], aspect-ratio [2], valency [2] and salt-concentration [1, 3] dependence of the ionic distributions and PE interactions at room temperature. Furthermore, we have investigated the orientation of spheroidal ions in systems composed of single and double rod-like PEs. Following electrostatics, we observe that spheroidal ions have a tendency to align along the PE backbone, and this tendency is enhanced by increasing their aspect ratio. Moreover, anisotropic ions induce an unexpected ion-valency and shape-anisotropy-dependent orientational ordering in the ionic double layer. The response affects ion condensation on the PE, PE charge reversal, and PE-PE interactions. For example, Fig. 1(b) shows that attraction between two parallel PEs is enhanced with trivalent ions as compared to divalent ones.

Our findings demonstrate that by considering the shape and steric effects alongside concentration and valency, one can systematically tune the type, range, and strength of the PE-PE interactions. We have also demonstrated that the binding energy between PEs (the amount of energy required to separate two PEs from their equilibrium distance to infinity) is greater when their counterions are spherical and with higher valency (more charged) than when they are elongated and with lower valency (less charged). In summary, our work provides guidelines for regulating PE self-assembly in aqueous solutions by salt specificity.

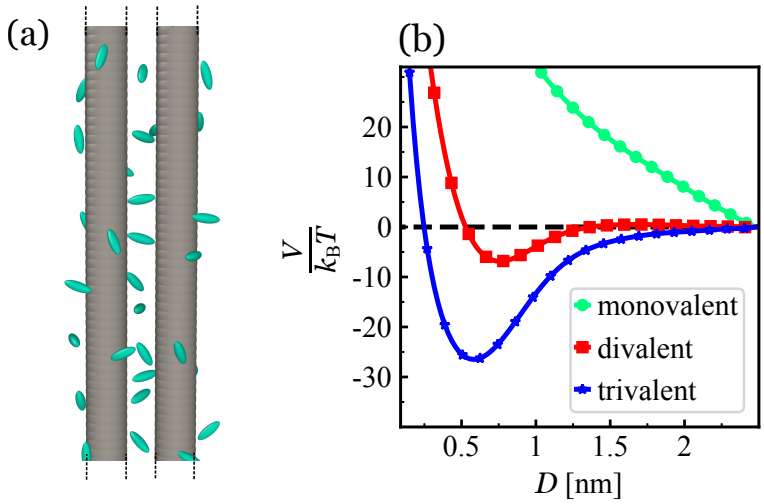

Fig. 1: (a) A schematic representation of the two coarse-grained PE rods with spheroidal counterions. (b) Qualitative presentation of the dimensionless potential of mean force $V/(k_B T)$ between two parallel PEs as a function of the surface-to-surface PE distance D, where the counterions are either monovalent (green curve), divalent (red curve), or trivalent (blue curve). Here k_B denotes the Boltzmann constant and T the temperature of the system.

References

[1] **H. Vahid**, A. Scacchi, X. Yang, T. Ala-Nissila, and M. Sammalkorpi, "Modified Poisson–Boltzmann theory for polyelectrolytes in monovalent salt solutions with finite-size ions", *The Journal of Chemical Physics*, **156** (21), 214906 (2022).

[2] **H. Vahid**, A. Scacchi, M. Sammalkorpi, and T. Ala-Nissila, "Interactions between polyelectrolytes mediated by ordering and orientation of multivalent non-spherical ions in salt solutions", *arXiv preprint*, arXiv:2210.03492 (2022).

[3] X. Yang, A. Scacchi, **H. Vahid**, M. Sammalkorpi, and T. Ala-Nissila. "Interaction between two polyelectrolytes in monovalent aqueous salt solutions", *Physical Chemistry Chemical Physics*, **24** (35), 21112 (2022).

*Corresponding author: maria.sammalkorpi@aalto.fi
†Corresponding author: tapio.ala-nissila@aalto.fi

Explorations to the auroral zone: All-sky-camera project in Lapland – “Revot”

J. Rautiainen[*1], **E. Tanskanen** [1], **J. Similä** [1], **T. Raita** [1], **T. Ulich** [1], **J. Jussila** [2]
1. Sodankylä Geophysical Observatory, University of Oulu, Pentti Kaiteran katu 1, FI-90014 Oulu, Finland
2. Boreal Vision, Torpantie 63 FI-90230 Oulu, Finland

Auroras are spectacular phenomena created in the Sun-Earth interaction as the plasma of the solar wind and the plasma captivated by the geomagnetic field travel along the geomagnetic field lines and collide with atoms and molecules in the atmosphere of Earth. If the collisions are energetic enough, the precipitating electrons and protons can excite the atoms and molecules that upon de-excitation emit photons with wavelengths unique to the energies spend in the excitation processes. The auroras are mainly observed in the oval shaped regions surrounding the geomagnetic poles while depending on the solar activity the regions where the aurora are likely to appear are called auroral zones.

To explore the auroral zone in northern Finland we are launching a ground-based coherent network of all-sky-camera (ASC) units called “SKY-i”s. The SKY-i network monitors the near-Earth space plasma processes over Lapland in the visible wavelength regime by imaging the sky in 2 second intervals. The SKY-i utilises commercial fisheye lens with field-of-view of 185°, low-noise and high dynamical range CMOS detector and single board computer Raspberry Pi into relatively low cost, flexible, and compact concept, that with our setup outputs 5 million images annually per unit and is capable of sub-second interval imaging.

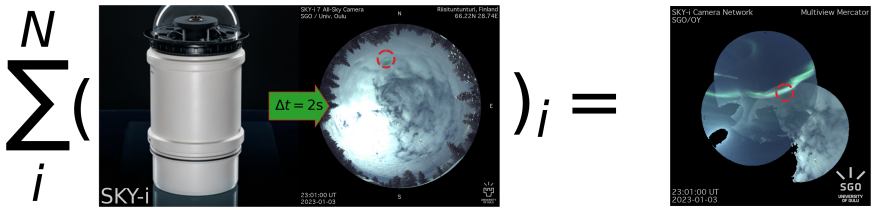

Fig. 1: Some data losses can be compensated by the peer instruments in the SKY-i Network. In the rightmost image we have projected the images to mercator coordinate system by assuming altitude of $h = 110$ km for the aurora, revealing structures obscured by the cloud coverage in the image on the left.

With the cost efficient concept of SKY-i, we are able span dense SKY-i network in the auroral zone that allows the spatial distribution and statistics of the aurora to be observed at multiple locations. Overlapping areas in the simultaneous multi-location imaging can for instance be used to study the temporal height structure of the aurora. The locations of SKY-i are, nevertheless, sparse enough and the number of imagers high enough that the local weather conditions and the possible instrument downtimes should pose a minimal impact on the visual awareness and the continuity of the observations on geomagnetic conditions over Lapland. This way we are able to provide scientifically and publicly meaningful, continuous record of visible aurora statistics over Lapland as well as information on the location specific observational conditions. The continuously accumulated data can be used in the development of aurora predictions and real time monitoring, the amount of the data solely provides a ground for a variety of image recognition tasks as data-storage optimisation using modern deep learning techniques and amass of valuable outreach material will be produced during the project.

Depending on the solar activity and the local weather conditions the aurora are not always observable by the instruments which can result in unnecessary storage costs by increasing the need of storage space or clean up activities. On a cloudy night with full moon the instruments might produce significant amount of unusable data and manually inspecting millions of images one-by-one would take a paramount number of working hours and storing such data is not optimal. A traditional way to deal with this is by building an image over the observing night that encapsulates time and activity along the latitude direction, called keograms, that tells us whether activity was observed during the night. Alternatively machine learning can be used to identify images and the irrelevant images such as those with full cloud coverage can be discarded. We will discuss this problem and the possibilities using modern convolutional neural network (CNN) called ResNet50 to perform data-storage optimisation and share our findings on this topic.

One of the project goals is to act as outreach for the public and particularly promote the science and technical work-prospectives in Lapland and in Sodankylä Geophysical Observatory (University of Oulu). To combine the educational and science scenes, we collaborate with different education facilities in Lapland. We engage the facilities in the technical and science aspects of the project while simultaneously provide amass of data with products of high educational value and utility in the scientific research on auroras. To enhance the public aspect of the project we will display products from the SKY-i network on a dedicated webpage.

The people in the northern regions are accustomed in observing the visible aurora “Northern Lights”, representing the most brightest displays of the aurora that are also a major attraction for the traveling industry. People are curious in nature and while we often question our observations of Nature, the means and options available to work with the intriguing topics might be obscure for the prospective young scientists and can be made clearer by the scientific community. Providing comprehensive knowledge and material on the different science and technical aspects involved in the study of the aurora or other fields in physics is especially important when we breach the cap between the science and public scenes and those prospective youngsters that dream to work in any field of science and perhaps do so in the arctics with attitude.

[*]Corresponding author: joona.rautiainen@oulu.fi

Hybrid-Vlasov simulation of soft X-ray emissions at the Earth's dayside magnetospheric boundaries

Maxime Grandin[*1], **Hyunju K. Connor**[2], **Sanni Hoilijoki**[1], **Markus Battarbee**[1], **Yann Pfau-Kempf**[1], **Urs Ganse**[1], **Konstantinos Papadakis**[1], **Minna Palmroth**[1,3]

1. Department of Physics, University of Helsinki, Helsinki, Finland
2. NASA Goddard Space Flight Center, Greenbelt, MD, 20771, USA
3. Space and Earth Observation Centre, Finnish Meteorological Institute, Helsinki, Finland

Solar wind charge exchange produces emissions in the soft X-ray energy range which can enable the study of near-Earth space regions such as the magnetopause, the magnetosheath and the polar cusps by remote sensing techniques. The Solar wind–Magnetosphere–Ionosphere Link Explorer (SMILE) and Lunar Environment heliospheric X-ray Imager (LEXI) missions aim to obtain soft X-ray images of near-Earth space thanks to their Soft X-ray Imager (SXI) instruments. While earlier modeling works have already simulated soft X-ray images as might be obtained by SMILE SXI during its mission, the numerical models used so far are all based on the magnetohydrodynamics description of the space plasma. To investigate the possible signatures of ion-kinetic-scale processes in soft X-ray images, we use for the first time a global hybrid-Vlasov simulation of the geospace from the Vlasiator model. The simulation is driven by fast and tenuous solar wind conditions and purely southward interplanetary magnetic field. We first produce global X-ray images of the dayside near-Earth space by placing a virtual imaging satellite at two different locations, providing meridional and equatorial views. We then analyze regional features present in the images and show that they correspond to signatures in soft X-ray emissions of mirror-mode wave structures in the magnetosheath and flux transfer events (FTEs) at the magnetopause. Our results suggest that, although the time scales associated with the motion of those transient phenomena will likely be significantly smaller than the integration time of the SMILE and LEXI imagers, mirror-mode structures and FTEs can cumulatively produce detectable signatures in the soft X-ray images. For instance, a local increase by 30% in the proton density at the dayside magnetopause resulting from the transit of multiple FTEs leads to a 12% enhancement in the line-of-sight- and time-integrated soft X-ray emissivity originating from this region. Likewise, a proton density increase by 14% in the magnetosheath associated with mirror-mode structures can result in an enhancement in the soft X-ray signal by 4%. These are likely conservative estimates, given that the solar wind conditions used in the Vlasiator run can be expected to generate weaker soft X-ray emissions than the more common denser solar wind. These results will contribute to the preparatory work for the SMILE and LEXI missions by providing the community with quantitative estimates of the effects of small-scale, transient phenomena occurring on the dayside.

[*]Corresponding author: maxime.grandin@helsinki.fi

Hale cycle in solar hemispheric radio flux and sunspots: Evidence for a northward shifted relic field

Kalevi Mursula[*,1]
[1] Space Climate Group, Space Physics and Astronomy Research Unit, University of Oulu, Oulu, Finland

Solar and heliospheric parameters occasionally depict notable differences between the northern and southern solar hemisphere. Although the hemispheric asymmetries of some heliospheric parameters vary systematically with the 22-year solar magnetic (Hale) cycle, this has not been found to be commonly valid for solar parameters. Also, no verified physical mechanism exists which can explain possible systematic hemispheric asymmetries.

We here use a novel method of high heliolatitudinal vantage points to increase the fraction of one hemisphere in solar 10.7 cm radio fluxes and sunspot numbers. We study if solar radio fluxes and sunspot numbers, the two most fundamental solar parameters, depict systematic, possibly mutually similar patterns in their hemispheric activities during the last 75 years. We use three different sets of time intervals with increasing mean heliographic latitude and calculate corresponding hemispheric high-latitude radio fluxes and sunspot numbers. We also normalise the high-latitude fluxes by yearly means in order to study the variation of fluxes in the two hemispheres over the whole 75-year time interval.

We find that cycle maximum radio fluxes and sunspot numbers in each odd solar cycle (19, 21, 23) are larger at northern than southern high latitudes, while maximum fluxes and numbers in all even cycles (18, 20, 22 24) are larger at southern than northern latitudes. This alternation indicates a new form of very similar 22-year Hale-cycle related variation in both parameters. Hemispheric differences at cycle maxima are, on an average, 15% for radio flux and 23% for sunspot numbers. The differences are largest during cycle 19 and smallest in cycle 24. Normalised radio fluxes depict a dominant Hale cycle variation in both hemispheres, with an opposite phase and overall amplitude of about 5% in the north and 4% in the south. Thus, there is systematic Hale-cycle alternation in hemispheric dominance of magnetic flux emergence.

Hemispheric asymmetry varying at the Hale cycle can be explained if there is a northward directed relic magnetic field (constant magnetic field from the time of the birth of the solar system), which is also slightly shifted northward. Then, in odd cycles, the northern hemisphere is enhanced more than the southern hemisphere, while in even cycles, the northern hemisphere is reduced more than the southern hemisphere, establishing the observed hemispheric alternation. The temporal change of asymmetry during the 7 cycles can be explained if the relic shift oscillates at the 210-year Suess/deVries period. Oscillating relic field would also give a physical cause to this periodicity. We note that earlier evidence exists from long-term geomagnetic activity, which relates the Suess/deVries cycle to solar hemispheric asymmetry. In this interpretation, the 80-100-year Gleissberg cycle of solar activity is explained as one off-equator excursion of the relic, forming one half of the 210-year relic shift oscillation cycle.
We also discuss how a relic field in the Sun can offer interesting possibilities for century-scale forecasting of solar activity.

[*]Corresponding author: kalevi.mursula@oulu.fi

The escape and propagation electron beams following acceleration by solar shock waves

Diana E. Morosan, Jens Pomoell, Anshu Kumari, Rami Vainio, Emilia Kilpua

Energetic particle populations are ubiquitous throughout the Universe and often found to be accelerated by astrophysical shocks. One of the most prominent sources for energetic particles in our solar system are huge eruptions of magnetised plasma from the Sun called coronal mass ejections (CMEs), which usually drive shocks that accelerate charged particles up to relativistic energies. Accelerated electrons, in particular, can be observed either remotely as low-frequency radio bursts or in situ as large particle fluxes detected by spacecraft. However, it is currently unknown where electrons accelerated in the early phases of such eruptions propagate and when they escape the solar atmosphere. Here, we report the first results on the acceleration, escape, and propagation directions of electrons during the early evolution of shock waves in the solar corona. The study uses a three-dimensional (3D) representation of the particle acceleration locations in relation to the overlying coronal magnetic field, location of solar eruptions, magneto-hydrodynamic (MHD) models of the solar corona, and radio spectropolarimetric and imaging observations from ground-based observatories. The synthesis of these methods allow us to combine in a unique manner the temporal evolution of the location of radio sources to the location of the expanding low coronal shocks. We show convincing evidence that the first radio emission in the CME eruption comes from electrons that initially propagate in regions of low Alfvén speeds and along closed magnetic field lines and most likely escape later during the eruption.

Engineered structural relaxation of amorphous phase-change memory materials via the application of electric fields

Konstantinos Konstantinou[*,1], **Jaakko Akola**[1,2], **Stephen R. Elliott**[3]

[1] Computational Physics Laboratory, Tampere University, Tampere FI-33014, Finland
[2] Department of Physics, Norwegian University of Science and Technology (NTNU), Trondheim NO-7491, Norway
[3] Physical and Theoretical Chemistry Laboratory, University of Oxford, Oxford OX1 3QZ, United Kingdom

Structural relaxation of amorphous phase-change memory materials has been attributed to defect-electronic-state annihilation from the band gap, leading to a time-dependent drift in the electrical resistance (see Figure 1), which hinders the development of multi-level memory devices with increased data-storage density. In this computational study, the target is to achieve an understanding, at the atomistic level, of the effect that an applied electric field has on localized mid-gap defect electronic states in the glassy state of phase-change memory materials. We utilize the Berry-phase formalism, within the modern theory of polarization, to apply external, finite, periodic electric fields to glassy models of $Ge_2Sb_2Te_5$ (GST), combined with density-functional-theory calculations of the electronic structure using non-local exchange-correlation functionals. The results highlight that the application of a sufficiently high external electric field removes mid-gap defect states from the band gap of the glass and transforms them into electronic states lying at the bottom of the conduction band, due to the electric-field-induced atomic relaxations of the amorphous structure [1]. A lowering of the coordination number of Ge atoms seem to be essential for delocalization of conduction-band-edge states. We illustrate how the weak, polarizable bonds in 5-coordinated Ge atoms can break under the application of electric fields, resulting in an engineered (i.e. without thermal annealing) annihilation of mid-gap defect states from the band gap of the glassy GST model [1]. In that way, we demonstrate a materials-engineering concept for the structural relaxation of glassy phase-change memory materials by controlling the localized states in the band gap of the chalcogenide glass. We also show that spontaneous electron and hole trapping at the intrinsic near-linear triatomic environments from the axial bonds in “see-saw” 4-coordinated or 5-coordinated configurations within the amorphous GST network results in weakening and potential breaking of the axial bonds in these defective octahedral-like sites [2].

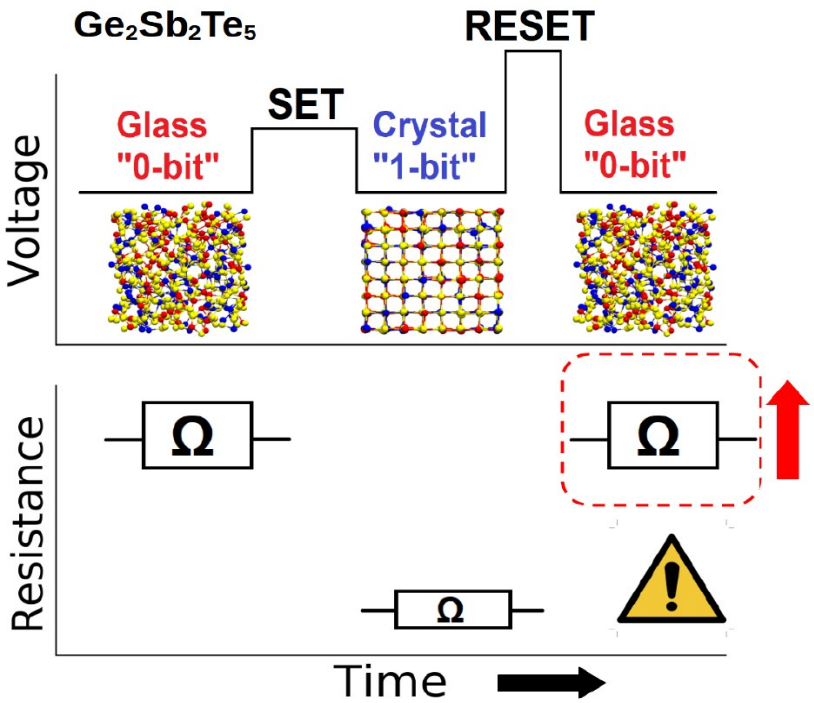

Figure 1: Operation principle of a phase-change memory and the time-dependent resistance "drift" issue.

References

[1] K. Konstantinou, F. C. Mocanu, J. Akola, S. R. Elliott, Acta Mater. **223**, 117465 (2022).
[2] K. Konstantinou, S. R. Elliott, J. Akola, J. Mater. Chem. C **10**, 6744 (2022).

*Corresponding author: konstantinos.konstantinou@tuni.fi

Designing a ferroelectric valley valve with a van der Waals heterostructure

Adolfo O. Fumega[*1], **Jose L. Lado**[† 1]
1. Department of Applied Physics, Aalto University, 02150 Espoo, Finland

Layered van der Waals materials are a fruitful platform to engineer emergent physical phenomena. In particular, AB-stacking bilayer graphene, when subjected to an external electric gate, develops a topological gap leading to a valley-Hall insulating behavior. In this talk we show that this phenomenology can be found in a van der Waals ferroelectric heterostructure [1]. We demonstrate that AB bilayer graphene encapsulated in ferroelectric $MoTe_2$ acts as a valley valve that displays a switchable built-in topological gap, leading to ferroelectrically driven topological channels. Using a combination of *ab initio* calculations and low energy models, we show that the ferroelectric order of $MoTe_2$ allows the control of the gap opening in bilayer graphene and leads to topological channels between different ferroelectric domains. Moreover, we analyze the effect of the natural moiré modulation between $MoTe_2$ and graphene layers on the topological modes. We show that the edge states are robust against moiré modulations of the ferroelectrically-induced electric potential. Therefore, these results put forward ferroelectric/graphene heterostructures as versatile platforms to engineer switchable built-in topological channels without requiring an external electric bias.

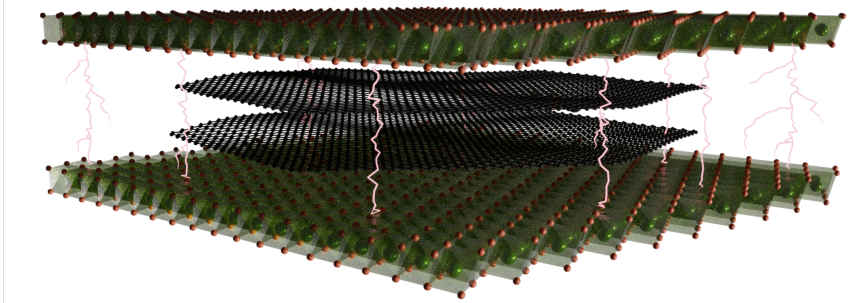

Fig. 1: Ferroelectric valley valve made with a van der Waals heterostructure.

References

[1] Adolfo O. Fumega, Jose L. Lado, Nanoscale, 2023, Advance Article (2023)

[*]Corresponding author: adolfo.oterofumega@aalto.fi
[†]Corresponding author: jose.lado@aalto.fi

Free Energy of Small Water Clusters from Nucleation Experiments and Quantum Simulations

Ali Afzalifar*[,1], George C. Shields[2], Vance R. Fowler[2], Robin H. A. Ras[1,3]

[1] Department of Applied Physics, Aalto University School of Science, Puumiehenkuja 2, 02150 Espoo, P.O. Box 15100, Aalto FI-00076, Finland

[2] Department of Chemistry, Furman University, Greenville, South Carolina 29613, United States

[3] Department of Bioproducts and Biosystems, Aalto University School of Chemical Engineering, P.O. Box 16000, Aalto FI-00076, Finland

Among all substances, water is of utmost significance due to its central role in numerous scientific and technological processes and in general the process of life on earth. A better understanding of water properties and mysterious behavior is inextricably depended on our accuracy in calculation of free energy of water clusters. In addition, nucleation is the initial and the major step in a first order phase transition, and thus it is a topic of special interest to fields as diverse as atmospheric science, nanotechnology, transformation of metals and cosmology.

Our work first addresses several general (and specific to water) defects of classical nucleation theory (CNT), after that it unravels and quantifies the free energy of small water clusters, and also identify the departure trend of the actual cluster energies from the values predicted by the macroscopic approach. It is shown that at higher temperatures (~250 K<T) the ratio of the extracted free energy to CNT's prediction behaves non-monotonically by varying the size of water cluster: toward the smallest clusters this ratio continuously falls to almost zero for monomers, while as cluster size increases this ratio goes above one and exhibits at least one maximum before returning toward one when the cluster becomes large enough. For lower temperatures (T<~250 K), this ratio is always below one for almost all experiments, though it rises as the cluster size increases. In addition, a state-of-the-art quantum mechanics model is used to compute free energies of water clusters containing 2-14 molecules. The simulation results also show a behavior change according to temperature, but for temperatures below and above ~298 K. Two different model chemistries, DLPNO-CCSD(T)/CBS//ωB97xD/6-31++G** and G3, are compared with one another and the values for formation of the water dimer derived from the second virial coefficient in the virial equation of state for water. [1]

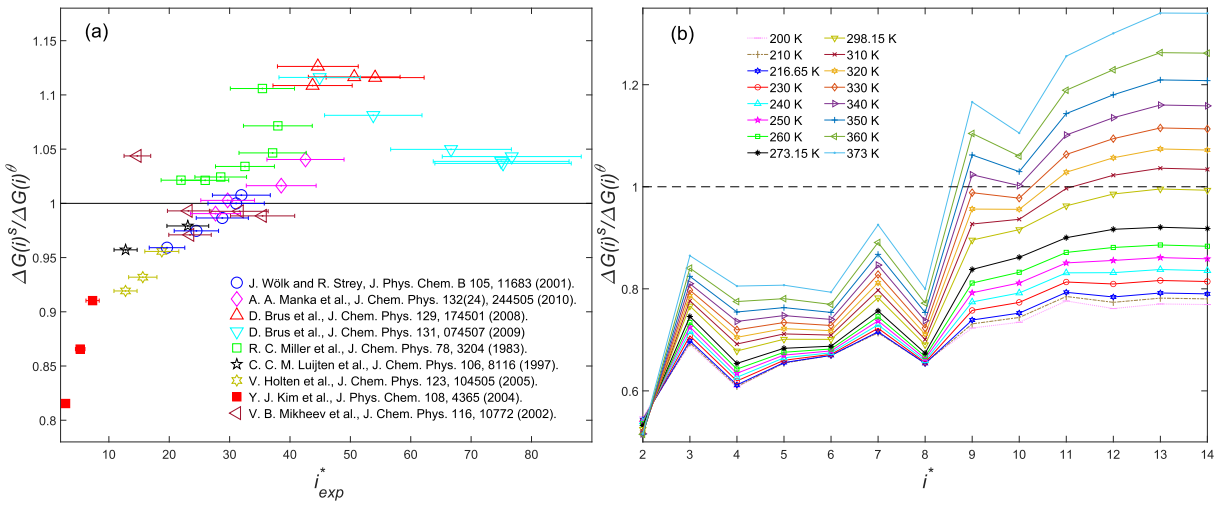

Figure 1. (a) Comparison of the actual cluster free energy which is extracted from the nucleation experiments $\Delta G^s(i)$ with CNT's prediction $\Delta G^\theta(i)$, The error bars indicate the uncertainty in the cluster size. (b) Comparison of the cluster free energy $\Delta G^s(i)$ from quantum mechanical simulation with CNT's prediction $\Delta G^\theta(i)$. Data from [1].

References

[1] A. Afzalifar, G. C. Shields, V. R. Fowler and R. H. A. Ras, J. Phys. Chem. Lett. **13**(34), 8038–8046 (2022).

*Corresponding author: ali.afzalifar@aalto.fi

Biased surface diffusion in Cu under electric field gradient captured in electrostatics–molecular dynamics

Jyri Kimari[*1], **Ye Wang** [2], **Andreas Kyritsakis** [2], **Veronika Zadin** [2], **Flyura Djurabekova** [1]
1. Helsinki Institute of Physics and Department of Physics, University of Helsinki, PO Box 43 (Pietari Kalmin katu 2), FI-00014 Helsinki, Finland
2. Institute of Technology, University of Tartu, Nooruse 1, 50411 Tartu, Estonia

Vacuum-facing metal surfaces are exposed to strong electric fields in many devices, such as particle accelerators, free-electron lasers and fusion reactors. Under sufficiently strong fields, current can arc through the vacuum, disrupting and damaging these devices. Despite decades of research, the precise mechanisms of the vacuum arc breakdowns are still unknown. The interplay of different physical phenomena, as well as their associated length and time scales, pose numerous challenges in experiments and simulations.

In our earlier study [1], we showed in simulation that a runaway process of Cu nanotip melting and evaporation can produce the necessary material for the formation of plasma that will conduct the electric current through vacuum. An open question remains of the growth of these nanotips, as well as their sharpening for enhanced field emission and heating.

A proposed mechanism of biased diffusion under electric field gradient could contribute to mass transfer toward the extremities of any initial protrusions or roughness on the surface [2]. In the study at hand [3], we simulated Cu surface diffusion directly in these conditions using molecular dynamics (MD). The implementation of the electric field involves concurrently solving the Laplace equation of macroscopic electric field on a finite elements method (FEM) mesh that follows the discrete atomic system and extends beyond it—see Fig. 1 for illustration. Furthermore, we extended the time scale of our simulations by the collective variable -driven hyperdynamics (CVHD) method for better collection of diffusion statistics. Finally, we estimated the surface polarization characteristics from our MD simulations, and compared them directly to density functional theory (DFT) calculations, finding good agreement.

In this talk, we will discuss the evidence we found for biased diffusion on Cu surface, as well as the practicalities of coupling CVHD-accelerated MD with FEM.

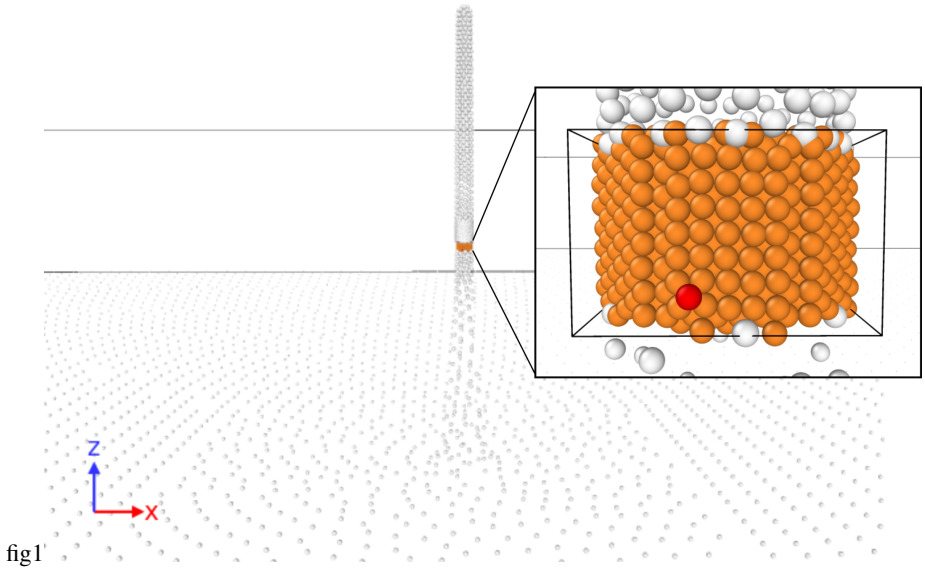

fig1'

Fig. 1: Extended simulation system, with the MD region (zoomed into in the inset) in copper color and the static, continuous FEM extension in gray.

References

[1] Kyritsakis, Andreas, et al. *Journal of Physics D: Applied Physics* **51**.22 (2018): 225203.
[2] Kyritsakis, Andreas, et al. *Physical Review B* **99**.20 (2019): 205418.
[3] Kimari, Jyri, et al. *Journal of Physics D: Applied Physics* **55**.46 (2022): 465302.

*Corresponding author: jyri.kimari@helsinki.fi

Predicting elastic and plastic properties of small iron polycrystals by machine learning

Marcin Mińkowski[*1], **Lasse Laurson** [1]
1. Computation Physics Laboratory, Tampere University

Deformation of crystalline materials is an interesting example of complex system behaviour. Small samples typically exhibit a stochastic-like, irregular response to externally applied stresses, manifested as significant sample-to-sample variation in their mechanical properties. In this work the predictability of the sample-dependent shear moduli and yield stresses of a large set of small cube-shaped iron polycrystals generated by Voronoi tesselation, is studied by combining molecular dynamics simulations and machine learning. Training a convolutional neural network to infer the mapping between the initial polycrystalline structure of the samples and features of the ensuing stress-strain curves reveals that the shear modulus can be predicted better than the yield stress. The results are discussed in the context of the sensitivity of the system's response to small perturbations of its initial state.

[*]Corresponding author: marcin.minkowski@tuni.fi

Avalanches and rate effects in strain-controlled discrete dislocation plasticity of Al single crystals

David Kurunczi-Papp[*1], **Lasse Laurson** [1]
1. Tampere University, P.O. Box 692, FI-33014 Tampere, Finland

Three-dimensional discrete dislocation dynamics simulations are used to study strain-controlled plastic deformation of face-centered cubic aluminium single crystals. After describing the rate and size dependence of the average stress-strain curves, we study the power-law distributed strain bursts, and find a universal power-law exponent $\tau \approx 1.0$ for all imposed strain rates. This is then followed by the characterization of the average avalanche shapes which reveals the two key physical regimes in dislocation plasticity dominant at small and large strain rates, respectively. We discuss the dependence on the loading rate and compare our observations with previous studies of strain-controlled two-dimensional systems of discrete dislocations as well as of quasistatic stress-controlled loading of aluminium single crystals.

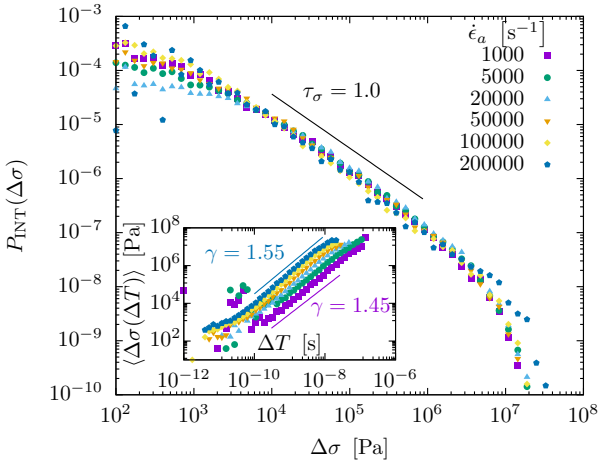

Fig. 1: Integrated distributions of the stress drop magnitudes $P_{\mathrm{INT}}(\Delta\sigma)$ for varying imposed strain rates $\dot{\varepsilon}_a$, described by the power law $\tau_\sigma = 1.00 \pm 0.05$ with exponential cutoff. The inset shows the scaling of the average stress drop magnitude $\langle\Delta\sigma(T)\rangle$ with the event duration T, where the lines correspond to the power laws obtained for the lowest and highest $\dot{\varepsilon}_a$, respectively. (b) Integrated distributions of the strain increments $P_{\mathrm{INT}}(\Delta\varepsilon)$ for varying imposed strain rates $\dot{\varepsilon}_a$, described by the power law $\tau_\varepsilon = 1.0 \pm 0.05$ with exponential cutoff. The inset shows the corresponding event duration distributions (proportional to the strain increments) obeying the same power law $\tau_T = 1.0 \pm 0.05$.

References

[1] D. Kurunczi-Papp, L. Laurson, Phys. Rev. Materials **7** 013605 (2023)
[2] D. Kurunczi-Papp, L. Laurson, Phys. Rev. E **104** 025008 (2021)

*Corresponding author: david.kurunczi-papp@tuni.fi

Asymmetric Roughness of Elastic Interfaces at the Depinning Threshold

Esko Toivonen*, **Matti Molkkari, Esa Räsänen, Lasse Laurson**
Computational Physics Laboratory, Tampere University, P.O. Box 692, FI-33014 Tampere, Finland

The dynamical response of elastic interfaces in random media to external driving forces is a universal phenomenon exhibited by e.g. contact lines in wetting, ferromagnetic domain walls and crack fronts in disordered solids. This response arises from the interaction between elasticity, external driving forces and the quenched disorder. A characteristic property of these interfaces is their roughness, which is typically understood to be described by a single roughness exponent ζ. The roughness exponent is usually obtained from the scaling of the mean squared interface width or that of a correlation function.

We show that at the depinning threshold, due to symmetry breaking caused by the direction of the driving force, elastic interfaces exhibit *asymmetric* roughness [1]. This asymmetry is present in interfaces with local, long-range and mean-field elasticity, and it is manifested as a skewed distribution of the local interface heights. Furthermore, this asymmetric roughness can be quantified by using detrended fluctuation analysis [2] with a scale-dependent segmentation method to compute a spectrum of local, segment-level scaling exponents [3]. This analysis reveals an approximately linear relationship between the local scaling exponents and the difference of the segment height from the mean interface height.

Our observations challenge the prevailing viewpoint that interface roughness can be characterized by a single roughness exponent. Instead, one needs to consider the whole spectrum of local scaling exponents. Our results are relevant for related problems such as the scaling properties of anisotropic fracture surfaces and call for experimental studies of diverse systems ranging from domain walls in ferromagnetic thin films to planar crack fronts.

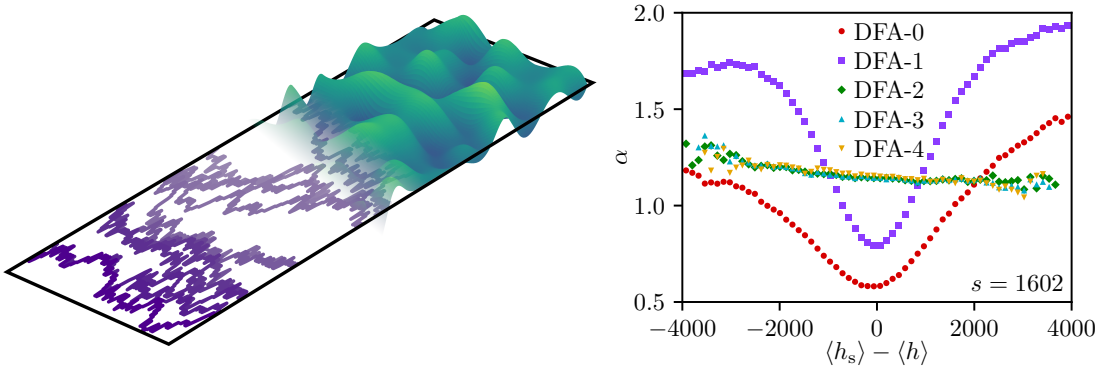

Fig. 1: Left: Schematic picture of sequential rough interface configurations moving in a random potential. Right: Convergence of the scaling exponent α of detrended fluctuation analysis (DFA) up to the 4th order (DFA-4) for the segments of the quenched Edwards-Wilkinson equation describing an elastic string with local elasticity [1]. The observed linear dependence of α on $\langle h_s \rangle - \langle h \rangle$, i.e., the difference of the mean segment height and the mean interface height, is a manifestation of asymmetric roughness.

References

[1] E. Toivonen, M. Molkkari, E. Räsänen, L. Laurson, Physical Review Letters **129**, 175701 (2022).
[2] C.-K. Peng, S. V. Buldyrev, S. Havlin, M. Simons, H. E. Stanley, A. L. Goldberger, Physical Review E **49**, 1685 (1994).
[3] M. Molkkari, G. Angelotti, T. Emig, E. Räsänen, Scientific Reports **10**, 13627 (2020).

*Corresponding author: esko.toivonen@tuni.fi

Topological transitions of lasing states in a plasmonic hexamer array

Grazia Salerno[1], Rebecca Heilmann[1,*], Kristian Arjas[1], Kerttu Aronen[1], Jani-Petri Martikainen[1], Päivi Törmä[1]
[1] Department of Applied Physics, Aalto University School of Science, P.O Box 15100, Aalto FI-00076, Finland

Metallic nanoparticles interacting with light give rise to plasmonic resonances, which enhance light-matter interaction due to high local field confinement and sensitivity to their environment. If such nanoparticles are arranged in periodic lattices and interact with light, surface lattices resonances (SLRs) are formed, which are dispersive plasmonic-photonic modes. Combined with emitters, such as organic dye molecules, plasmonic lattices emerged as an effective platform for strong light-matter coupling, lasing, and Bose-Einstein condensation.

Bound states in continuum (BICs) are resonant states lying within a continuum of other states, however they are completely decoupled from these. In case of plasmonic lattices, this means that BIC modes are decoupled from free-space radiation and appear as dark states, however by coupling them to leakage channels, they can be observed. Such BICs can be viewed as vortex centres of light polarization, where the polarization winds around the BIC. This polarization vortex can be described by a quantized topological charge, which describes the direction of the winding as well as how many times the polarization winds.

Here, we experimentally observe lasing in a plasmonic lattice from a quasi-BIC with a topological charge q = -2 and demonstrate several topological transitions as a structural parameter of the unit cell is changed [1]. The system we study consists of cylindrical gold nanoparticles arranged in hexamers. Such hexamers belong to a C_6 symmetry class which hosts 12 eigenmodes that can be understood as the irreproducible representations (IR) of this symmetry class. The topological charges of modes corresponding to an IR can be calculated. We find quasi-BIC modes with charges of q = -2, q = -1, and q =1, as well as bright modes with q = 0. In the experiments, we study arrays composed of gold nanoparticle hexamers arranged in a triangular lattice. We vary the size of the hexamers and combine the arrays with organic emitters. Under optical pumping we observe lasing in this system. Arrays with different hexamer sizes show different lasing behaviour. With polarization resolved measurements, we identify lasing modes as quasi-BIC modes and measure their topological charge q. We identify four regimes, where modes with different topological charges lase: we observe lasing in three quasi-BIC modes with charges of q = -2, q = -1, and q = 1, as well as a bright mode (q = 0). Hence, by changing the size of the hexamer, we induce a topological transition of lasing modes with different topological charges.

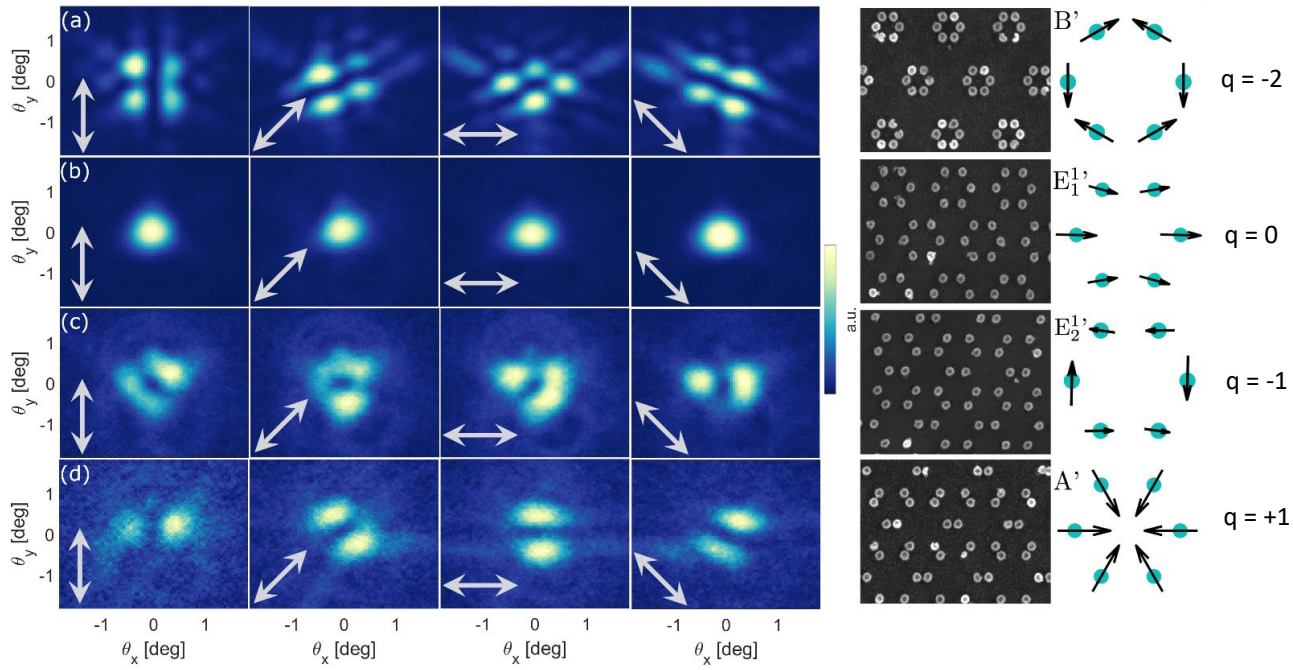

Figure 1: Polarization resolved measurements in K-Space for different regimes. In rows (a)-(d) the hexamer size is gradually increased as shown in the SEM images of the corresponding arrays. The white double-headed arrows depict the orientation of the polarizer. The lasing modes are depicted in the last column, where the arrows correspond to the polarization orientation of each site within the hexamer and q is the topological charge of each lasing mode.

References

[1] G. Salerno, R. Heilmann, K. Arjas, K. Aronen, J. P. Martikainen, P. Törmä, Phys. Rev. Lett. **129**(12),173901 (2022).

*Corresponding author: rebecca.heilmann@aalto.fi

Extended depth of field of an imaging system with an annular aperture

Panu Hildén[*1] **and Andriy Shevchenko**[1]
1. Department of Applied Physics, Aalto University, P.O Box 13500, FI-00076 Aalto, Finland

In optical imaging, there is a trade-off between resolution and depth of field. In order to form a high-resolution image, a lens needs to have a high numerical aperture, due to which even a slight displacement of the object along the optical axis results in a blurred image. This problem can be addressed by a $4f$-type imaging system with an annular aperture in the front focal plane of the second lens, like the one shown in Fig. 1. The aperture acts as a spatial filter, which turns the light from a single point in the object plane into a nearly non-diverging Bessel-like beam [1,2]. Bessel beams can be superposed to form more complicated non-diverging optical fields [3,4], such as the field forming an image. Such images stay sharp independently of the longitudinal coordinate of the object, which makes the depth of field of the system infinite. In a realistic system of this type, non-diverging Bessel-like beams have a certain finite length limiting the depth of field.

We compare the performance of the system with that, in which the annular aperture is replaced with a circular one of the same diameter. Both spatially coherent and incoherent illuminations are considered. Our results show a considerable extension of the depth of field. However, for the image to have a high quality, the illumination must be incoherent. The results presented in this work can be used to design many practical devises with the extended depth of field, such as high-resolution microscopes and optical systems for imaging three-dimensional objects.

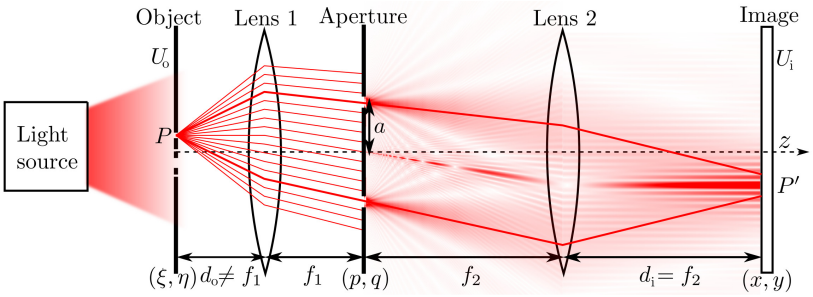

Fig. 1: An imaging system with an extended depth of field. The image is formed by Bessel-like beams owing to the presence of an annular aperture in the common focal plane of the two lenses.

References

[1] W. T. Welford, J. Opt. Soc. Am. **50** 749–753 (1960)
[2] D. McGloin, K. Dholakia, Contemp. Phys. **46** 15–28 (2005)
[3] Z. Bouchal, Opt. Lett. **27** 1376–1378 (2002)
[4] A. Zannotti, C. Denz, M. A. Alonso, M. R. Dennis, Nat. Commun. **11** 3597 (2020)

[*]Corresponding author: panu.hilden@aalto.fi

High efficiency interface between multi-mode and single-mode fibers

Oussama Korichi*,[1], Markus Hiekkamäki[1], Robert Fickler[1]
[1] Photonics Laboratory, Physics Unit, Tampere University, Tampere FI-33720, Finland

Multi-mode fibers (MMFs) and Single-mode fibers (SMFs) are widely used in communication networks. Choosing to utilize either MMFs or SMFs depends on many factors. For example, in applications that require distances of up to 500 m - 600 m, MMFs are the practical choice in terms of cost. Beyond that, SMFs are necessary due to the modal dispersion in MMFs [1]. Hence, a device for efficiently interfacing an MMF with an SMF would be beneficial to optical telecommunication.
In this work, we present a method capable of achieving this interfacing between an MMF and SMF using a multi-plane light conversion scheme (MPLC) [2]. With our method, and discluding the losses in the optics, we demonstrate that only 3 phase modulations, realized with a single spatial light modulator (SLM), are enough to achieve MMF to SMF coupling efficiencies of 72% ± 7%, 60% ± 3%, 50% ± 4%, and 29% ± 3%, using MMFs with core diameters of 8.2 µm, 25 µm, 50 µm, and 200 µm, respectively [3].

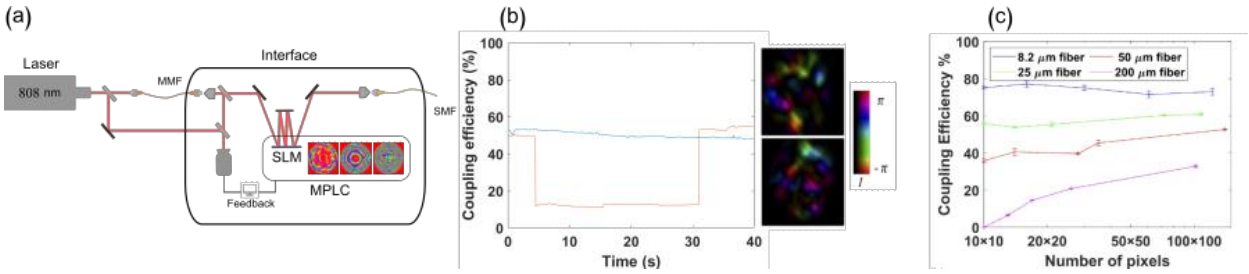

Figure 1. (a) Sketch of the experimental setup for efficient MMF to SMF coupling using an MPLC implemented with an SLM. (b) Stability of coupling efficiency without disturbance (blue) and automatized correction after a strong deformation of an MMF with 50 µm of core diameter (orange). The insets on the right correspond to the complex field before (top) and after (bottom) the deformations (c) SMF coupling efficiencies after the mode transformation for different MMFs and resolutions of the reconstructed field. The efficiencies were obtained from 200 measurements within a time frame of 35 s, and the errors represent the standard deviation of the respective dataset.

In the experiment, we sent an 808 nm laser into an MMF and reconstructed the complex transverse amplitude of the output field from an interferogram [4]. We then used the obtained full field information to calculate the 3 phase modulation screens with wavefront matching [5]. The phase screens were optimized to transform the multi-mode field into the Eigenmode of the SMF, i.e., a Gaussian beam profile, such that the transformed field could be efficiently coupled into the SMF (see Fig. 1a). Because the field reconstruction, as well as the mode transformation, were updated in real-time, the obtained coupling efficiency remains stable even if the output field of the MMF changes entirely, for example through strong deformation of the fiber (see Fig. 1b). We additionally tested the influence of the resolutions for both, the field reconstruction and MPLC system, on the coupling efficiencies. The former is shown in Fig. 1c. For both, we found that commercially available devices with increased speed and efficiency, such as wavefront sensors and deformable mirrors, would be enough to establish an MMF to SMF interface working in the kHz-regime.
The presented method might find applications in optical telecommunication and could also be adapted to correct for very strong atmospheric disturbances in long distance free space communication.

References

[1] Peng, G. D. (Ed.). (2019). Handbook of Optical Fibers. Berlin/Heidelberg, Germany: Springer.
[2] Labroille, G., Denolle, B., Jian, P., Genevaux, P., Treps, N., & Morizur, J. F. (2014). Efficient and mode selective spatial mode multiplexer based on multi-plane light conversion. Optics express, 22(13), 15599-15607.
[3] O. Korichi, M. Hiekkamäki, R.Fickler, (2021) High-efficiency interface between multi-mode and single-mode fibers, arXiv:2211.15438
[4] Takeda, M., Ina, H., & Kobayashi, S. (1982). Fourier-transform method of fringe-pattern analysis for computer-based topography and interferometry. J. Opt. Soc. Am. , 72(1), 156-160.
[5] Fontaine, N. K., Ryf, R., Chen, H., Neilson, D. T., Kim, K., & Carpenter, J. (2019). Laguerre-Gaussian mode sorter. Nature communications, 10(1), 1-7.

*Corresponding author: Oussama.korichi@tuni.fi

Live Imaging Alpha Radiation Sources via Radioluminescence in Nitrogen-Flushed Glovebox

Teemu Koivisto[†,1], **Dixon Sajan**[1,2], **Juha Toivonen**[1]
[1] Laboratory of Photonics, Tampere University, 33720 Tampere, Finland
[2] International School of Photonics, CUSAT, 682022 Kerala, India

Traditional methods for detecting alpha radiation are limited by the alpha particles short range of about 4 cm in air. Detectors that rely on direct interaction with alpha particles can be inconvenient and hazardous to operate. This range limitation can be overcome by utilizing the radioluminescent light induced by the alpha particles in air. A review paper by Wu et. al [1] describes several demonstrations for locating alpha sources by imaging the radioluminescent light. However, due to the weakness of the radioluminescence signal, the data integration times have always been in scale of minutes.

In this work, we demonstrate for the first time a method for real-time imaging of the radioluminescence of americium-241 with frame rates down to 1 s under normal room lighting conditions. Rapid radioluminescence imaging in daylight conditions is possible in a N_2 atmosphere with a small concentration of NO. Compared to a normal atmosphere, this has the effect of increasing the conversion efficiency from alpha particles kinetic energy to radioluminescent light significantly. Furthermore, the radioluminescent wavelengths are shifted into the UV-C band, which has minimal background radiation [2]. A highly sensitive scientific camera and an UV-C filter are used to record the radioluminescent light highlighting possible alpha sources. Simultaneously, the scene is recorded with a 3D camera to obtain visible light video of the background with depth information. Utilizing the depth information, the radioluminescence frames can be mapped accurately to the visible light frames revealing the locations of possible alpha sources. An illustration of this method is presented in Figure 1, where an UV-C LED equivalent with approximately a 10 MBq alpha source in N_2 with 2 ppm of NO was imaged with a 1 second exposure time. The imaging capability with americium-241 sources will be included in the presentation. The method for live imaging alpha active materials is targeted to monitor nitrogen-flushed gloveboxes, where hazardous and unknown radioactive materials are handled, increasing the operator's safety and awareness of the materials and their locations.

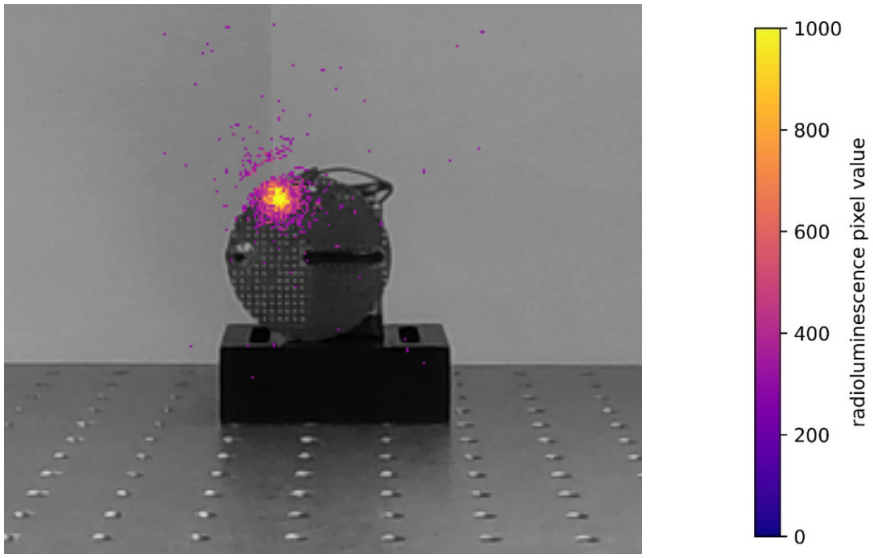

Figure 1. UV-C LED equivalent with approximately a 10 MBq alpha source simultaneously imaged with a scientific camera and a 3D camera revealing the location of the source. An integration time of 1 s is used in the detection allowing live imaging of the source location. The radioluminescence heatmap is drawn exclusively with the pixels greater than a threshold value.

References

[1] Z. Wu, J. Cheng, M. Xu, Q. Wang, A. Yu, Y. Zhang, W. Wen, Y. Wu, Z. Tang, Sensors (Basel) **22**(1), 202 (2021)
[2] T. Kerst, J. Toivonen, Opt. Express **26**, 33764-33771 (2018)

[†]Corresponding author: teemu.koivisto@tuni.fi

Time-varying photonics, relativity, and the arrow of time

Matias Koivurova[*1], **Charles W. Robson**[1], **Marco Ornigotti** [1]
1. Tampere Institute for Advanced Study, Tampere University, 33100 Tampere, Finland
2. Faculty of Engineering and Natural Sciences, Tampere University, 33720 Tampere, Finland

Recently, time-varying media has risen as a new paradigm in wave mechanics, in particular for the case of electromagnetic radiation [1]. This is due to the emergence of highly nonlinear materials, such as epsilon-near-zero media, which may feature large and fast modulation to the dielectric function under specific conditions. In such media, the time dependent dielectric function induces a varying speed to a wave propagating within it, which in turn causes a longitudinal acceleration of the wave.

In the framework of modern physics, it is normal practice to take the speed of light as a strictly constant value [2]. However, we encounter situations where it varies every day: whenever light interacts with matter, it appears to slow down. Of course, this is not a modification to the vacuum speed of light but it is an essential property nonetheless. Importantly, longitudinally accelerating waves are *not* a solution of the standard wave equation. To study such waves rigorously, we have derived the accelerating wave equation in 1+1 dimensions,

$$\frac{\partial^2 f(x,t)}{\partial t^2} = c(t)^2 \frac{\partial^2 f(x,t)}{\partial x^2} - \dot{c}(t)\frac{\partial f(x,t)}{\partial x}, \tag{1}$$

where $f(x,t)$ is the wave, $c(t)$ is the time dependent speed of the wave, and $\dot{c}(t)$ is the acceleration. If we choose c_0 as the (constant) vacuum speed of light, and write the speed variations as a modulation to the vacuum speed, such that $c(t) = c_0/n(t)$, we can find the general plane wave solution to the accelerating wave equation as in

$$f(x,t) = A\exp(i\omega t' - ikx) + B\exp(i\omega t' + ikx). \tag{2}$$

Here, A and B are amplitude coefficients and $k = \omega/c_0$ is the wavenumber. Moreover, we have defined an *intrinsic* time for the electric field as $t' = \int n(t)^{-1} dt$, which is the time experienced by the wave. Intriguingly, this is fully equivalent to the definition of proper time in general relativity [2]. In other words, if we allow waves to accelerate, they exhibit properties that have natural parallels in the theory of relativity, such as time dilation and length contraction.

To test the applicability of accelerating waves to photonics, we have investigated simple refraction problems, as well as the more exotic disordered photonic time crystal [3]. Our results are entirely consistent with earlier studies, and our formulation is able to treat material interfaces *without* boundary conditions (i.e. our solutions are analytical and continuous over the whole domain). Lastly, we have gained important new insight into two long standing problems in physics: the Abraham–Minkowski controversy and the arrow of time. To be more specific, by considering the effects of longitudinal acceleration, the Abraham–Minkowski controversy can be solved without dividing the overall momentum to wave and material portions. Moreover, accelerating waves are able to move only towards positive time, thus shedding light on the microscopic arrow of time.

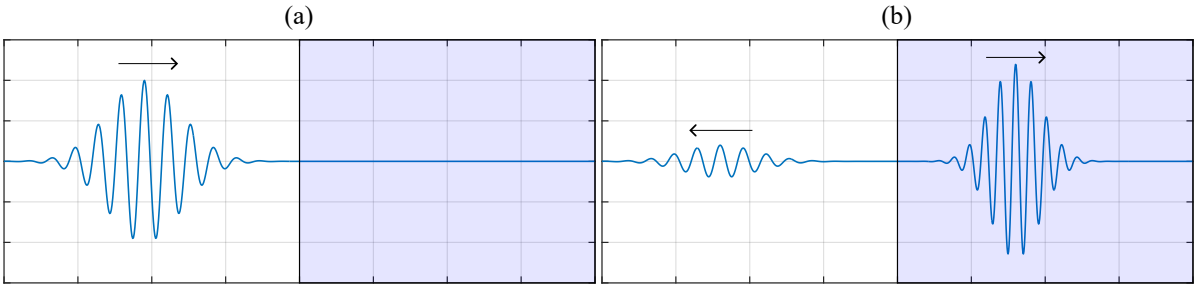

Fig. 1: Electric field at an interface, as seen in the laboratory frame. (a) Gaussian pulse incident on a dielectric, travelling from left to right (indicated by right pointing arrow), (b) the reflected pulse (leftarrow) and the transmitted pulse (right arrow). This pulse was analytically simulated with continuous functions. The wavenumber of light does *not* change inside the dielectric, but rather, the pulse experiences length contraction.

References

[1] E. Galiffi, R. Tirole, S. Yin, H. Li, S. Vezzoli, P. A. Huidobro, M. G. Silveirinha, R. Sapienza, A. Alù, and J. B. Pendry, Adv. Photon. **4**, 014002 (2022).
[2] L. D. Landau and E. M. Lifshitz, *The Classical theory of Fields* (Butterworth-Heinemann, 1975).
[3] Y. Sharabi, E. Lustig, and M. Segev, Phys. Rev. Lett. **126**, 163902 (2021).

*Corresponding author: matias.koivurova@tuni.fi

Single-laser feedback cooling of optomechanical resonators

Arvind Shankar Kumar[*,1], **Joonas Nätkinniemi**[1], **Henri Lyyra**[1] **and Juha Muhonen**[†,1]
[1] Department of Physics and Nanoscience Center, University of Jyväskylä, PO Box 35, FI-40014 University of Jyväskylä, Finland

Keywords: Quantum optics, optomechanics, nanostructures

Measurement-based control has emerged as an important technique to prepare mechanical resonators in pure quantum states for applications in quantum information processing and quantum sensing [1-3]. Conventionally this has required two separate channels, one for probing the motion (which is typically measured using a balanced homodyne detector) and another one acting back on the resonator.

In this work [4], we analyze and experimentally demonstrate a technique of single-laser feedback cooling, where one laser is used for both probing and controlling the mechanical motion through homodyne feedback. We show using an analytical model, numerical simulations and experiments on Silicon nanobeam resonators that feedback cooling is feasible in this mode as long as certain stability requirements are fulfilled.

Our results show that, in addition to being more experimentally feasible construction, the interference effects of the feedback can actually be used to enhance cooling at some parameter regimes.

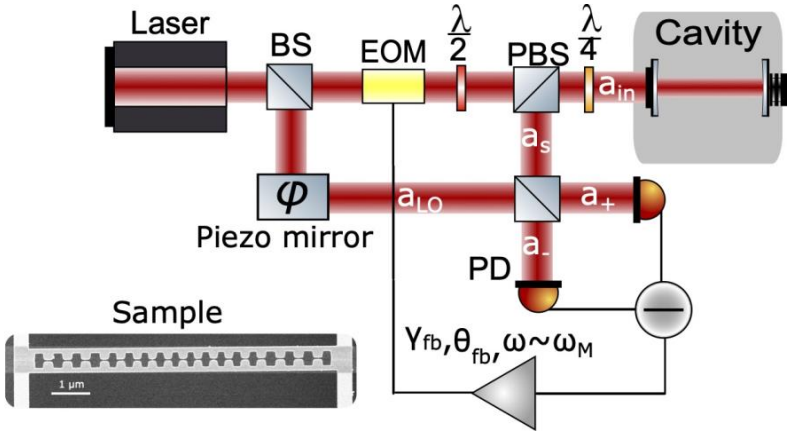

Figure 1. Schematic of experimental setup for single-laser feedback cooling and Scanning electron microscope image of Silicon nanobeam resonator sample.

References

[1] M. Rossi, D. Mason, J.Chen, Y. Tsaturyan and A. Schliesser "Measurement-based quantum control of mechanical motion," Nature **563**, 53–58 (2018)
[2] Jingkun Guo, Richard Norte, and Simon Gröblacher "Feedback Cooling of a Room Temperature Mechanical Oscillator close to its Motional Ground State" Phys. Rev. Lett. **123**, 223602 (2019)
[3] A. Borrielli, M. Bonaldi, E. Serra, P. M. Sarro, and B. Morana "Active feedback cooling of a SiN membrane resonator by electrostatic actuation" Journal of Applied Physics **130**, 014502 (2021)
[4] Arvind Shankar Kumar, Joonas Nätkinniemi, Henri Lyyra, Juha T. Muhonen " Single-laser feedback cooling of optomechanical resonators " arXiv:2209.06029 (2023)

[*]Corresponding author: arvind.s.kumar@jyu.fi
[†]Corresponding author: juha.t.muhonen@jyu.fi

Two color fast switching in epsilon-near-zero hyperbolic metamaterial

Alessandro Pianelli[*1], **Rakesh Dhama**[1], **Jarosław Judek**[2], **Rafał Mazur**[3], **Humeyra Caglayan**[†1]

1. Tampere University, Faculty of Engineering and Natural Sciences, 33720, Tampere, Finland

2. Institute of Microelectronics and Optoelectronics, Warsaw University of Technology, Koszykowa 75, 00-662 Warsaw, Poland

3. Institute of Applied Physics, Military University of Technology, 2 Kaliskiego Str., 00-908, Warsaw, Poland

All-optical fast switches enabled by artificial materials are considered the forefront of the next generation of quantum photonic communications and data processing [1],[2]. One class of materials considered promising for all-optical control of light is the so-called Hyperbolic Metamaterials (HMMs) [3]. They provide exotic functionalities such as tunability [4], enhancement of photonic density of states (PDOS) [3], canalization of light at the nanoscale [5], and all-optical ultra-fast switching, particularly at epsilon-near-zero (ENZ) regime where the dielectric permittivity vanishes [6].

Here, we propose novel HMMs based on complementary metal–oxide–semiconductor (CMOS) materials that possess two resonant epsilon-near-zero in visible and telecom windows (Fig. 1(a)). The HMM is composed of subwavelength stacked layers of Titanium Nitride (TiN) and Indium-tin-oxide (ITO) used as a building block (sketched in the inset of Fig. 1(a)). Taking advantage of low losses, ENZ regime, and excellent plasmonic properties of TiN/ITO at optical wavelengths, we could observe, with pump and probe measurements, a fast switching time at both ENZ regions at a wavelength equal to 657 nm and at 1318 nm O band of telecom wavelengths. (Fig.1 (b,c)). Such optical metamaterials can function as double-switching devices featuring an all-optical modulation response within the range of 2.1 - 3.3 THz. Our results envision the possibility of engineering meta-devices that act as fast modulators operating at multiple wavelengths simultaneously. Such metamaterials have a prominent outlook and launch a new paradigm towards hybrid configuration for ultra-fast modulators based on quantum photonic integrated circuits.

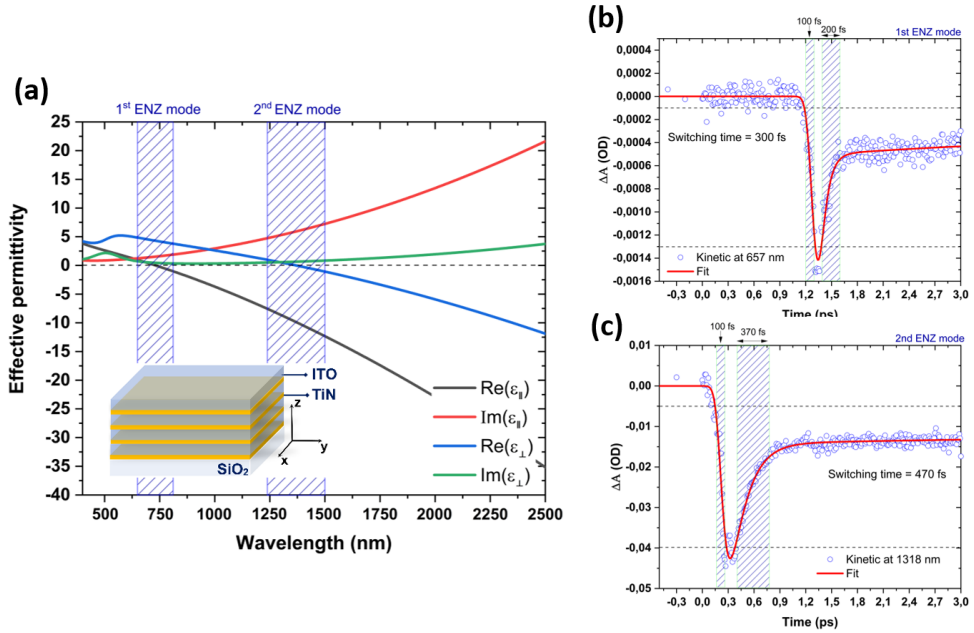

Fig. 1: (a) Effective permittivity of TiN/ITO based HMM, (b),(c) fast switching responses respectively at the two resonant frequencies in visible and Near-IR range

References

[1] Zheludev, Nikolay I and Kivshar, Yuri S, Nature materials **11** 917–924 (2012)

[2] Dhama, Rakesh and Panahpour, Ali and Pihlava, Tuomas and Ghindani, Dipa and Caglayan, Humeyra **13** 1–9 (2022)

[3] Guo, Zhiwei and Jiang, Haitao and Chen, Hong, Journal of Applied Physics **127** 071101 (2020)

[4] Habib, Mohsin and Briukhanova, Daria and Das, Nekhel and Yildiz, Bilge Can and Caglayan, Humeyra, Nanophotonics **9** 3637–3644 (2020)

[5] Pianelli, A., Caligiuri, V., Dudek, M. et al., Scientific Reports **9** 3637–3644 (2020)

[6] Rashed, Alireza R and Yildiz, Bilge Can and Ayyagari, Surya R and Caglayan, Humeyra, Physical Review B **16** 165301 (2020)

We acknowledge the financial support of the European Research Council (Starting Grant project aQUARiUM; Agreement No. 802986), Academy of Finland Flagship Programme (PREIN), (320165).

[*]Corresponding author: alessandro.pianelli@tuni.fi

[†]Corresponding author: humeyra.caglayan@tuni.fi

Engineering of Hiqh-Q Lattice Resonances in Plasmonic Bipartite Arrays through Nanoparticle Geometry and Orientation

Timo Stolt[*1], **Jussi Kelavuori**[1], **Ali Panahpour**[1], **Mikko J. Huttunen**[1]
1. Photonics Laboratory, Physics Unit, Tampere University, FI-33014 Tampere, Finland

Periodic arrays of plasmonic nanoparticles (NPs) show potential for realizing novel photonic devices, including flat lenses, lasers, and nonlinear components [1–3]. The optical responses of such structures can be boosted by utilizing collective resonances known as surface lattice resonances (SLRs), which are associated with high quality-factors (Q-factors) and strong local-field enhancements [4,5]. Particularly, arrays exhibiting multiple SLRs show promise for tunable and efficient nonlinear devices [6,7]. However, different SLRs in such multiresonant designs often occur for orthogonal polarization states. This results in poor spatial overlap between different SLR modes, and consequently, limited light–matter interaction. Here, we address this issue by designing plasmonic bipartite NP arrays that exhibit two SLRs for the same incident polarization. We show that by changing the NP geometry and orientation, the Q-factors and mutual mode-overlaps of the occurring SLRs can be improved, which is essential for enhancing nonlinear processes taking place in such NP arrays.

We numerically investigate (COMSOL Multiphysics) the optical properties of three metasurface designs consisting of gold nanoparticles arranged in a bipartite array along the metasurface y-axis. They have the same lattice periodicity that gives rise to SLRs for x-polarized light at 1200 nm and 800 nm, named SLR1 and SLR2, respectively. The three samples, named S1, S2, and S3, differ in the NP geometry and orientation. S1 has rectangular NPs, while S2 and S3 have one side of the NPs shortened. The difference between S2 and S3 is in NP orientation. For S2, the narrow ends of each NP point in the same direction along the y-axis. For S3, every second NP is rotated so that the short sides of NPs are pointing at each other. These NP modifications do not significantly affect the spectral location of the occurring SLRs but rather their associated local-field distributions and Q-factors. First, the narrowing of the NPs increases the Q-factor of SLR1 from 300 for S1 to roughly 1000 for S2 and S3. However, only narrowing the NPs decrease the Q-factor of SLR2 significantly: for S1 it is approximately 50 000, while for S2 it has decreased significantly to approximately 12 000. Interestingly, this effect can be compensated by flipping every second NP in the array. Thus, for S3, the SLR2 near 1200 nm has a considerably high Q-factor of roughly 30 000. Furthermore, S3 has improved mode overlap between the two analyzed SLR modes, which is expected to boost nonlinear frequency-mixing processes, such as sum-frequency generation, difference-frequency generation, and four-wave-mixing.

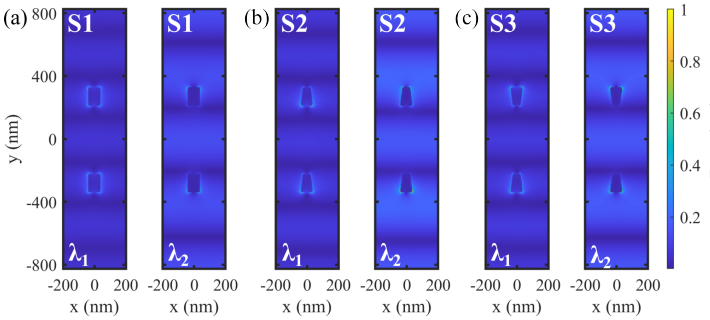

(d)

	S1	S2	S3
λ_1 (nm)	800.8	798.5	798.4
Q_1	342	969	1 020
λ_2 (nm)	1195.8	1195.7	1195.7
Q_2	55 119	12 834	31 626

Fig. 1: (a)-(c) Normalized electric field profiles for plasmonic bipartite arrays at the occurring surface lattice resonance (SLR) wavelengths λ_1 and λ_2. We investigated three sample designs, S1, S2, and S3, which differ in nanoparticle shape and orientation. (d) The differences in nanoparticle geometry and orientation have only a very limited impact on the SLR wavelength. However, they do affect the quality-factors (Q) of the occurring SLRs dramatically.

To conclude, we numerically investigated plasmonic NP arrays with bipartite lattice configuration. The lattice periodicities were selected such that the NP arrays exhibit SLRs at two separate wavelengths in the near-infrared region. We modified the NP geometry and mutual orientation, which had a considerable impact on the Q-factors of the occurring SLRs. NP modification also impacted the local-field distributions associated with SLRs, which is expected to have a significant impact on the nonlinear responses of the studied structures. Next, we will characterize the nonlinear properties of our sample designs and present the results at the conference.

References

[1] J. Hu, D. Wang, D. Bhowmik, T. Liu, S. Deng, M. P. Knudson, X. Ao, and T. W. Odom, ACS Nano **13**, 4613-4620 (2019)
[2] T. K. Hakala, H. T. Rekola, A. I. Väkeväinen, J. P. Martikainen, M. Nečada, A. J. Moilanen, and P. Törmä, Nat. Commun. **8**, 13687 (2017)
[3] L. Michaeli, S. Keren-Zur, O. Avayu, H. Suchowski, and T. Ellenbogen, Phys. Rev. Lett. **118**, 243904 (2017)
[4] A. D. Utyushev, V. I. Zakomirnyi, and I. L. Rasskazov, Rev. Phys. **6**, 100051 (2021)
[5] M. S. Bin-Alam, O. Reshev, Y. Mamchur, M. Z. Alam, G. Carlow, J. Upham, B. T. Sullivan, J. Ménard, M. J. Huttunen, R. W. Boyd, and K. Dolgaleva, Nat. Commun. **12**, 974 (2021)
[6] T. Stolt, A. Vesala, H. T. Rekola, P. Karvinen, T. K. Hakala, and M. J. Huttunen, Opt. Express, **30**, 3620–3631 (2022)
[7] T. Lim, Y. Vaddi, M. S. Bin-Alam, L. Cheng, R. Alaee, J. Upham, M. J. Huttunen, K. Dolgaleva, O. Reshev, and R. W. Boyd, ACS Nano **16**, 5696–5703 (2022)

*Corresponding author: timo.stolt@tuni.fi

Taming the Cosmic Mustang

T. Kurki-Suonio[*,1], T. Tala[2], S. Lazerson[3], O. Asunta[4], J. Varje[4], S. Scott[5]
[1] Aalto University, Espoo,
[2] VTT, Espoo, Finland
[3] Max Planck Institute, Greifswald, Germany
[4] Tokamak Energy Ltd, Oxford, U.K.
[5] MIT and Commonwealth Fusion Systems, Massachusetts, U.S.A.

The year 2022 was filled with fusion-related records, even breakthroughs: First, the JET magnetic fusion facility sets a new world energy record on energy produced by fusion reactions in a tokamak [1], then ST40 reached a record ion temperature for a spherical tokamak, 100 million degrees [2], and later in the year NIF laser fusion facility announced a genuine breakthrough in this technology: the deuterium-tritium pellet exploded releasing more energy from fusion reactions than what it had absorbed from the laser beams [3].

With this contribution we wish to elaborate on these results and on their significance for the progress in harnessing the power of the stars for terrestrial, peaceful use. We also touch upon the earlier world record in fusion *power* [4], illuminating what the difference of that is to the records achieved last year. After this, the listener should be able to make conclusions on whether it would be time to start constructing the first fusion power plant on the Pyhäjoki site, recently abandoned by the planned sixth nuclear power plant in Finland.

Even if the answer were 'yes', it would probably not be the first fusion power plant in the world. There are several privately and semi-privately funded fusion enterprises with very aggressive schedules to introduce a working demonstration reactor that would produce a fusion gain in excess of 10 already in early 2030s. In this contribution, we elaborate the ideas and solutions of two of these, Tokamak Energy Ltd, Oxford, England, and Commonwealth Fusion Systems, Cambridge, Massachusetts, USA.

The contribution is concluded by briefly introducing the black horse galloping to the front from the 50's: the stellarator concept. The availability of super-computers made it possible to optimize this readily reactor-relevant technology, leading to the construction of Wendelstein 7-X at Max Planck institute, Greifswald, Germany. Recently, even private companies are hopping in the stellarator wagon: Renaissance Fusion at Fontaine, France, and Princeton Stellarators at New Jersey, USA.

The research efforts of the Finnish fusion community, FinnFusion, within these remarkable projects are also outlined.

References

[1] C. Maggi et al., "Overview of T and D-T Results in JET with ITER-like Wall", in 29th IAEA Fusion Energy Conference (FEC 2023) 16-21 October 2023, London, United Kingdom.
[2] S. McNamara et al., "Achievement of ion temperatures in excess of 100 million degrees Kelvin in the compact high-field spherical tokamak ST40" (Submitted to Nuclear Fusion)
[3]https://www.llnl.gov/news/national-ignition-facility-experiment-puts-researchers-threshold-fusion-ignition
[4] M. Keilhacker et al., Nuclear Fusion **39** (1999) 209

[*]Corresponding author: taina.kurki-suonio@aalto.fi

Fusion-born alpha particle power loads in ITER: sensitivity on the radial displacement of wall tiles and field coils

Otso Hyvärinen[*1], **Antti Snicker**[†1], **Lucia Sanchis**[‡1]
1. Department of Applied Physics, Aalto University, FI- 00076 AALTO, FINLAND

In Southern France, ITER, to date the largest thermonuclear fusion experiment is being built. It represents a new era of fusion experiments where fusion products are planned to dominantly heat the plasma. The plasma is said to be burning in these conditions. To achieve burn conditions, fusion-born alpha particles need to be confined well enough inside the magnetic cage. If the opposite is true, alpha particle losses could lead to not only significant loss of power but also potential damage to the first wall of the device. One of the earlier neglected processes to increase these losses is the engineering accuracy of several components. This work addresses this issue by performing a sensitivity analysis of the alpha particle loss patterns in the first wall on the radial displacement of the first wall tiles and the magnetic field generating toroidal field coils. The results show that while the small displacement of toroidal field coils causes changes in the alpha particle losses barely measurable within the Monte Carlo simulations, displacement of the first wall tiles even by 1 cm could be of significant importance.

All the fusion-alpha simulations are carried out using the Monte Carlo orbit-following code ASCOT [1]. The wall loads of six simulations with varying radial displacements of a chosen limiter tile are analyzed. The exponential increase of the wall loads in this tile is observed with a characteristic scale of 11 mm, as illustrated in the figure below. The exponential increase in limiter wall loads due to displacement coincides with the radial displacement of the banana-trapped particle orbits due to toroidal ripple [2]. Due to the 3D nature of the magnetic field, the mirroring points of the banana orbits are not located in the same (R,z) position and the orbits will experience a small radial drift causing fractions of these particles to drift all the way to the first wall. The mean step size of these radial jumps is of the order of < 10 mm. Hence, the protruding tile will collect most of these drifting alphas.

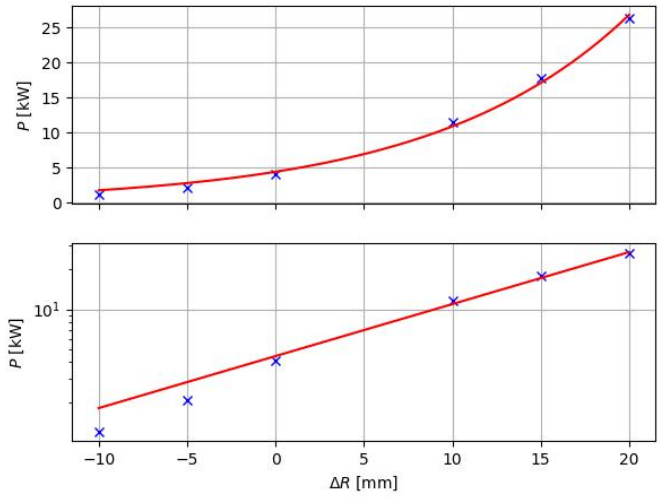

Fig. 1: Linear and logarithmic total wall load in limiter as data points, and the corresponding exponential fit.

The wall loads sensitivity to the radial displacement of TF-coils is investigated using three different scenarios: 1) The first coil is located in 11 radial positions. The wall loads do not exhibit any significant difference, but the most sensitive displacement is determined to be -2 mm. 2) The local wall loads of the first 6 coils with a -2 mm radial displacement are analyzed, and the second coil is determined to be the most sensitive coil. 3) All coils are displaced by a random distance, representing a realistic scenario. In all three scenarios, the local wall loads were not found to have significant changes, and the discrepancies were found to decrease when the Monte Carlo error was decreased.

In conclusion, the fusion-alpha wall loads in displaced limiter tiles were found to experience exponential increase, with characteristic scale of 11 mm. These local differences could potentially cause additional local erosion and even endanger the integrity of the first wall elements in a scenario where the absolute total power load is large enough. The wall loads were not found affected by radial displacements of the TF coils.

References

[1] Hirvijoki, Eero, et al. "ASCOT: Solving the kinetic equation of minority particle species in tokamak plasmas." Computer Physics Communications 185.4 (2014): 1310-1321.
[2] Goldston, Robert J., R. B. White, and Allen H. Boozer. "Confinement of high-energy trapped particles in tokamaks." Physical review letters 47.9 (1981): 647.

[*]Corresponding author: otso.hyvarinen@aalto.fi
[†]Corresponding author: antti.snicker@aalto.fi
[‡]Corresponding author: lucia.sanchis@aalto.fi

Advances in flow harmonic analysis of LHC collisions: From large to small systems

Dong Jo Kim[*1], **Anna Önnerstad**[†1], **Cindy Mordasini**[‡1]
1. University of Jyväskylä and Helsinki Institute of Physics

One of the primary goals of heavy-ion physics is to understand the transport properties of the quark-gluon plasma (QGP), which is composed of the smallest constituents of matter, the quarks and gluons, and which filled up our universe a few microseconds after the Big Bang. The present most challenging question in this research field is to pin down the critical point of the QGP, where the shear viscosity over entropy ratio is at its minimum. As of now, the QGP has the smallest observed value of eta/s, close to the theoretical minimum of 1/4pi. Significant advances based on flow harmonic analysis have recently been made. There are, however, still a few remaining challenges in both experiment and theory to constrain the temperature dependence of η/s and ζ/s of the QGP. In this talk, I will highlight the latest advances made from LHC experiments in this regard and discuss aforementioned challenges.

[*]Corresponding author: dong.jo.kim@cern.ch
[†]Corresponding author: anna.onnerstad@cern.ch
[‡]Corresponding author: cindy.mordasini@cern.ch

Unravelling the electronic structure of uranium: the case of MUO3 (M = K, Na and Rb)

S. Orlat[1], R. Bes[2], F. Tuomisto[2], P. Martin[1], P. Moisy[1], G. Leinders[3], K. Kvashnina[4,5]

1 CEA, DES, ISEC, DMRC, University of Montpellier, Marcoule, France
2 Department of Physics, University of Helsinki, P.O. Box 64, FI-00014 Helsinki, Finland
3 Belgian Nuclear Research Centre (SCK CEN), Institute for Nuclear Materials Science, Boeretang 200, B-2400 Mol, Belgium.
4 The Rossendorf Beamline at ESRF, The European Synchrotron, CS40220, 38043 Grenoble Cedex 9, France
5 Institute of Resource Ecology, Helmholtz Zentrum Dresden-Rossendorf (HZDR), PO Box 510119, 01314 Dresden, Germany

Uranium is a key chemical element of the nuclear industry and has a complex chemistry due to the large number of oxidation states allowed by its $[Rn]7s^26d^15f^3$ ground state electronic configuration. Even if this element has been the focus of substantial research, its electronic structure remains difficult to study theoretically due to the same magnitude of the crystal field splitting, spin orbit coupling and electron-electron interaction. The core of this contribution, is to present recent effort made to overcome this difficulty by studying U(V) compounds such as alkali metal uranates KUO_3, $NaUO_3$ and $RbUO_3$. More precisely, the analysis of high energy resolution fluorescence detected data obtained at the U-L_3 edge measuring the Lβ_5 emission line for enhanced spectral resolution [1,2] will be discussed in the light of new theoretical calculation results obtained using the Finite Difference Method for Near-Edge Structure (FDMNES) code [3] as illustrated in Figure 1. As shown by recent results obtained on KUO_3 [4] and on $NaUO_3$ [5], such combined experimental and theoretical approach allows to better understand the impact on the uranium valence electronic structure induced by the change in the U-O interatomic distances and the associated local structural distortions.

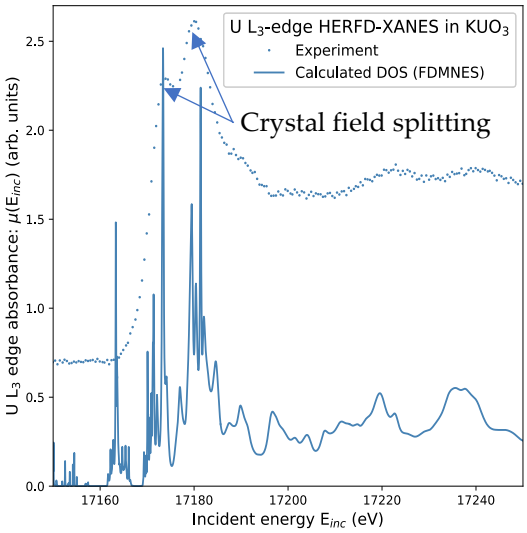

Figure 1: uranium L_3-edge HERFD-XANES in KUO_3 and corresponding simulated spectrum using *FDMNES* [3]

References

[1] K. O. Kvashnina et al., J. Electron Spectrosc. Relat. Phenom. 194, 27 (2014).
[2] K. O. Kvashnina et al., Anal. Chem. 87, 8772 (2015).
[3] O. Bunău et al., J. Phys. Condens. Matter. 21, 4260 (2009).
[4] R. Bes et al., J. Synch. Rad. 29, 21 (2022) 21.
[5] S. M. Butorin et al., Chem. Eur. J. 22, 9693 (2016).

*Simon Orlat: simon.orlat2@cea.fr

Inherently Charged Particle (ICP) Sensor: Measuring particles based on their natural charge

L. Salo[1*], A. Rostedt[1], H. Kuuluvainen[1], K. Teinilä[2], R.K. Hooda[2], Md. H. Rahman[3], A. Datta[3], V.P. Sharma[3], S. Subudhi[3], A. Hyvärinen[2], H. Timonen[2], E. Asmi[2], S. Martikainen[1], P. Karjalainen[1], B. Lal[3], J. Keskinen[1], T. Rönkkö[1]

[1]Aerosol Physics Laboratory, Tampere University, 33720, Tampere, Finland
[2]Atmospheric Composition Research, Finnish Meteorological Institute, 00101, Helsinki, Finland
[3]The Energy and Resources Institute, New Delhi, 110003, India

Ambient particles are a major cause of premature deaths globally [1]. While there are many instruments suitable for scientific measurements of aerosols, better methods for long-term monitoring are still needed, especially low-maintenance, affordable solutions for ultrafine particles. We present a new sensor prototype, the ICP (Inherently Charged Particle sensor) [2]. It uses the naturally occurring charge of the particles to detect them. The ICP-sensor prototype was tested in a highly polluted traffic location. We also compared the measured charged concentration to the equilibrium concentration of ambient aerosols, calculated from the particle number distribution measured with ELPI+ (Electrical low-pressure impactor, Dekati Ltd.).

The results from the field measurements show the sensor's performance in a suggested application. In Figure 1, the charge concentration measured with the ICP-sensor is compared to three particle metrics (measured with ELPI+). All three metrics have a reasonable correlation, but the best correlation is to particle surface area. In Figure 2, the ICP charge concentration is compared to a theoretical charge concentration based on the assumption that the ambient charge distribution has reached an equilibrium state described by the Wiedensohler formulation [3].

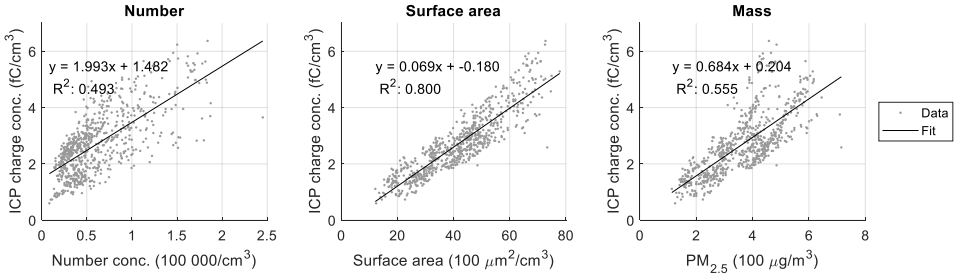

Figure 1: Charge concentration measured with the ICP-sensor compared to different particle metrics.

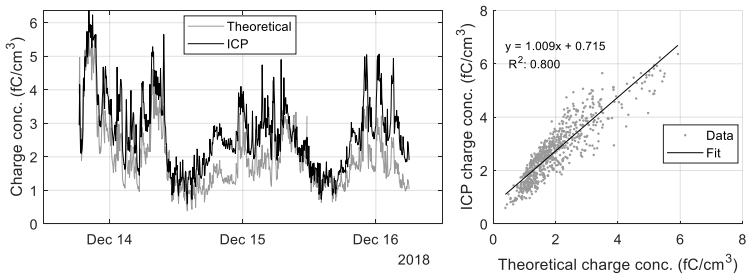

Figure 2: A time series of the measured and calculated theoretical charge concentration as well as a scatter plot.

The ICP sensor worked well in the demonstrated application of monitoring highly polluted ambient air, producing a good correlation with surface area concentration. We also showed that by pairing the sensor with another instrument, information can be gathered on the charge state of the particle population. The benefit of the ICP compared to previous electrical particle sensors is that no charger is required, whereas the downside is that it requires higher particle concentrations for accurate measurement.

This work was in part funded by Business Finland project TAQIITA (grant number 2763/31/2015) & the Department of Biotechnology, India. The work was made in the Academy of Finland Flagship: The Atmosphere and Climate Competence Center (ACCC). Grant numbers: 337551 (Tampere University) and 337552 (Finnish Meteorological Institute). Laura Salo gratefully acknowledges funding from the Doctoral School of Tampere University of Technology (now Tampere University).

References

[1] Burnett, R. *et al.* (2018) 'Global estimates of mortality associated with longterm exposure to outdoor fine particulate matter', *Proceedings of the National Academy of Sciences of the United States of America*, 115(38), pp. 9592–9597.
[2] Salo, L. *et al*., 'Inherently Charged Particle (ICP) Sensor Design', *IEEE Sensors Journal*, doi: 10.1109/JSEN.2022.3232509.
[3] Wiedensohler, A. (1988) 'An approximation of the bipolar charge distribution for particles in the submicron size range', *Journal of Aerosol Science*, 19(3), pp. 387–389.

*Corresponding author: laura.salo@tuni.fi

Characterizing Atmospheric Molecules for Machine Learning

Hilda Sandström[†,1,2] **and Patrick Rinke**[*,1,2]
[1] Department of Applied Physics, Aalto University, Espoo, Finland
[2] Virtual Laboratory for Molecular Level Atmospheric Transformations (VILMA) Centre of Excellence

Aerosols in the atmosphere impact air quality and contribute to climate change. A great number of atmospheric molecules and chemical processes lead to aerosol formation. This combinatorial complexity is well-suited for study using machine learning. However, for many applications, large datasets of atmospheric molecules, which are needed for machine learning, are not available. In this contribution, I present an investigation into the similarity, as seen through molecular descriptors and fingerprints, between a dataset of atmospheric molecules and several available molecular datasets from other research domains. Preliminary results demonstrate little overlap between the atmospheric dataset and the others. The implication of this study suggests that the atmospheric science community needs a joint effort to collect and curate large atmospherically relevant datasets.

[*]Corresponding author: patrick.rinke@aalto.fi
[†]Presenting author: hilda.sandstrom@aalto.fi

Infiltration of outdoor particulate matter into indoor spaces

Ville Silvonen[*,1], **Laura Salo**[1], **Tuomas Raunima**[2], **Juha Vinha**[2], **Panu Karjalainen**[1], **Topi Rönkkö**[1]

[1] Aerosol Physics, Faculty of Engineering and Natural Sciences, Tampere University, Tampere, 33720, Finland
[2]Building Physics, Faculty of Built Environment, Tampere University, Tampere, 33720, Finland

The assessment of a person's exposure to particulate matter frequently relies on information from outdoor environments. However, because so many people spend most of their time indoors, using data only from the outside can be deceptive. To accurately describe the exposure to particulate matter, it is therefore necessary to also study indoor environments.

A typical indoor setting is an office. According to Bo et al. [1], the majority of airborne particles in offices come from outdoor sources and are brought indoors through ventilation, open doors and windows, or leaks in the building envelope. Gravimetric techniques are frequently used to study indoor/outdoor particulate pollution, but high time and size resolution measurements are required to fully comprehend the mechanisms governing particle infiltration.

Our study's objective was to describe the physical characteristics of indoor and outdoor particles in four European office buildings. We looked at how different factors, like wind direction and pressure differences over the building envelope, affected particle concentrations and characteristics both indoors and outdoors. We also studied how various factors affected the percentage of outdoor particles that made it indoors.

The measurements were performed in office rooms in Helsinki, Tampere, Prague, and Dusseldorf. Particle size distributions and alveolar deposition of particles were measured from indoor and outdoor air with electrical low-pressure impactors (ELPI+).

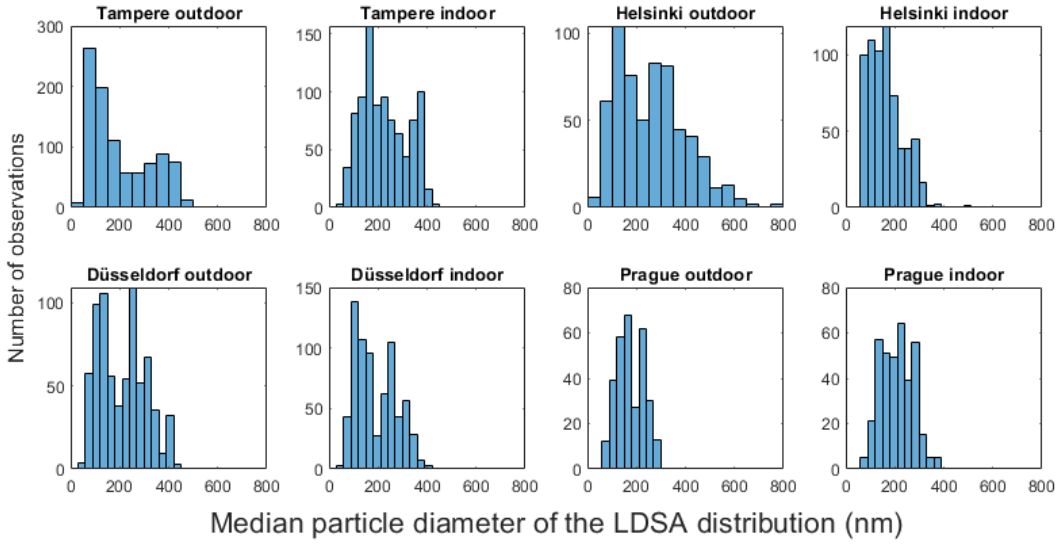

Figure 1: Histogram representation of the median particle size of the LDSA (lung deposited surface area) distribution in different cities. One observation corresponds to the 30 minute median size of the distribution. The data is preliminary.

We found that the outdoor particle concentration significantly influenced the indoor concentration in all the studied offices. The ambient particle size distribution had a considerable impact on the infiltration of particles, and we observed decreased infiltration when the outdoor particle size distribution shifted towards larger particles. Aged (larger) aerosol particles are likely to be less harmful to health than fresh traffic emission particles [2] and the stronger infiltration of traffic emissions highlights their importance in terms of indoor exposure.

This study was funded by Business Finland project Future Spaces (grant number: 33250), with industry funding from Koja Ltd., A-Insinöörit Suunnittelu Ltd., Tampereen Tilapalvelut Ltd., TPI Control Ltd. and Dekati Ltd.

References

[1] M. Bo, P. Salizzoni, M. Clerico, and R. Buccolieri, "Assessment of Indoor-Outdoor Particulate Matter Air Pollution: A Review," *Atmosphere*, vol. 8, no. 8, p. 136, 2017, doi: http://dx.doi.org/10.3390/atmos8080136.
[2] M. Park *et al.*, "Differential toxicities of fine particulate matters from various sources," *Sci Rep*, vol. 8, no. 1, Art. no. 1, Nov. 2018, doi: 10.1038/s41598-018-35398-0.

*Corresponding author: ville.silvonen@tuni.fi

Comparison of thin film surfaces to study salivary biomarkers of oral diseases by Surface-Enhanced Raman Spectroscopy

Miia Hurskainen[*,1], **Hannu Korhonen**[1], **Sami Myllymaa**[1], **Reijo Lappalainen**[1]

[1] Department of Technical Physics, University of Eastern Finland, FI-70211 Kuopio, Finland

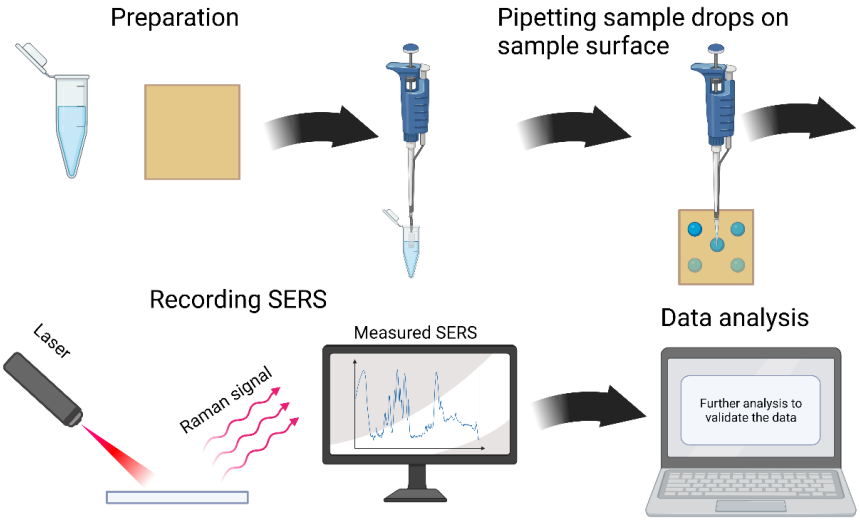

Figure 1 Schematic presentation of the study.

Six thin film surfaces, Bi, Ti, Al_2O_3, Ag, Au, and C, were prepared on Si substrates to investigate which are the most efficient ones for detection of salivary biomarkers with surface-enhanced Raman spectroscopy (SERS). Two oral cancer biomarkers, L-Fucose and L-Proline, and one oral disease biomarker, N-acetylneuraminic acid, were used in this two-phase study [1,2,3]. In the first phase, 5 mg of each substance was diluted in 1 ml of Millipore water and the same amount of substance was diluted in 1 ml of artificial saliva in the second phase. SERS spectra were recorded for each solution and spiked saliva samples. Raw spectra were normalized using standard normal variate (SNV) and then smoothed using a Savitzky-Golay filter (degree = 3, window = 31). Area normalization was calculated for the smoothed SNV spectra as shown in equation

$$S_{AN} = \frac{S}{\sum|S_p|},$$

where S_{AN} is area normalized spectra and S_p is a point in spectrum. A cubic k-nearest neighbor's (kNN) was tested for both aqueous solutions and artificial salivas' spectra, and their respective confusion matrixes and F1-scores were calculated.

Based on both visual inspection of the spectra and computing confusion matrixes and their F1-scores four surfaces, namely Bi, Al_2O_3, Ag, and Au on Si substrates were chosen to the second phase. The results from the second phase with spiked artificial saliva confirmed that the four surfaces are the most suitable ones. Besides typically used gold and silver [4,5], our study shows that also bismuth and aluminium oxide coated silicon surfaces work well in SERS-based detection of salivary biomarkers.

Future studies should use spiked saliva samples collected from healthy volunteers and samples from patients suffering from oral diseases such as oral squamous cell cancer to confirm the results of this study. Furthermore, compositional and microtextural modifications can significally improve the performance when applied to tested thin films surfaces.

References

[1] J.J.W. Mikkonen, S.P. Singh, M. Herrala, R. Lappalainen, S. Myllymaa, A.M. Kullaa, J.Periodontal. Res., **51**, 431–437 (2016).
[2] J.J.W. Mikkonen, S.P. Singh, R. Akhi, T. Salo, R. Lappalainen, W.A. González-Arriagada, M. Ajudarte Lopes, A.M. Kullaa, S. Myllymaa, Oncol. Lett., **16**, 6795-6800 (2018).
[3] A. Hernández-Cedillo, M. G. García-Valdivieso, A. C. Hernández-Arteaga, N. Patiño-Marín, A.A. Vértiz-Hernández, M. José-Yacamán, H. R. Navarro-Contreras, Oral Dis., **25**, 1627-1633, (2019)
[4] E. Vinogradova, A. Tlahuice-Flores, J.J. Velazquez-Salazar, E. Larios-Rodriquez, M. Jose-Yacaman, J. Raman Spectrosc., **45**, 730-735 (2014).
[5] K.V. Hacksaw, J.S. Miller, D.P. Aykas, L.Rodriguez-Saona, Molecules, **25**, 4725 (2020)

*Corresponding author: miia.hurskainen@uef.fi

The combination of Langmuir-Blodgett trough and synchrotron X-ray techniques: Unique tools to study tear film components

Mira Viljanen[†1,2], Tuomo Viitaja[*1], Ryan Trevorah[2], Filip Ekholm[1], Kirsi Svedström[*2]
[1] Department of Chemistry, University of Helsinki, P.O.B 55 (A. I. Virtasen aukio 1), 00014 University of Helsinki
[2] Department of Physics, University of Helsinki, P.O.B 64 (Gustaf Hällströmin katu 2), 00014 University of Helsinki

The tear film covers the ocular surface of the eye. It offers protection from the environment and contributes to the maintenance of eye health [1]. The tear film consists of two separate phases: A thick, muco-aqueous layer, coated by a thin tear film lipid layer (TFLL). The TFLL is secreted by the Meibomian glands and it forms the outermost barrier between the ocular surface and the environment. The TFLL has a highly conserved composition featuring a number of unique lipid classes such as wax esters (WE), cholesteryl esters (CE), *O*-acyl- ω-hydroxy fatty acids (OAHFA) and diesters (DiE). The interactions between these species and functional properties of the TFLL on the whole are not well-known [2] but a link between TFLL composition changes and development of ocular surface diseases, such dry eye disease, has been noted.
By studying the biophysical and structural properties of individual lipid species under physiological conditions [3,4], insights on their potential contributions to the overall function of the TFLL can be gathered. This information is not only important to understanding the functional base of this unique biological membrane, but also central to the development of new treatments and diagnostic tools for ocular surface diseases.
We have recently studied the properties of individual lipid species using a Langmuir-Blodgett trough setup and synchrotron grazing incidence X-ray diffraction (GIXD) and reflectivity (XRR) techniques at the ESRF and Soleil facilities. The data collected from these experiments reveal novel characteristics of individual TFLL lipid classes and will lead to an increased understanding on TFLL structure and function.

References

[1] J.P. Craig et al., The ocular surface, 15(3), 276-283 (2017).
[2] I.A. Butovich, Experimental eye research, 163, 2-16 (2017).
[3] R.O. Paananen et al., The ocular surface, *18*(4), 545-553 (2020).
[4] T. Viitaja et al., Nano Lett., *21*(18), 7676-7683 (2021).

[*]Corresponding author: tuomo.viitaja@helsinki.fi
[†]Corresponding author: mira.viljanen@helsinki.fi

Machine learning in localization of electrodes in the brain of epilepsy patients

Johannes Halkoaho[*1,2] **Eero Salli** [2] **Tuomas Kaseva** [2] **Sauli Savolainen** [1,2]
1. Department of Physics, Faculty of Science, University of Helsinki, PL 64 (Gustaf Hällströmin katu 2a), 00014
2. HUS Diagnostic Center, Radiology, University of Helsinki and Helsinki University Hospital, PL 340 (Haartmaninkatu 4), 00029 HUS

Up to 30% of people suffering from epilepsy are resistant to epileptic drugs [1]. In these cases the surgical removal of the epileptic area can be considered as a treatment for the epilepsy. In order to successfully accomplish this task it is necessary to locate the epileptic zone as accurately as possible. This localization can be performed using Stereoelectroencephalography (SEEG) [2]. SEEG is a procedure where electrodes are implanted into a patients brain in order to measure electric signals to locate the epileptogenic focus. The electrodes are then imagined using a CT scan and the location of the electrodes are aligned with an MR image. The localization of the electrode contacts are usually marked either manually or semi-automatically which is a time consuming task. Automatic segmentation and localization of the electrode contacts increases the speed of the process in a significant manner.

The use of machine learning in medical applications has increased in the recent years and medical image segmentation is not an exception. Machine learning can be used to segment the electrode contacts [3] and electrode sticks. We focus on finding of the center points of the electrode contacts and clustering them together into electrode sticks using deep learning model V-net [4]. We train two different models, one for finding the electrode contacts and one for finding the electrode sticks.

The data consists of 89 CT scans with 64 scans used for validation and training. The test set consists of 25 randomly selected scans. The localization of the electrode contacts of the scans were done manually by trained experts. The preliminary results for the validation set in terms of the dice score is 0.73 for contact segmentation and 0.845 for stick segmentation. As the contacts are very small compared to the entirety of the volume dice score is not the best metric for measuring success. A better metric for evaluation can be considered such as the median distance of the predicted center point compared to the ground truth and the number of missing/extra contacts along with their locations (in the skull or the brain).

After both prediction have been made it is possible to use other methods to cluster together the segmented contacts that belong to a specific segmented electrode. The method can be integrated to a workflow to be used in clinical situations.

We will be presenting the basics of machine learning based segmentation along with some of its common limitations using the case above as an example.

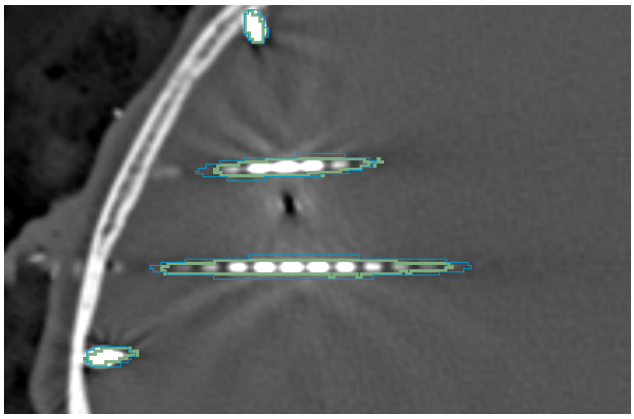

Fig. 1: Model prediction on the sticks for a scan from [5]. The model was trained with additional data from [5] in order for it to be able to perform on the scan. The green outlines mark the prediction and the blue outlines the ground truth.

References

[1] Kwan P, Brodie MJ. Early identification of refractory epilepsy. N Engl J Med. 342(5):314-319 (2000)
[2] Miller C, Schatmeyer B, Landazuri P, et al. Epilepsia Open. 6(4):694-702 (2021)
[3] Anja Pantovic, Irène Ollivier, Caroline Essert, Computer Methods in Biomechanics and Biomedical Engineering: Imaging & Visualization (2022)
[4] F. Milletari, N. Navab and S. -A. Ahmadi, 2016 Fourth International Conference on 3D Vision (3DV) pp. 565-571 (2016)
[5] Wang, Kang, SEEG, MRI, CT for BrainQuake analysis (2021)

[*]Corresponding author: johannes.halkoaho@helsinki.fi

Convolutional neural network -based phantom image scoring for mammography quality control

Veli-Matti Sundell[*,1,2], **Teemu Mäkelä**[1,2], **Anne-Mari Vitikainen**[2], **Touko Kaasalainen**[2]
[1] Department of Physics, University of Helsinki, P.O. Box 64, FI-00014 Helsinki, Finland
[2] HUS Diagnostic Center, Radiology, University of Helsinki and Helsinki University Hospital, P.O. Box 340, Haartmaninkatu 4, 00290 Helsinki, Finland

Visual evaluation of phantom images is an important part of mammography quality control (QC). However, it is a time-consuming and subjective task. To overcome these, an automated scoring systems can be used. Convolutional neural networks (CNNs) have been used recently with a high accuracy to solve a wide range of image classification problems [1]. The aim of this work was to automate mammography QC phantom scoring task by training CNN model to mimic a human reviewer. CNN was trained for detecting targets in American College of Radiology (ACR) accreditation phantom images and the results were compared with human scoring. The ACR phantom is made of acrylic, and it has wax insert which contains six fibres, five microcalcification groups and five masses. Figure 1 shows image of ACR mammography phantom and automatic pre-processing steps for phantom image. Different CNN structures were developed for scoring. For training and validation data one reviewer visually evaluated regular and artificially degraded/improved phantom images from eight mammography devices (2640 images in total). Additionally, four reviewers evaluated visually a separate test data set consisting of daily QC images from the eight devices and separately acquired images with varying dose levels (160 images in total). Each target was scored separately. Test data set were considered the ground truth for CNN performance testing. The best CNN structure had six convolutional layers and a scoring accuracy of 95% was achieved in test data. Figure 2 shows total scores (sum of each target type scores) of automated CNN analysis as a function of reviewers' consensus scores. At lowest dose levels, deviation between the CNN and the reviewers was the highest. However, no significant difference was found between the visual reviews and the CNN results except in case of smallest masses. In conclusions, a CNN-based automatic mammography QC phantom scoring system scores phantom images in a good agreement with human reviewers. Thus, it can be of benefit in mammography QC.

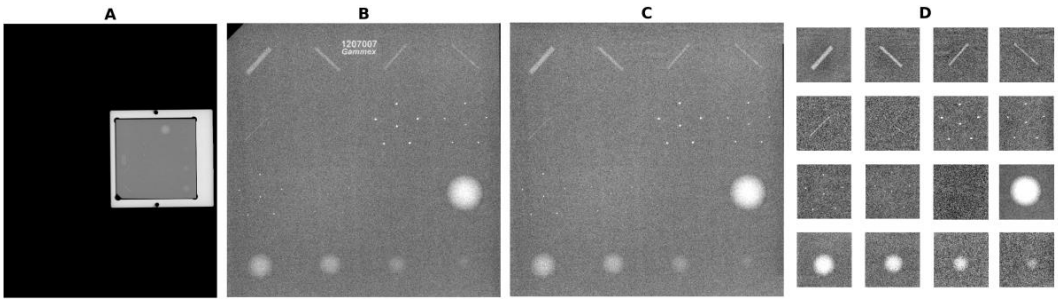

Figure 1. Pre-processing steps for a phantom image (A). At First, the wax area was cropped and rotated in right orientation (B), and then the phantom name and corners were replaced with noise (C). At the end, each fibre, microcalcification group, and mass was separated into an individual sub-image (D). Reprinted from work Sundell et al. [2].

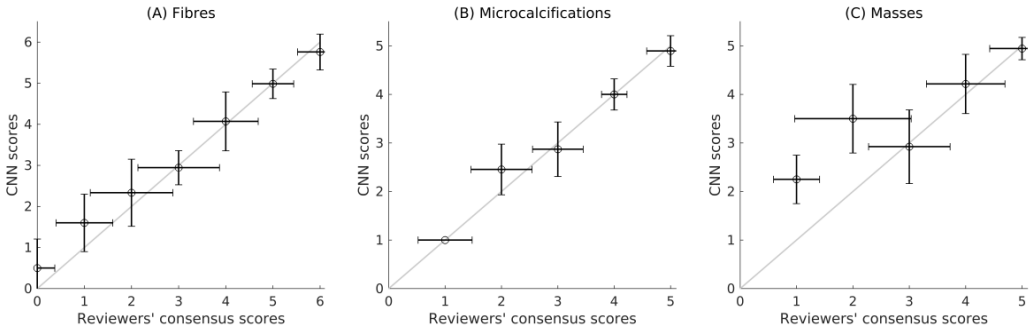

Figure 2. Total scores (sum of each target type scores) of automated CNN analysis as a function of reviewers' consensus scores. The error bars represent ±1 standard deviation for visual and automated scoring. Equal reviewer and CNN scoring is represented with the light grey line. Reprinted from work Sundell et al. [2].

References

[1] Szegedy C, Liu W, Jia Y, Sermanet P, Reed S, Anguelov D et al. Going deeper with convolutions. Proceedings of the IEEE Conference on Computer Vision and Pattern Recognition (CVPR), 1–9 (2015).

[2] Sundell V-M, Mäkelä T, Vitikainen A-M, Kaasalainen T. Convolutional neural network -based phantom image scoring for mammography quality control. BMC Med Imaging **22**, 216 (2022).

[*]Corresponding author: veli-matti.sundell@helsinki.fi

Dynamical Detrended Fluctuation Analysis of Heart Rate Variability

Teemu Pukkila*, **Matti Molkkari, Esa Räsänen**
Computational Physics Laboratory, Tampere University, P.O. Box 692, FI-33014 Tampere, Finland

The time intervals between successive heart beats, that is, the interbeat intervals (IBIs), fluctuate in time in a complex manner. These fluctuations are commonly referred to as the heart rate variability (HRV). The HRV reflects the state of the autonomic nervous system, and it is widely utilized in most wrist monitors today to characterize, e.g., stress, sleep, physical performance and recovery [1].

The conventional HRV analysis is based on simple time- and frequency-domain measures computed from the IBIs. However, the IBI time series are highly non-stationary, irregular and contain trends dictated by the heart rate. Hence, *nonlinear* time-series analysis methods are needed to obtain detailed information on the IBI fluctuations. Detrended fluctuation analysis (DFA) stemming from random-walk theory in statistical physics [2] has been established as one of the main methods to describe the internal correlations of the IBI series through the scaling exponent α computed from the behavior of the fluctuation function [3] – see Fig. 1(a-c) as an example.

We have developed *dynamical* DFA (DDFA) that computes the scaling exponent $\alpha(t,s)$ as functions of both scale and time [4] – see Fig. 1(d) as an example. The fluctuation functions are calculated in maximally overlapping windows, yielding optimal time precision and thus a detailed view on the dynamic properties of the IBI correlations – and their changes – in real time. This is extremely useful in, e.g., detecting relevant physiological changes beyond the conventional and/or time-averaged HRV methods. DDFA has already been utilized in multiple HRV studies to characterize physical performance [4], sleep stages [5], and even the properties of heart cells under limited oxygen [6].

Here we focus on our most recent advances in the application of the DDFA method for HRV. In particular, we show how different cardiac diseases such as long-QT syndrome [7] can be detected and classified with the new measures – and how even the mortality can be assessed through the rest HRV alone. Secondly, we show how DDFA can be utilized to estimate the aerobic and anaerobic thresholds in the testing of athletic performance.

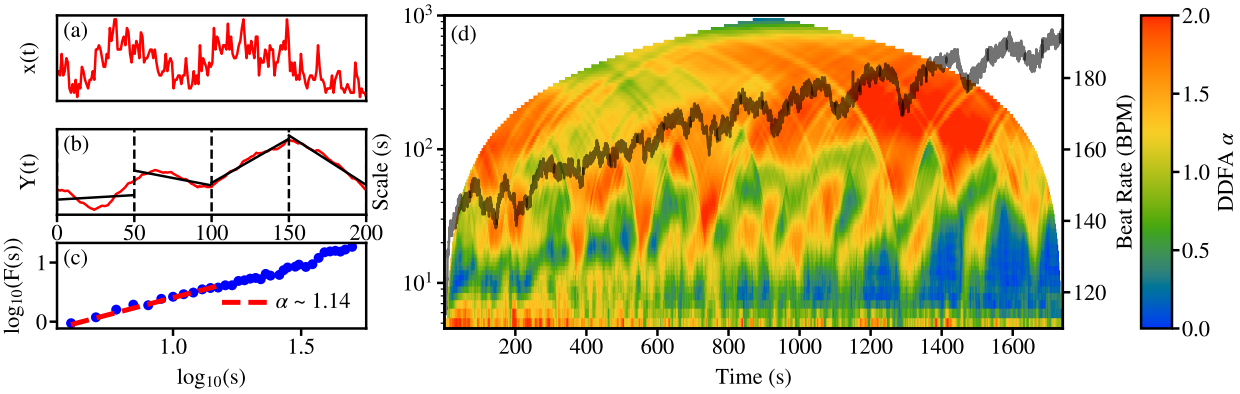

Fig. 1: Examples of detrended fluctuation analysis (DFA) and dynamical DFA (DDFA) algorithms. (a) Time series of 200 interbeat intervals (IBIs). (b) Integral of the IBIs split to 50-beat segments, together with their linear trends (least-squares fit). (c) Scaling exponent α calculated as the slope of the fluctuations as a function of the scale (in log-log scale). (d) DDFA landscape of $\alpha(t,s)$ (in colorscale) as functions of time and scale for running activity. Increasing effort towards the end of the activity is characterized by anticorrelations in the IBIs with $\alpha(t,s) < 0.5$ (blue regions).

References

[1] F. Shaffer, JP. Ginsberg, Frontiers in Public Health **5**, 258 (2017).
[2] C.-K. Peng, S. V. Buldyrev, S. Havlin, M. Simons, H. E. Stanley, A. L. Goldberger Physical Review E **49** 1685 (1994).
[3] C.-K. Peng, S. Havlin, H. E. Stanley, A. L. Goldberger, Journal of Nonlinear Science **5**, 1 (1995).
[4] M. Molkkari, G. Angelotti, T. Emig, E. Räsänen, Scientific Reports **10**, 13627 (2020).
[5] M. Molkkari, M. Tenhunen, A. Tarniceriu, A. Vehkaoja, S. L. Himanen, E. Räsänen, Computing in Cardiology **46** (2019).
[6] J. Kim, D. Shah, M. Molkkari, A. Lönnrot, K. Aalto-Setälä, E. Räsänen, Submitted to PLOS One (2023).
[7] T. Pukkila, M. Molkkari, J. Kim, E. Räsänen, Computing in Cardiology **49** (2022).

*Corresponding author: teemu.pukkila@tuni.fi

Halcyon and Ethos radiotherapy beam Monte Carlo model with CAD geometry implementation

Linda Laakkonen[*,1,2], **Jouko Lehtomäki**[1], **Antti Kulmala**[3], **Ari Harju**[1]
[1]Varian Medical Systems, a Siemens Healthineers Company, Helsinki, Finland
[2]Department of Physics, University of Helsinki, Finland
[3]Clinical Research Institute HUCH Ltd., Helsinki, Finland

Monte Carlo (MC) simulations can serve as computational model of the radiotherapy beams, and as such can explore the machine accuracy limits. The purpose of this work was to generate a computational model of the Halcyon and Ethos (Varian Medical Systems, a Siemens Healthineers Company) radiotherapy beam. The MC model was built on top of Geant4 and had a detailed representation of the treatment head geometry. The static treatment head components were modeled closely following the engineering drawings and the dual-layer multileaf collimator (MLC) was imported as computer-aided design (CAD) files. The information for the incident electron beam hitting to the target was achieved from an iterative electromagnetic solver.[1]

The Geant4 physics list "QGSP_BIC_EMZ" including extended electromagnetic physics configuration "EM Opt4" was used. The production cuts for secondary particle generation were set to 0.1 mm. The MC model was validated with high-precision measurements. With a high accuracy implementation of the MLC, the MC model was shown to be able to reproduce the radiation beam characteristics with both static and modulated plans. The static square fields were used to validate and confirm the incident electron beam model. The studied output factors for square fields were within 1% and the largest differences of 5% were found in the build-up region of PDDs and the penumbra region of profiles.

The MLC geometry was validated with more complicated MLC-shaped fields. Figure 1 shows dose planes at 5 cm depth of the film measurement, MC data, and the voxelwise difference between the MC and the measured data. The leaf movement direction is parallel to X-axis. In the positive Y-axis range, a tongue and groove design of the MLC edges has a clear impact on the dose distribution. On the negative Y-axis, where the collimation is static, three small gaps parallel in the leaf movement are created. The smallest static 2 mm gap is located between -1.0 cm and 0.0 cm, the 4 mm gap between -3.5 cm and -1.5 cm, and the largest 8 mm gap between -6.0 cm and -4.0 cm. The largest differences were found in the MLC leaf tip region due to the uncertainty of the MLC positioning and the machine-specific mechanical leaf gap (MLG). One feature of the positioning uncertainty is a known difference between a drive position (defined by a control point) and an actual position of the MLC leaf, i.e., the mechanical slack. This feature of a collimator design is significant especially when small fields and dual-layer MLC are introduced.[2]

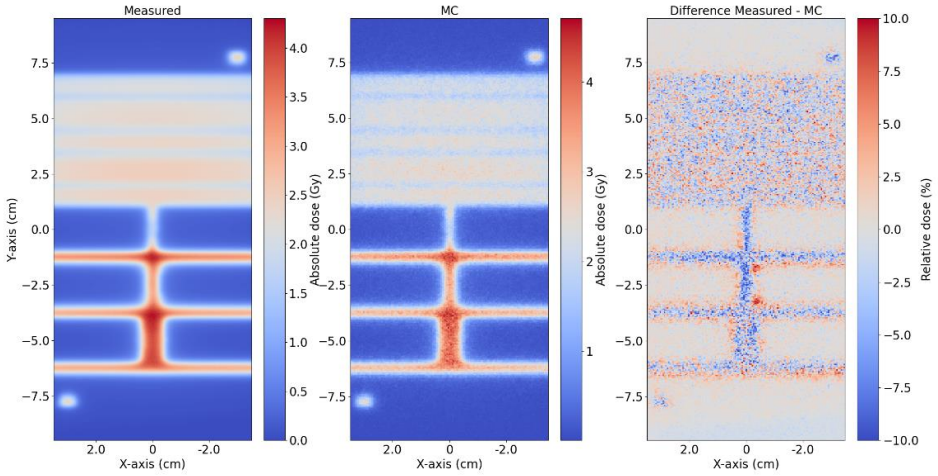

Figure 1 - Dose planes at 5 cm depth of the film measurement, MC data, and the voxelwise dose difference between the measured and MC data.

References

[1] L. Laakkonen, J. Lehtomäki, A. Cahill, M. Constantin, A. Kulmala, and A. Harju, Monte Carlo modeling of Halcyon and Ethos radiotherapy beam using CAD geometry: Validation and IAEA-compliant phase space, *Phys. Med. Biol.*, https://doi.org/10.1088/1361-6560/acb4d9, (2023)
[2] A. Kulmala, A. Rintala, L. Koivula, V. Petäjä and M. Tenhunen, A robust method for determining backlash of a multileaf collimator, poster, ESTRO (2022)

[*]Corresponding author: linda.laakkonen@varian.com

Can a one-day event trigger interest in quantum physics at the university level?

Daria Anttila[*,1], **Antti Lehtinen**[2,3], **Pekka Koskinen**[†,4]
[1] Department of Physics and Astronomy, University of Turku, 20014 Turku, Finland
[2] Department of Physics, University of Jyväskylä, 40014 Jyväskylä, Finland
[3] Department of Teacher Education, University of Jyväskylä, 40014 Jyväskylä, Finland
[4] NanoScience Center, Department of Physics, University of Jyväskylä, 40014 Jyväskylä, Finland

The ongoing second quantum revolution and the growing impact of quantum technologies on our society and economy are making quantum physics education ever more important. Consequently, there is a lot of research on quantum physics education for university students and even the general public. However, studying quantum physics or any other topic is primarily voluntary and thus a matter of personal interest – and it can only grow from a seed planted earlier. Here, we describe and analyze a one-day event designed to trigger interest and change perceptions about quantum physics among physics and mathematics students at a Finnish university. The data was collected from participants through questionnaires and complementary interviews. We found that the event made attitudes and views toward quantum physics more positive, versatile, and realistic. Although the event was too short to notably or permanently elevate the phase of interest when evaluated externally on a four-level scale, self-evaluations still reported an increased interest for most participants. Thus, it appears that even a short event can cultivate the ground to make it fertile for maintaining and developing interest further, for example, by well-designed and -timed quantum physics curriculum.

[*]Corresponding author: dariale@utu.fi
[†]Corresponding author: pekka.j.koskinen@jyu.fi

Student attitudes before, during and after the pandemic

Teemu Hynninen[*1], **Henna Pesonen** [1], **Olli Lintu** [1], **Petriina Paturi** [1]
1. Department of Physics and Astronomy, University of Turku, FI-20014, Turku, Finland

The COVID-19 pandemic lead to an extended period of remote teaching, which has had both positive and negative effects on student performance and wellbeing. It is likely that there are also long-term consequences, and we as teachers should seek to understand these consequences in order to help students overcome the problems they cause.

In this work, we study the attitudes of first year physics students towards physics before, during and after remote teaching [1]. We do this by comparing results from the Colorado Learning Attitudes about Science Survey from 2018 to 2022. We see that before the pandemic, students displayed a high level of expertlike attitudes both at the beginning of their studies and a year afterwards. In contrast, the students who had to study remotely during their first year at the university showed a decline in expertlike thinking after their first year of studies. Finally, the class that began their studies in 2021, after a year of remote learning in high school, displayed a lower level of expertlike thinking already as they began their studies. Some improvement was seen in their expertlike thinking after their first year of studies at the university, but these gains were not enough to close the gap compared to the students who began their studies before the pandemic.

References

[1] T. Hynninen, H. Pesonen, O. Lintu, P. Paturi, Phys. Rev. Phys. Educ. Res. **19**, 010101 (2023)

[*]Corresponding author: first.author@email.com

Assessment and physics instructional laboratories: A literature review and a model to design assessment for lab work

Laura Ketonen[1*], Antti Lehtinen[1,2†], Pekka Koskinen[2]
[1] Department of Teacher Education, University of Jyväskylä, P.O. 35, 40015 University of Jyväskylä
[2] Department of Physics, University of Jyväskylä, P.O. 35, 40015 University of Jyväskylä

Recent research on physics instructional labs for undergraduate education has highlighted many factors that increase the quality of teaching and learning e.g. the focus on learning objectives related to experimental skills [1] and the inclusion of open-ended elements in the lab tasks [2]. But as lab instruction is moving forward, what is the situation with educational assessment of lab work - is it moving forward as well? Generally, the research on educational assessment (i.e. assessment that produces information to the students themselves) has highlighted to need to conduct also formative assessment [3] i.e. assessment for learning, alongside with the summative assessment, i.e. assessment of learning. Research has also focused on the possible benefits of self and peer assessment alongside with the teacher assessment [4]. But have these suggestions made it through to physics instructional labs?

We have conducted a literature review (under review) focusing on educational assessment of labs. The review focused on studies published between the years 2000 and 2022. As the number of studies concentrating on physics instructional labs was quite small, we chose to also include chemistry education studies to the review. Through a screening process, 34 journal articles were chosen for the review.

The results show that 50 % of the studies concentrated at least partly on the assessment of experimental skills, 33 % on content knowledge and 24 % on so-called "meta skills" such as teamwork. Almost all the studies concentrated on at least partly on summative assessment and 59 % of studies focusing on at least partly on formative assessment. The most common form of formative assessment was feedback from the teachers or TAs that was given to a draft or the final product, e.g. lab report. 94 % of the reviewed studies focused on assessment conducted by a teacher or a TA with 23 % and 21 % focusing on self and peer assessment, respectively.

All in all, research on educational assessment and labs emphasizes assessment that is summative, teacher-led, and focuses on experimental skills and content knowledge. The scenery could be described with the word “traditional”. On the other hand, many of the studies presented new and experimental approaches to assessment.

Based on the results of the literature review and other literature on educational assessment we propose a model for designing educational assessment of labs. This model focuses on choosing appropriate learning objectives, assessment purposes and agents of assessment for any lab course.

References

[1] C. Walsh, H. J. Lewandowski, N. G. Holmes, Phys. Rev. Phys. Educ. Res. **18**, 010128 (2022).
[2] B. R. Wilcox, H. J. Lewandowski, Phys. Rev. Phys. Educ. Res. **12**, 020132 (2016).
[3] P. Black, D. William, Assess. Educ. **5**, 1 (1998).
[4] A. Jonsson, Act. Learn. High. Educ. **14**, 63 (2013).
[5] J. Tai, R. Ajjawi, D. Boud, P. Dawson, E. Panadero, High. Educ. **76**, 467 (2018).

*Corresponding author: laura.k.ketonen@jyu.fi
†Corresponding author: antti.t.lehtinen@jyu.fi

Defect generation in single-layer graphene upon sputter deposition of thin metal films

Franck L. Nadji Adjim*, Kostas Sarakinos
Department of Physics, University of Helsinki, Helsinki, Finland
*email: franck.nadjiadjim@helsinki.fi

Deposition of multifunctional metal contacts on two-dimensional (2D) materials is a key step in the fabrication of a wide array of optoelectronic, catalytic, and sensing devices. For the performance of such devices to be optimized, metal layers (i.e., contacts) should exhibit a well-defined morphology, while control of the structure and chemistry of the metal/2D-crystal interface is also required, without substantially modifying the pristine properties of the 2D material. Nowadays, metal layers (i.e., thin films) are routinely synthesized on 2D materials via vapor condensation using thermal or electron beam evaporation. Besides vapor-based methods, wet-chemistry approaches and electroless deposition have been employed for decorating graphene-based surfaces with metal nanoparticles [1-3]. All the above-mentioned deposition strategies suffer from lack of lateral film thickness and properties uniformity, while they do not provide the ability to control the atomic assembly kinetics during growth; a prerequisite for tuning metal-layer morphologies and film/substrate interface properties.

Magnetron sputtering is a vapor-based deposition technique that meets the requirements of large-scale film thickness and properties uniformity, while it offers access to a wide range of process parameters for tuning growth kinetics. However, it has been, up to now, deemed incompatible with metal-layer deposition on 2D materials, as it generates ample amounts of energetic neutral and ionized species, which create defects that compromise the pristine electronic and transport properties of the 2D crystals [1-3]. Recent combined experimental and theoretical data [1] indicated that defects during magnetron-sputter-deposition of Au layers on graphene primarily emanate from energetic species generated during neutralization and backscattering of Ar^+ ions at the sputtering cathode (i.e., target). This suggests that accurate and careful control of backscattered Ar energy and flux may allow defect-free deposition of metals on 2D crystals.

In this work, study defect generation in single-layer graphene (SLG) during deposition of metal layers using magnetron sputtering. Different metals layers (Au, Ag, Al, and Cu) with thicknesses of 20 Å are deposited on SLG/SiO_2/Si at two different working pressures (5 and 20 mTorr) with the purpose of investigating the the way by which the working pressure and the atomic mass of the sputtered species influence the vibrational properties of the underlying SLG substrate, as probed by Raman spectroscopy. The Raman spectrum of graphene exhibits three main vibrational modes (D ~ 1345 cm^{-1}, G ~ 1585 cm^{-1}, and 2D ~ 2680 cm^{-1}), while the intensity ratios I_D/I_G and I_{2D}/I_G provide information about the graphene structure. The data presented in this work show that the increase in working pressure induces fewer defect in the SLG. Moreover, increase of the atomic mass of the target material results in more pronounced damage in the SLG, most notably at low sputtering pressures. This provides further support to the the notion that damage is primarily caused by energetic backscattered Ar species.

[1] N. Pliatsikas, O. Karabinaki, M. Zarshenas, G.A. Almyras, I. Shtepliuk, R. Yakimova, J. Arvanitidis, D. Christofilos, K. Sarakinos, Appl. Surf. Sci. 566 (2021) 150661.
[2] M. Politou, I. Asselberghs, I. Radu, T. Conard, O. Richard, C.S. Lee, K. Martens, S. Sayan, C. Huyghebaert, Z. Tokei, S. De Gendt, M. Heyns, Appl. Phys. Lett. 107 (15) (2015) 153104.
[3] T. Cusati, G. Fiori, A. Gahoi, V. Passi, M.C. Lemme, A. Fortunelli, G. Iannaccone, Sci. Rep. 7 (2017) 5109.

Time Evolution of Transient Currents under the CdTe Metal Layer

Mihaela Bezak[*1,2], **Erik Brücken** [2], **Maria Golovleva** [1,2], **Matti Kalliokoski** [2], **Stefanie Kirschenmann** [2], **Nikita Kramarenko** [1,2], **Panja-Riina Luukka** [1,2], **Eija Tuominen** [2]

1. Lappeenranta-Lahti University of Technology, Yliopistonkatu 34, FI-53850 Lappeenranta, Finland

2. Helsinki Institute of Physics, University of Helsinki, Gustaf Hällströmin katu 2, FI-00014 University of Helsinki, Finland

CdTe is a prominent material for X-ray and γ-ray detection due to its high atomic number, wide band gap, and ability to operate under room temperature conditions. Like other compound semiconductors, it is difficult to grow it as a single crystal. In-homogeneities, such as precipitates and inclusions are the most common forms of defects present in the crystals. Not only do they make the material brittle, but they also influence the stability of the detector, especially pronounced in the Schottky-type, metal-semiconductor, configuration [1]-[2].

To study the impact of the in-homogeneities we used the scanning laser Transient Current Technique (TCT). With this method, electron-hole pairs are produced at a depth depending on the laser wavelength. Measurement of the produced current transients give us information about signal rise time, charge drift, and accumulation of charge in different parts of the detectors. Example of such measurements of area scan of titanium metallized CdTe surface with red laser are presented in Figure 1. Such detailed spatial maps of current transients can directly be linked to the electrical field deviations. Precipitates act as efficient trapping centres as well as they distort the linearity of the field around them. High concentrations of precipitates lead to progressive degradation of energy resolution and loss in charge collection efficiency, depending on their number, density, and size.

In this contribution, we present a detailed analysis of the current pulse shapes, effects of charge trapping and polarization on charge mobility and charge collection efficiency, and link the losses to different precipitates. We also investigate the ALD alumina-CdTe interface and negative fixed charge trapping using passivated CdTe crystals[3]-[4].

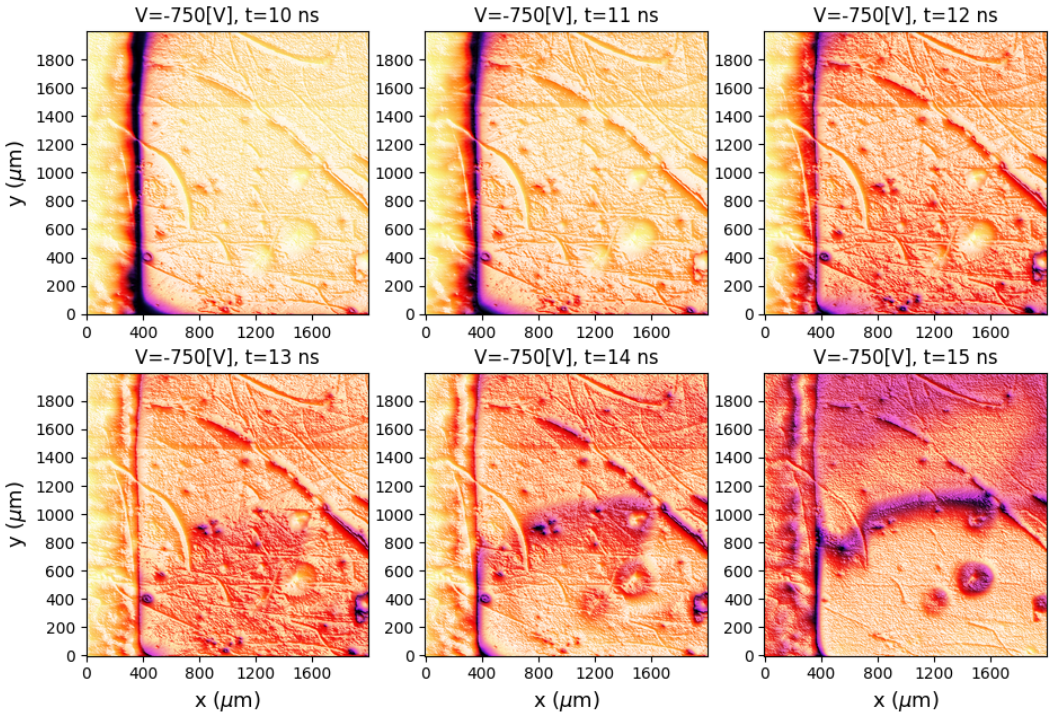

Fig. 1: Charge accumulation and drift over a time period of 5ns. Electron-hole pairs were generated by 660nm red laser light. Images were reconstructed from 202500 current waveforms recorded in the period of 72h.

References

[1] M. Kalliokoski et al., *Characterization and Identification of Defects in CdTe Detectors Using Scanning Laser Transient Current Technique*, Proceedings of 2020 IEEE Nuclear Science Symposium and Medical Imaging Conference (NSS/MIC) (2021)

[2] C. Buis et al., *Effects of dislocation walls on charge carrier transport properties in CdTe single crystal*, Nucl. Instrum. Meth. A **735** (2014), p.188-192.

[3] A. Gädda, et al., *Cadmium telluride X-ray pad detectors with different passivation dielectrics*, Nucl. Instrum. Meth. A, **924** (2019), pp. 33 – 37

[4] M. Bezak, et al., *Analysis and Characterization of CdTe Material Surface Defects*, J. Inst (2023), *In press, accepted for publication.*

*Corresponding author: mihaela.bezak@lut.fi

Micromagnetic simulations of magnetic domain wall dynamics in steel thin films

Sami Kaappa[*1], **Suvi Santa-aho** [2], **Mari Honkanen** [3], **Minnamari Vippola** [2,3], **Lasse Laurson** [1]

1. Computational Physics Laboratory, Tampere University
2. Materials Science and Environmental Engineering, Tampere University
3. Tampere Microscopy Center, Tampere University

Barkhausen noise is increasingly used in non-destructive testing (NDT) in various fields of industry that use steel. Barkhausen noise is understood as the noise signal in the magnetic response of a ferromagnetic material, driven by an applied field. This is generally known to originate from the jerky movement of magnetic domain walls as induced by the pinning effect of impurities in the microstructure of the material. Magnetic domain walls and their movement in thin films can be directly imaged via transmission electron microscope (TEM) in Lorentz mode [1]. In the on-going Academy of Finland -funded project BarFume we aim to connect the magnetic response of different types of steels to their microstructure, especially via the Barkhausen noise signal, by combining TEM imaging, state-of-the-art Barkhausen noise measurements, and micromagnetic simulations.

In the talk, we give a brief introduction on the Academy project and concentrate on the computational physics aspects of the problem. We simulate the dynamics of the magnetization via the Landau-Lifschitz-Gilbert equation

$$\frac{\partial \vec{M}}{\partial t} = \frac{\gamma}{1+\alpha^2}\left(\vec{M}\times\vec{H}_{\text{eff}} + \alpha\vec{M}\times\left(\vec{M}\times\vec{H}_{\text{eff}}\right)\right), \tag{1}$$

where $\vec{M}$ is the magnetization, $\vec{H}_{\text{eff}}$ the effective field, and γ and α constants. Using such a framework, we are able to reproduce some of the experimental TEM findings such as pinning of domain walls on carbide (Fe_3C) impurities in ferritic steel, as illustrated in Fig. 1. Similar but weaker pinning effect is predicted to occur by introduction of dislocations, whose magnetostrictive effect can be modeled via extra anisotropy terms in the effective field $\vec{H}_{\text{eff}}$ in Eq. 1.

The results obtained in the project deepen the understanding of the magnetic domain wall dynamics in the micron scale, as well as enhance the power of the Barkhausen noise applications by offering more accurate, physics-based predictions on ferromagnet microstructures based on the measured Barkhausen signal.

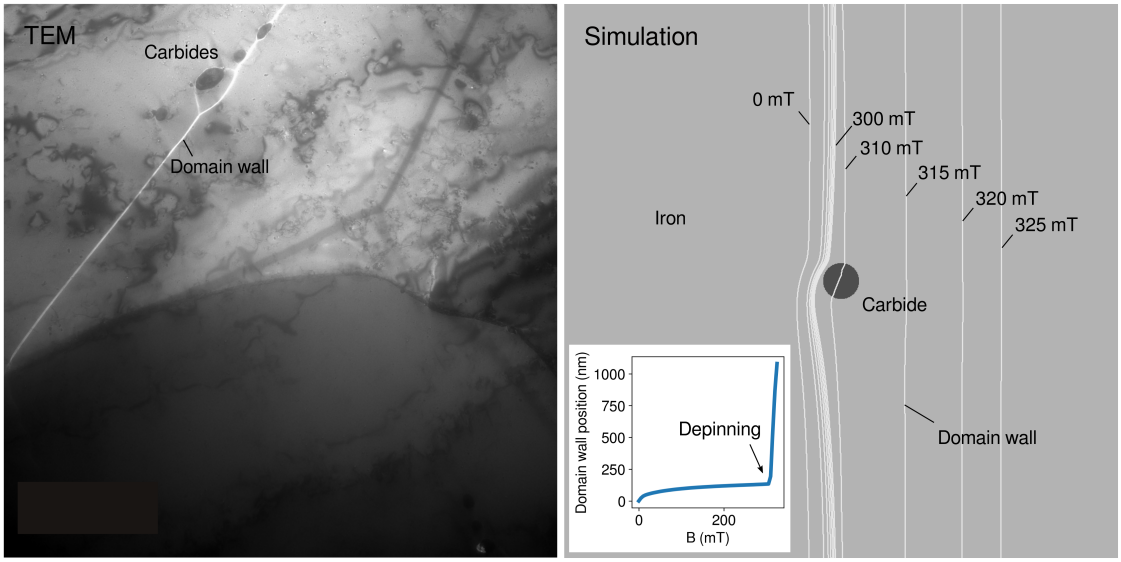

Fig. 1: Left: Overfocus TEM image (Lorentz mode). The domain wall is pinned by carbide impurities in the iron matrix. Image width is approximately 15 µm. Right: Micromagnetic simulation of a single magnetic domain wall moving over a spherical carbide. The domain wall configuration is shown at different out-of-plane field strengths, indicating the depinning field strength of approximately 310 mT. Sudden depinning of domain walls creates crackling noise in the magnetic response, referred to as Barkhausen noise. Image width approximately 3 µm.

References

[1] M. Honkanen, S. Santa-aho, L. Laurson, N. Eslahi, A. Foi, M. Vippola, Acta Materialia **221**, 117378 (2021)

[*]Corresponding author: sami.kaappa@tuni.fi

Superconducting properties of ion-irradiated disordered thin films

Katja Kohopää[*,1], Dibyendu Hazra[†,1], Alberto Ronzani[1], Robab Najafi Jabdaraghi[1], Arijit Bera[1], Mario Ribeiro[1], Emma Mykkänen[1], Jorden Senior[1], Mika Prunnila[1], Joonas Govenius[1], Janne Lehtinen[1], Antti Kemppinen[1]
[1] Institute 1, VTT Technical Research Centre of Finland Ltd, P.O. Box 1000, FI-02044 VTT, Finland

Ever since P. W. Anderson's celebrated work [1] on the Theory of Dirty Superconductors, it had been a paradigm that the critical temperature (T_c) of an S-wave superconductor is unaffected by disorder, as long the time-reversal symmetry is intact. However, it has been revealed that even a moderate amount of disorder can alter the T_c of S-wave superconductors. Subsequently, a large wealth of physics has been unearthed on different S-wave superconductors, for instance, the observation of the superconductor-insulator transition, strong phase fluctuations, pseudo-gap at normal state and inhomogeneous superconducting properties in a spatially homogeneous film.

In recent times, there has been a resurgence in the study of disordered S-wave superconductors, primarily driven by circuit quantum electrodynamics experiments at high magnetic field, and kinetic inductance and optical single photon detection— thanks to very high upper critical field and kinetic inductance of disordered S-wave superconductors. These, in turn, demand an understanding of the change in superconducting properties with the nature and quantity of the disorder for optimal device design and performance.

Here, we experimentally study the effect of the disorder on many different superconducting thin films, for instance, MoSi, NbN and Al [2,3]. The disorder in the films was introduced by ion irradiation, leading to the amorphization of these films. We characterize these films using high-resolution transmission electron microscopy and low-temperature electrical transport measurement and correlate their superconducting and structural properties. To discuss the variation in Tc of the studied films, we analyze the possible role played by the Coulomb interaction and the change in the Debye temperature. We comment on the fabrication parameter space for which the films are suitable for the application, for instance, for optical single photon detection.

References

[1] P. W. Anderson, Journal of Physics and Chemistry of Solids, **11**, 26 (1959)
[2] K. Kohopää, A. Ronzani, R. N. Jabdaraghi, A. Bera, M. Ribeiro, D. Hazra, E. Mykkänen, J. Senior, M. Prunnila, J. Govenius, J. Lehtinen, A. Kemppinen, in preparation (2023)
[3] E. Mykkänen, A. Bera, J. S. Lehtinen, A. Ronzani, K. Kohopää, T. Hönigl-Decrinis, R. Shaikhaidarov, S. E. de Graaf, J. Govenius, M. Prunnila, Nanomaterials, **10(5)**, 950 (2020)

[*]Corresponding author: first.author@email.com
[†]Corresponding author: presenting.author@email.com

Constructing two-dimensional heavy fermions in $NbSe_2$ heterstructures

Xin Huang (黄鑫)[*,1], Somesh C. Ganguli[1], Jiangxu Li (李江旭)[2], Jani Sainio[1], Jose L. Lado[†,1], Peter Liljeroth[§,1]
[1] Department of Applied Physics, Aalto University, Aalto, Finland
[2] Institute of Metal Research, Chinese Academy of Sciences, Shenyang, China

Heavy fermion systems are a fascinating arena for studying multiple competing electronic orders in a strongly correlated system, while almost all heavy fermion systems are found in three-dimensional bulk compounds with heavy rare-earth elements with *f*-electrons. Here, we push this heavy concept into a lighter compound niobium diselenide ($NbSe_2$) with only *d*-electrons and construct heavy fermion systems with a simple recipe of vertical two-dimensional (2D) heterostructures, by coupling the conduction electrons in 1H-$NbSe_2$ with the localized moments of triangular spin lattice formed by the charge density wave in 1T-$NbSe_2$. We use low-temperature scanning tunneling microscopy (STM) and spectroscopy (STS) to probe local density of states (LDOS) of the different stacking heterostructures with different exposed surface. These simple heterostructures show complex correlating electrons behavior, namely, the Kondo resonance and heavy fermion hybridization gap in a mixed-valence Kondo lattice, a bit away from half-filling. These two-dimensional systems are an exciting playground for exploring heavy fermion phase diagram and quantum criticality compared to bulk compounds, since conduction electrons and spin lattice are now de-coupled into separate two component monolayers and can be engineered separately. These viable alternative designer artificial systems can on-demand provide new possibilities to process the old open puzzle on heavy fermions.

[*] xin.huang@aalto.fi
[†] jose.lado@aalto.fi
[§] peter.liljeroth@aalto.fi

Interface effects on the elongation of embedded metal nanoparticles during swift heavy ion irradiation

Ville Jantunen[*1], **Aleksi Leino** [1] **Mihkel Veske** [2], **Andreas Kyritsakis** [2], **Henrique Vázquez Muiños** [1], **Kai Nordlund** [1], **Flyura Djurabekova** [1]

1. University of Helsinki, Department of Physics, PO Box 43, FI-00014 Helsinki, Finland

2. University of Tartu, Faculty of Science, Institute of Technology, Nooruse 1, Tartu, EE 50411, Estonia

Embedded metal nanoparticles have interesting optical properties that depend on their material, size, and shape, which offers new opportunities for future optoelectronic applications. Swift heavy ion irradiation is a known method for controlling the shape of embedded metal nanoparticles. While experimentally well documented, there still does not exist a universally accepted model on how exactly this shape change occurs. This phenomenon has been studied by molecular dynamics simulations and the temperature evolution after a swift heavy ion impact of the nanoparticle-embedding material system has been studied with the finite-difference and similar methods. However, the interface between the nanoparticle and the embedding material is difficult to model and it had always been simplified in both types of simulations.

In molecular dynamics, the interactions at the interface were often reduced to repulsive interactions for simplicity. As a byproduct some ad-hoc tricks had been used, i.e. artificial recrystallization between SHI-impacts when studying cumulative effects from multiple impacts. Here we present the results from a new interatomic potential for Au-nanoparticle and silica, which is a commonly used embedding material. With the use of this new potential, we gained new insights into the shape-changing process by being able to include the surface adhesion effects in the simulations. This also allowed us to minimize the use of ad-hoc solutions, while offering interesting insights on the role of ions impacts in close vicinity to the irradiatied nanoparticle. [1]

By solving the coupled partial differential equations simultaneously for heat propagation in electronic and lattice subsystem, one can extimate the temperatures that develop in the nanoparticle after the swift heavy ion impact. In the previous modelling efforts, the interface between Au nanoparticle and its surrounding were approximated as if only the thermodynamic parameters changed when moving from one material to another. We now address the issue of such simplification, which is likely to lead to inaccuracies in the temperature evolution. We consider the physics of interactions in the interface in greater details, taking into account the difference in the Fermi-level in Au and the bottom of the conduction band in silica as well as increased electron-phonon scattering at the interface and thermal insulance between the materials.[2]

Our improved model shows that surface adhesion plays important role in the evolution of Au nanoparticles embedded in silica irradiated with swift heavy ions and that the interface affects the thermal evolution of such systems. We find, that in both cases the interface has a major role in the results of the simulations and should be taken into account whenever studying swift heavy ion-induced shape modification.

References

[1] Aleksi Leino, Ville Jantunen, and Flyura Djurabekova. arXiv preprint arXiv:2204.10023 (2022)

[2] Ville Jantunen, Aleksi Leino, Mihkel Veske, Andreas Kyritsakis, Henrique Vázquez Muiños, Kai Nordlund, and Flyura Djurabekova. Journal of Physics D: Applied Physics 55, no. 27 (2022): 275301.

[*]Corresponding author: ville.jantunen@helsinki.fi

Determination of the magnetic twist in solar magnetic flux ropes

Ville-Vertti Linho*, **D. J. Price, J. Pomoell, E. K. J. Kilpua**
Department of Physics, University of Helsinki

Coronal Mass Ejections (CMEs) are gigantic magnetized plasma clouds erupting regularly from the Sun. They contribute to the energetic particle acceleration and some of them pass by the Earth and drive geospace storms with various space weather disturbances. The integral ingredient of CMEs are magnetic flux ropes. They are defined as coherent structures where magnetic field lines wind about a common axis. One of the key parameters related to solar flux ropes is the magnetic twist number, i.e., how much field lines wind about the common axis. The distribution of the twist can vary within the flux rope from one field line to another as well as the rate of the twist along the field line. Twist number is important to flux rope stability. If it exceeds a critical value the flux rope becomes kink unstable and can erupt from the Sun. Its number is, however, not straightforward to determine for practical purposes. This presentation introduces the concept of magnetic twist and presents the implications of different analytical flux rope models on twist.

*Corresponding author: ville-vertti.linho@helsinki.fi

MAFIAT: Magnetic Field Analysis Tools

D. J. Price, J. Pomoell, E. K. J. Kilpua
Department of Physics, University of Helsinki (daniel.price@helsinki.fi)

Magnetic flux ropes are coherent bundles of twisted magnetic field lines that wind about a common axis. These structures, formed at the Sun, evolve through footpoint motions, magnetic reconnection, and other processes. The degree of twist in the flux rope helps us to understand their evolution and potential eruption. This twist can be difficult to compute so it is often approximated such that the geometry of the flux rope is neglected. However, despite the relative simplicity of their computation, the results of these approximations require careful analysis to ensure proper understanding. Consequently, the magnetic field analysis tools (MAFIAT) Python package has been developed to compute the geometrically-based twist of coronal flux ropes. Here we describe MAFIAT's initial features, its Jupyter notebook-based operation, its scientific relevance, and our plans for its future development.

Modelling the interaction of Alfvénic fluctuations with Coronal Mass Ejections in the low solar corona

Chaitanya Sishtla[*1], **Jens Pomoell** [1], **Emilia Kilpua** [1], **Simon Good** [1], **Rami Vainio** [2]
1. Department of Physics, University of Helsinki, Helsinki, Finland
2. Department of Physics & Astronomy, University of Turku, Turku, Finland

Alfvénic fluctuations of various scales are ubiquitous in the solar wind[1], with their non-linear interactions and eventual cascade resulting in an important heating mechanism to accelerate the solar wind via turbulent heating[2]. These fluctuations may get processed by large-scale transient and coherent heliopsheric structures such as Coronal Mass Ejections (CMEs)[3]. In this study we investigate the interactions between solar wind Alfvénic fluctuations and CMEs using MHD simulations. We study the transmission of upstream solar wind fluctuations into the CME leading to the formation of CME sheath fluctuations. Additionally, we investigate the influence of the fluctuation frequencies on the extent of the CME sheath.

We use an ideal magnetohydrodynamic (MHD) model with an adiabatic equation of state. An Alfvén pump wave is injected into the quiet solar wind by perturbing the transverse magnetic field and velocity components, and a CME is injected by inserting a flux-rope modelled as a magnetic island into the quasi-steady solar wind. The resulting simulation snapshots are shown in Figure 1. The upstream Alfvén waves experience a decrease in frequency and change in the wave vector direction due to the non-spherical topology of the CME shock front. The CME sheath inhibits the transmission of low frequency fluctuations due to the presence of non-radial flows in this region. The frequency of the solar wind fluctuations also affect the steepening of MHD fast waves causing the CME shock propagation speed to vary with the solar wind fluctuation frequencies.

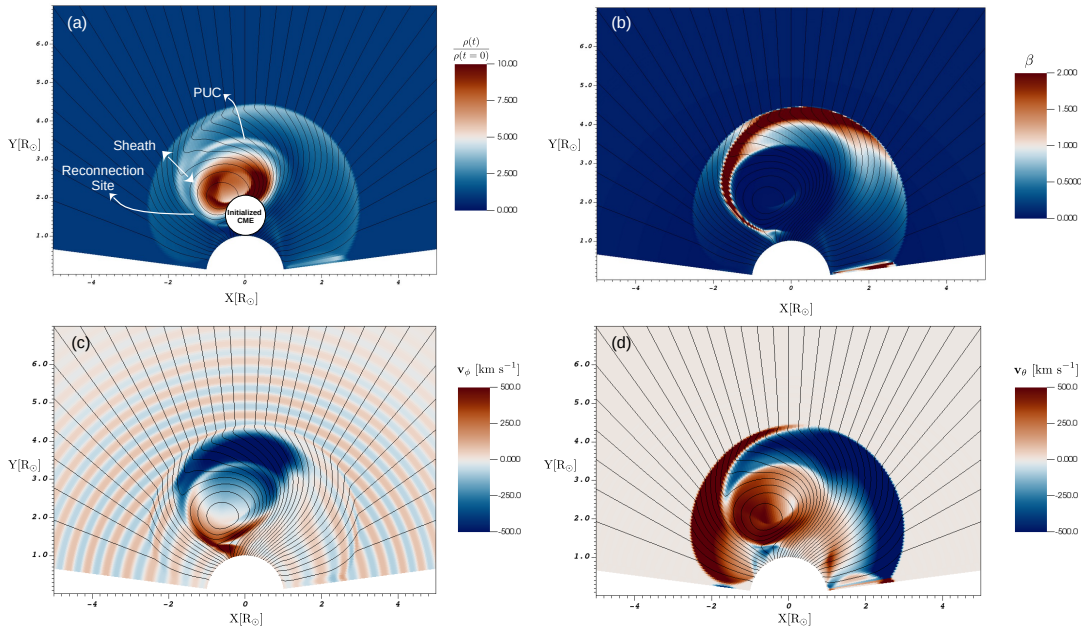

Fig. 1: Simulation snapshots of the propagating CME in the low corona at t = 10.8 mins. In (a) the colour intensity denotes the density compression compared to the quasi-steady solar wind, with annotations representing the PUC, sheath, and reconnection site. The plot in (b) shows the plasma beta, and (c), (d) present the out-of-plane velocity components $\mathbf{v}_\phi$ and $\mathbf{v}_\theta$ in the non-radial directions.

References

[1] Bale, S., Kellogg, P., Mozer, F., Horbury, T., Reme, H. 2005, Physical Review Letters, 94, 215002
[2] Zank, G. Matthaeus, W. 1992, Journal of plasma physics, 48, 85
[3] Kilpua, E. K., Fontaine, D., Good, S. W., et al. 2020 in , Copernicus GmbH, 999–1017

[*]Corresponding author: chaitanya.sishtla@helsinki.fi

Observing the Sun with the largest low-frequency radio telescope

Abstract

The Sun is a star that is very active in radio wavelengths. Solar eruptions such as flares and coronal mass ejections (CMEs) are dominated by the interactions between the magnetic fields and plasmas in the solar atmosphere. These processes can create supersonic shocks and accelerate particles that escaped into the heliosphere. Plasma shocks and the associated particle acceleration processes are usually accompanied by radio emissions, which can be used to diagnose the plasma parameters and pinpoint the location of particle acceleration. The Low-Frequency Array (LOFAR) radio telescope has made great contributions to solar and space weather studies in recent years. The high spatial, temporal, and frequency resolution and also high sensitivity have helped reveal unprecedented details of the radio emission from the Sun, including tracking electron beams in the solar atmosphere, high-spatial resolution observations of quiet Sun emission, and pinpointing emissions from CME shocks. Although LOFAR has excellent resolving power for plasma diagnostics and particle acceleration studies, it is not a solar-dedicated instrument but a general-purpose telescope. For solar and space weather observations, a dedicated solar observing campaign and continuous spectrum monitoring have been set up. In the observing campaign, there are simultaneous multi-mode observations providing high-time and -frequency resolution dynamic spectra and high spatial resolution interferometric imaging. For continuous spectrum monitoring, a prototype project is currently ongoing: Incremental Development of LOFAR Space Weather (IDOLS) using a single station to perform continuous calibrated dynamic spectrum observation for the Sun. Here, I will present the resolving capability of LOFAR in different observing modes, and how we use LOFAR imaging spectroscopy to inspect the energetic electrons and diagnose plasma parameters in the solar atmosphere.

Interstellar filament morphology and fragmentation in Orion Molecular Cloud 3

Emma Mannfors[*1], **Mika Juvela** [1], **Tie Liu** [2]
1. Department of Physics, University of Helsinki, Gustaf Hällströmin katu 2a, 00560 Helsinki, Finland
2. Shanghai Astronomical Observatory, Chinese Academy of Sciences, 80 Nandan Road, Shanghai 200030, People's Republic of China

Background
Stars are born within dense filaments in the cold interstellar medium (ISM). Thus, the properties of these filaments determine the characteristics of stars and planets. However, the formation mechanisms and evolution of filaments are still uncertain.

In recent decades, observations with the *Herschel* space telescope [1] have shown that filaments are ubiquitous within the ISM [2][3]. Filaments cover a wide range of scales, from the Galactic-scale Radcliffe wave [4], down to narrow fibers of widths ∼0.035 pc [5]. A filament may fragment into dense clumps and cores, which in the right conditions can form stars. Mass of forming stars is related to filament size, with the highest-mass stars almost exclusively being formed within dense infrared dark clouds with column densities above 10^{23} cm^{-2} [6]. In recent years, a universal filament width of ∼0.1 pc has been proposed [7][8][9], possibly indicative of changes in interstellar turbulence [10] or magnetohydrodynamic waves [11]. This universal width has, however, been called into question [12][13], as filament widths seem to be correlated with distance to the filament [14]. To understand this width would help to understand the internal mechanics of the ISM, the evolution of the gas, and the early stages of star formation (SF).

Aims
We have analyzed a massive star-forming filament at two angular resolutions, in order to gain a multiscale picture of the region. We study whether derived filament properties, such as mass, width, and clump gravitational stability, change depending on the resolution of the observations. We further study how fragmentation of the filament changes at various spatial scales.

Our source and observations
We have observed OMC-3, a dense star-forming cloud, in the infrared using the *Herschel* space telescope (resolution ∼ 20") and the ArTéMiS instrument (resolution ∼10" [15]) on the Atacama Pathfinder Experiment (APEX) telescope [16] (Fig. 1a,b). OMC-3 is located toward the northern end of the Orion Molecular Cloud (OMC), the nearest high-mass star-forming region (d ∼400 pc, [17]). It is at an early state of SF, with multiple young stellar objects along the OMC-3 filament [18][19]. Unlike the rest of the cloud, OMC-3 is not yet affected by feedback from young massive stars [20]. However, this region shows high column densities above 10^{23} cm^{-2} across the main filament. Studies of the magnetic field of OMC-3 suggest the region may represent filaments forming through collision-induced magnetic reconnection [21].

Results
The inclusion of higher-resolution data changes derived parameters. Using only *Herschel* data, we detect the characteristic 0.1 pc width, as well as large clumps which are not gravitationally bound. Observing the same region with the inclusion of ArTéMiS data reveals several bound clumps, as well as widths significantly under the characteristic width (Fig. 1c). The multi-scale, interconnected nature of the ISM is apparent within these data. We further have performed simulations on the accuracy of fitting filament properties, studying how various factors, such as observational noise, affect derived properties.

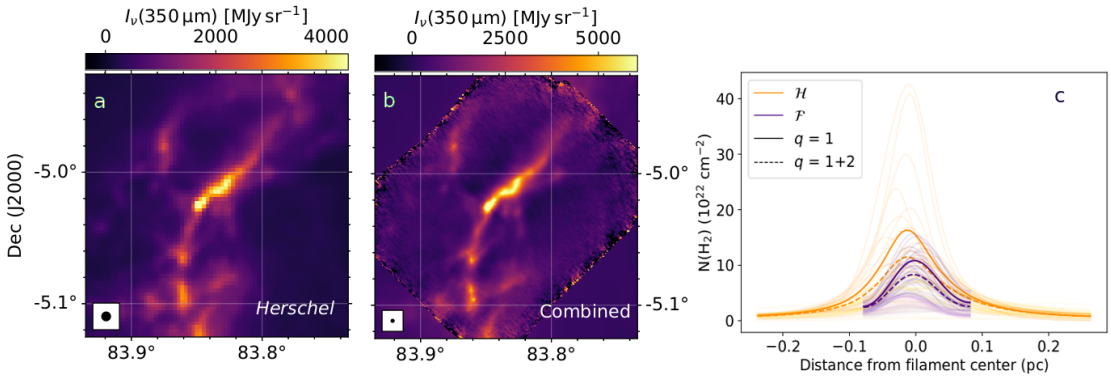

Fig. 1: (a-b) OMC-3 imaged with *Herschel* (a; FWHM∼20") and the combined *Herschel* and ArTéMiS data (b; FWHM∼10"). (c) The profiles of the *Herschel* data (orange) and combined data (purple). The bold lines show mean filament profiles in each dataset. q refers to the quality of the profile, with q = 1 profiles having the highest signal-to-noise.

References

[1] G.L. Pilbratt, J.R. Riedinger, et al., A& A **518** L1 (2010) [2] D.M. Elmegreen, B.G. Elmegreen, AJ, **84** 615 (1979) [3] P. André, A. Men'shchikov, et al., A& A **518** L102 (2010) [4] J. Alves, C. Zucker, et al., Nature **578** 237 (2020) [5] A. Hacar,M. Tafalla, et al., A& A **610** A77 (2018) [6] S.J. Carey, F.O. Clark, et al., ApJ **508** 721 (1998) [7] D. Arzoumanian, P. André, et al., A& A **529** L6 (2011) [8] P. André, J. Di Francesco, et al., Protostars and Planets VI **27** (2014) [9] M. Juvela, J. Malinen, et al., A& A **544** A141 (2012) [10] P. Padoan, M. Juvela, et al., ApJ **553** 227 (2001) [11] P. Hennebelle & P. André, A& A **560** A68 (2013) [12] R.J. Smith, S.C. Glover, et al., MNRAS **445** 2900 (2014) [13] G.V. Panopoulou, S.E. Clark, et al., A& A **657** L13 (2022) [14] A. Rivera-Ingraham, I. Ristorcelli, et al., A& A **591** A90 (2016) [15] V. Revéret, P. André, et al., SPIE conference series **9153** (2014) [16] R. Güsten, L.Å. Nyman, et al., A& A **454** L13 (2006) [17] J.E. Großschedl, J. Alves, et al., A& A **619** A106 (2018) [18] S.T. Megeath, R. Gutermuth, et al., AJ **144** 192 (2012) [19] S. Takahashi, P. Ho, et al., ApJ **763** 57 (2013) [20] S. Suri, Á. Sánchez-Monge, et al., A& A **623** A142 (2019) [21] S. Kong, D. Whitworth, et al., MNRAS **517** 4 (2022)

*Corresponding author: emma.mannfors@helsinki.fi

Analysis of observations of thermal dust emission: the complexity of the modified blackbody function

Mika Juvela[*1],
1. Department of Physics, University of Helsinki, Gustaf Hällströmin katu 2, FI-00014, University of Helsinki

The dust far-infrared (FIR) spectra are commonly fitted using the modified blackbody model (MBB) that consists of a single temperature component. This is known to result in biased column density estimates, because the real sources (such as interstellar clouds or entire galaxies) always contain a range of temperatures. With good multi-frequency observations, the bias could be reduced by the use of more complex models. These may employ parametric temperature distributions or multiple discrete temperature components, potentially also with different spectral indices. However, temperatures and spectral indices tend to be partly degenerate, which leads to large uncertainties when the temperature distributions are poorly constrained and the observation contain noise [1][2][3]. Bayesian models can mitigate the problems caused by the observational noise, although, by restricting the distributions of the temperature and spectral index values, they can also lead to some systematic errors [4]. The point process mapping (PPMAP) [5] is a widely used implementation of the Bayesian multi-component MBB fitting. However, it is computationally costly, meaning that the analysis of large FIR maps can take days.

We have investigated alternative implementations of the multi-component MBB model fitting routines. The models consist of a sum of N MBB functions with different discrete temperatures and fixed spectral indices (N-MBB models) or a sum of N more general template spectra (N-TMPL models). We analysed observations that range from simple toy models to synthetic observations of magnetohydrodynamic simulations of high-mass star forming regions.

We find that the reliability of multi-component models is limited by the need for strong regularisation, and one must be careful that the selected priors are appropriate for the observations in question. Contrary to common wisdom, the fitting can be done using standard numerical methods, even when the model includes convolutions with wavelength-dependent telescope beams. With some limitations on the priors, the N-TMPL models can be fitted in Fourier space, in which case the run times are counted in seconds rather than days, especially when the calculations are sped up by the use of GPU computing. However, also the single-MBB model remains a valid alternative due to its small number of parameters and well-understood bias properties. Combined with empirical corrections, it can provide a more robust and computationally faster alternative to the more complex MBB models.

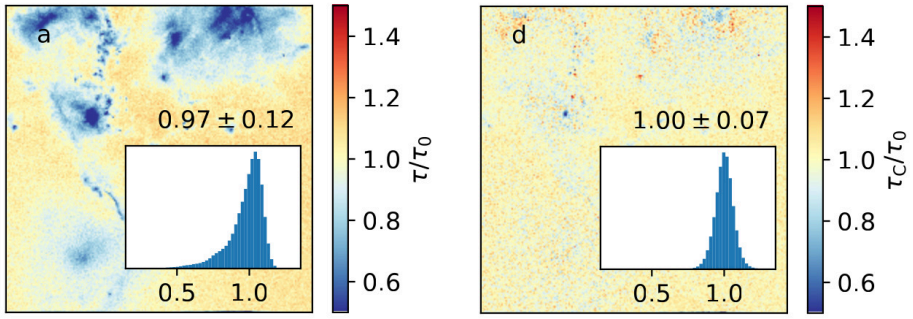

Fig. 1: Ratios between estimated and true optical depths in the case of a simulated star-forming cloud. The synthetic observations mimic those made with the *Herschel* satellite. On the left, the estimates have been calculated with basic 1-MBB fits that nevertheless use all the observed frequency maps at their native resolution. The right frame shows the estimates after a simple empirical correction that was derived by training a small neural net with similar synthetic observations.

References

[1] M. Juvela, N. Ysard, *The effect of temperature mixing on the observable (T,β)-relation of interstellar dust clouds*, Astronomy and Astrophysics, **539**, A71 (2012)
[2] M. Juvela, N. Ysard, *The degeneracy between the dust colour temperature and the spectral index. The problem of multiple χ^2 minima*, Astronomy and Astrophysics, **541**, A33 (2012)
[3] M. Juvela, J. Montillaud, *Estimation of high-resolution dust column density maps. Empirical model fits*, Astronomy & Astrophysics **5**57, A73, (2013)
[4] M. Juvela, J. Montillaud, N. Ysard, N., T. Lunttila, *The degeneracy between dust colour temperature and spectral index. Comparison of methods for estimating the $\beta(T)$ relation*, Astronomy and Astrophysics, **556**, A63 (2013)
[5] K .A. Marsh, A.P. Whitworth, O. Lomax, *Temperature as a third dimension in column-density mapping of dusty astrophysical structures associated with star formation*, MNRAS **454**, 4282
[6] M. Juvela, *Comparison of modified blackbody fits for estimation of dust optical depths*, submitted (2023)

[*]Corresponding author: mika.juvela@helsinki.fi

Lyman-α constraints on non-standard dark matter

Deanna C. Hooper[*1]

1. Department of Physics and Helsinki Institute of Physics, PL 64, FI-00014 University of Helsinki, Finland

The nature of dark matter remains one of the biggest mysteries in cosmology. In the standard model of cosmology – known as ΛCDM – dark matter is cold and collisionless. However, despite its remarkable success in explaining observations at many scales, the standard ΛCDM paradigm has been challenged lately by significant tensions and mismatches between different datasets. This has fuelled interest in beyond-ΛCDM models, such as those in which dark matter can interact or have non-negligible velocities. In these models (known by the umbrella term *non-standard dark matter*), dark matter prevents small cosmic structures from forming, therefore inducing a suppression of the matter power spectrum on small scales. This makes them an ideal target to be constrained with Lyman-α forest data, which maps the matter distribution in the intergalactic medium. In this talk I will discuss a new method we developed to use Lyman-α data without needing the usual computationally-expensive hydrodynamical simulations. I will also present our recent competitive bounds for several non-standard dark matter models, highlighting the broad range of applicability of this method.

[*]Corresponding author: deanna.hooper@helsinki.fi

Toward an unbiased flow measurements in LHC pp collisions

M. Virta[†,1,2], T. Kallio[*,1], D.J. Kim[††,1,2]
[1] *University of Jyväskylä, Department of Physics, P.O. Box 35, FI-40014 University of Jyväskylä, Finland*
[2] *Helsinki Institute of Physics, P.O Box 64, FI-00014 University of Helsinki, Finland*

Long-range correlations for pairs of charged particles with two-particle angular correlations are studied in pp at $\sqrt{s} = 13$ TeV with various Monte Carlo (MC) generators. The correlation functions are constructed as functions of relative azimuthal angle $\Delta\varphi$ and pseudorapidity separation $\Delta\eta$ for pairs of various particle species with the identified hadrons such as π, K, p, and Λ in wide η ranges.

Fourier coefficients are extracted for the long-range correlations in various high-multiplicity classes using the low-multiplicity template fit method [1]. The method allows to subtract the enhanced away-side jet fragments in high-multiplicity with respect to low-multiplicity events. However, we found that due to a kinematic bias on jets and differing model implementation of the flow and jet components, subtracting the non-flow contamination in small systems can bias the results. It was found that PYTHIA models where collective flow is not expected but the bias results in very large flow.

We found that mass ordering at low p_{T} and particle type grouping in an intermediate p_{T} range found in large systems such as PbPb collisions are also present in AMPT String Melting model. However, extracting flow signals from the EPOS and PYTHIA Shoving models is not possible because of flow signal introduced in the low-multiplicity events. In this talk, the summary of these results and a possible solution to overcome these biases will be discussed.

References

[1] G. Aad et al. (ATLAS), Observation of Long-Range Elliptic Azimuthal Anisotropies in $\sqrt{s} = 13$ and 2.76 TeV pp Collisions with the ATLAS Detector, *Phys. Rev. Lett.* 116, 172301 (2016), arXiv:1509.04776 [hep-ex].

[*]Corresponding author: teemu.p.kallio@student.jyu.fi
[†]Corresponding author: maxim.virta@cern.ch
[††]Corresponding author: dong.jo.kim@cern.ch

Multi-Jet Merging in Deep Inelastic Scattering with Pythia

Joni Laulainen[*1,2], **Ilkka Helenius** [1,2], **Christian T. Preuss** [3]
1. University of Jyvaskyla, Department of Physics, P.O. Box 35, FI-40014 University of Jyvaskyla, Finland
2. Helsinki Institute of Physics, P.O. Box 64, FI-00014 University of Helsinki, Finland
3. Institute for Theoretical Physics, ETH, CH-8093 Zürich, Switzerland

Deep inelastic scattering (DIS) in high-energy electron-proton collisions provides a clean process to study hadron structure and dynamics of quantum chromodynamics (QCD). In this process, the incoming electron interacts with the inner constituents of the hadron by exchanging a highly-virtual photon, breaking the hadron. Such processes have been extensively studied with the HERA collider in DESY. Thanks to the upcoming Electron-Ion Collider (EIC), planned to launch in the near future at Brookhaven National Laboratory [1], we expect to have plenty of new high-precision data for DIS within the next ten years. Furthermore, having accurate predictions and simulations will help the EIC collaborations to optimize the experiments that are currently being designed.

Monte Carlo (MC) event generators are the leading approach in the numerical modeling of scattering events. These are built upon collinear factorization where the hard scattering cross sections can be calculated from the perturbative QCD. The subsequent radiation is then generated with DGLAP-based parton showers that are complemented with a hadronization model to provide the full exclusive final state that can be directly compared to experimental results. The DGLAP equations are derived in a collinear and infrared limit, and as such, are not best suited to model hard, well-separated jets that are key observables for many QCD studies. In the recent years there have been plenty of development in event generators that have been driven by the data coming from proton-proton collisions at the LHC. In particular, a field that advanced significantly is the combination of parton-showers and higher order corrections to hard-scattering cross sections, allowing for complete simulations also for events with multiple high-energy jets. A key challenge in this procedure is to avoid double-counting of different event classes. Such jet merging algorithms have successfully been implemented for LHC-processes [2].

In our current project we aim to improve the modeling of DIS within Pythia, the most widely-used MC event generator among the LHC experiments [3]. As a first step we are working on adding the jet-merging capabilities also for DIS process. Here we will apply the recently implemented new parton shower Vincia, in which the merging can be efficiently performed. Instead of relying on the Born-level hard events and the parton shower algorithm to produce jets, we use external hard events with higher multiplicity final-states that are then combined with the parton shower. Such modelling has been performed for DIS within the Sherpa MC generator, where they found significant effects from jet merging to be necessary to describe experimental data [4]. In this talk we summarise the state of our project, and compare our results to experimental data from HERA [5].

References

[1] R. Abdul Khalek, A. Accardi, J. Adam, *et al.* Nucl. Phys. A **1026** (2022)
[2] H. Brooks and C. T. Preuss, Comput. Phys. Commun. **264** (2021)
[3] C. Bierlich, S. Chakraborty, N. Desai, *et al.*, SciPost Phys. Codebases 8 (2022)
[4] T. Carli, T. Gehrmann and S. Hoeche, Eur. Phys. J. C **67** (2010)
[5] H. Abramowicz *et al.* [ZEUS], Eur. Phys. J. C **70** (2010)

[*]Corresponding author: joollaul@jyu.fi

Improving Bayesian parameter estimation with the latest RHIC and LHC data including a new initial conditions model

Maxim Virta[*1], **Dong Jo Kim**[†1], **Jasper Parkkila**[‡ 2]
1. University of Jyväskylä,
2. CERN

The evolution of the strongly interacting medium is modelled with hydrodynamic models, which are driven by a large number of parameters quantifying properties of the medium. The need to find model parameters, which give the best description of the experimental data imposes a multidimensional optimization problem. The Bayesian analysis has shown to be very effective in constraining the parameter values [1], and the combined inclusion of LHC Pb–Pb 5.02 and 2.76 TeV data with additional flow observables has greatly narrowed down the uncertainties [2]. Figure 1 showcases the reduction in uncertainty for the specific shear and bulk viscosities.

In this talk, we present our latest study in inferring transport properties of the QGP by an improved Bayesian analysis using the RHIC Au–Au collision data in addition to the previous studies [1, 2] where only the LHC data were used. With the RHIC data more interest is evoking towards the initial state of the system. More interestingly it has been shown that the correlator $\rho(v_n^2, [p_T])$ is sensitive to the initial state parameters nucleon width and σ_{NN} [3]. To fully capture the initial state parameters we are employing another initial conditions model called EKRT while also studying the effect of $\rho(v_n^2, [p_T])$ on TRENTo model.

Furthermore, we will quantify the sensitivities of newly developed flow observables, Asymmetric Cumulants and Symmetry Plane Correlations as well as the $\rho(v_n^2, [p_T])$ observable to the model parameters.

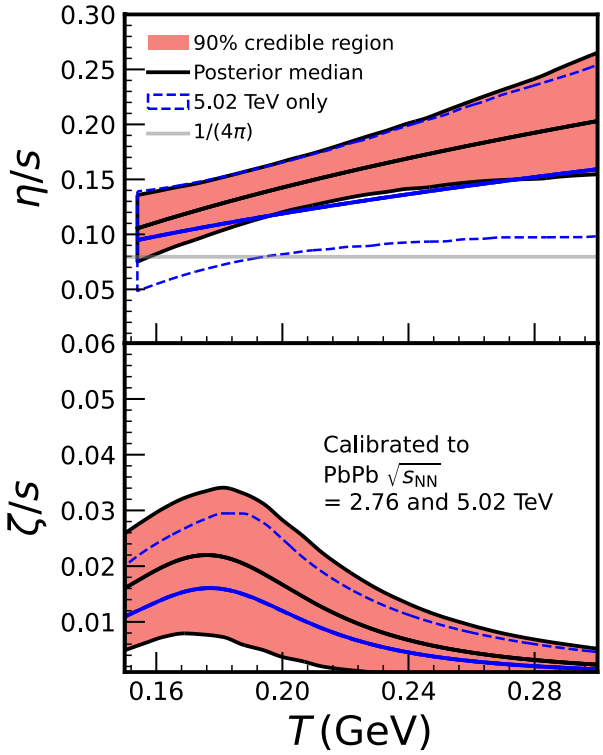

Fig. 1: Posterior distributions for specific shear and bulk viscosity are shown for results from Ref. [2] (red) in comparison with Ref. [1] (blue).

References

[1] J. E. Parkkila, A. Onnerstad, and D. J. Kim. Bayesian estimation of the specific shear and bulk viscosity of the quark-gluon plasma with additional flow harmonic observables. *Phys. Rev. C*, 104(5):054904, 2021.

[2] J.E. Parkkila, A. Onnerstad, S.F. Taghavi, C. Mordasini, A. Bilandzic, M. Virta, and D.J. Kim. New constraints for qcd matter from improved bayesian parameter estimation in heavy-ion collisions at lhc. *Physics Letters B*, 835:137485, 2022.

[3] Govert Nijs and Wilke van der Schee. Hadronic nucleus-nucleus cross section and the nucleon size. *Phys. Rev. Lett.*, 129:232301, Nov 2022.

[*]Corresponding author: maxim.virta@cern.ch
[†]Corresponding author: dong.jo.kim@cern.ch
[‡]Corresponding author: jasper.parkkila@cern.ch

Flavour-universal NSI and light mediators

Timo J. Kärkkäinen[*1], **Zoltán Trócsányi** [2]
1. National Institute of Chemical Physics and Biophysics, Rävala pst 10, Tallinn, Estonia
2. ELTE Eövtös Loránd University, Pazmany Péter sétány 1/A, XXXX Budapest, Hungary

Nonstandard neutrino interactions (NSI) arising from light and heavy mediators coupled to neutrinos. Production of these heavy NSI-mediator particles requires next-generation particle accelerator experiments, while the light NSI-mediators can be produced by improving the luminosity and intensity of particle accelerator instead of the centre-of-mass energy. Low energy neutrino experiments are an emerging field of research providing exciting research avenues on light NSI. For flavour-universal NSI neutrino oscillation is unaffected, but recent measurements on coherent elastic neutrino-nucleon scattering provide the first bound for flavour-universal light mediator NSI. In my talk, I will discuss light and heavy mediator NSI and the emerging bounds on flavour-universal models, and a specific example model, an U(1) extension of the Standard Model.

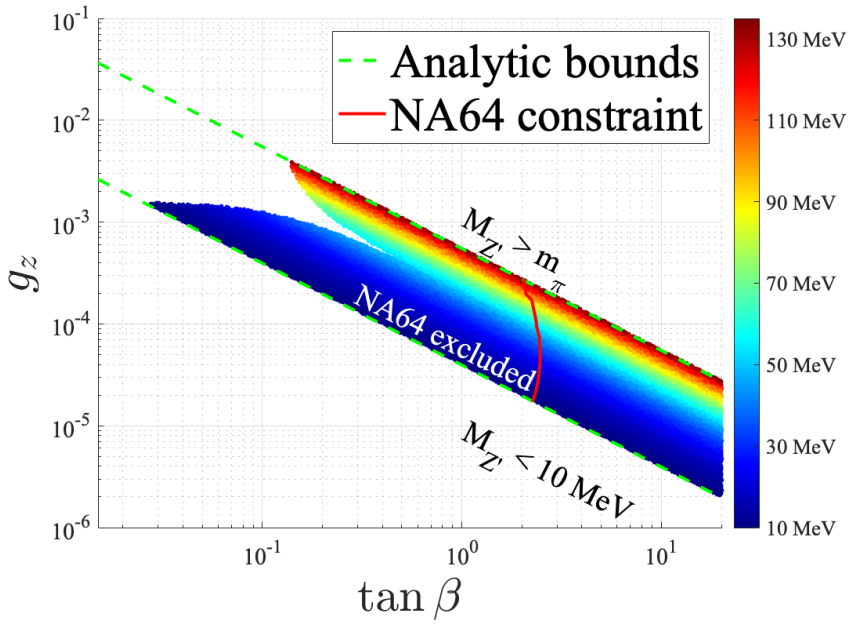

Fig. 1: Available parameter space in $(\tan\beta, g_z)$ plane, where $\tan\beta$ is the ratio of vacuum expectation values of the SM Higgs and the new scalar in U(1) extension, and g_z is the gauge coupling of the new U(1) gauge symmetry.

References

[1] T. J. Kärkkäinen, Z. Trócsányi, J.Phys.G **49** (2022) 4, 045004, arXiv: 2105.13360 [hep-ph]
[2] T. J. Kärkkäinen, Z. Trócsányi, arXiv: 2301.06621 [hep-ph]

*Corresponding author: karkkainen@kbfi.ee

Real scalar phase transitions: bubble nucleation, nonperturbatively

Oliver Gould[1], **Anna Kormu**[*2], **David Weir** [2]
1. School of Physics and Astronomy, University of Nottingham, Nottingham NG7 2RD, United Kingdom.
2. Department of Physics and Helsinki Institute of Physics, P.O. Box 64, 00014 University of Helsinki, Finland.

As the universe cooled down from its initial hot plasma state it might have gone through a phase transition at roughly one picosecond after the Big Bang. The transition can be thought of as the cosmological equivalent to the freezing of water. In the Standard Model (SM) of particle physics, no such transition is present, but in the so-called beyond the SM models this is a well-motivated possibility. First, they could help us with explaining why there is more matter than antimatter in the universe. Second, they could produce a gravitational wave (GW) signal that is still detectable today. Furthermore, this signal lies in the detection range of upcoming space-based GW detector LISA, that is launching in the early 2030s.

Modelling these GWs and the particle physics processes that give rise to them in the first place is challenging. Perturbation theory is commonly used to estimate the parameters that enter the calculation of GW spectra. However, perturbation theory is known to run into problems at the regime we are interested in and furthermore it is important to test the reliability of existing results. Here I will discuss our recent results where we studied a real singlet scalar model with a tree level potential barrier and performed nonperturbative simulations to determine the bubble nucleation rate. Our preliminary results show good agreement with perturbation theory, and we expect our findings to allow calibration of the systematic uncertainty in perturbative results.

[*]Corresponding author: anna.kormu@helsinki.fi

Neutrino density matrix formalism derived from Kadanoff-Baym equations

Henri Jukkala[*1,2], **Kimmo Kainulainen**[†1,2], **Harri Parkkinen**[‡1,2]
1. Department of Physics, PL 35 (YFL), 40014 University of Jyväskylä, Finland
2. Helsinki Institute of Physics, PL 64, 00014 University of Helsinki, Finland

When neutrinos propagate in medium, they encounter coherent and incoherent collisions. Due to the coherent collisions a background potential arises which modifies the energy eigenstates of neutrinos. Incoherent collision in turn lead to quantum damping which affects the dynamical evolution of neutrinos and can have significant effect on neutrino propagation.

In this talk it is discussed how to derive a formalism, which describes mixing of relativistic neutrino fields while including flavor coherence and all particle-antiparticle coherence effects, from the fundamental grounds of thermal quantum field theory [1]. We begin by deriving the general Kadanoff-Baym (KB) equations in the Wigner space starting from the contour Schwinger-Keldysh euqation. Next the KB equations are solved using the coherent quasiparticle approximation (cQPA). The key point of the cQPA scheme is that it relinquishes the approximation of translationally invariant propagators from which it follows that the phase space of the propagators consists of novel shell solutions in addition to the usual mass shell solutions. These new shells can be recognized to carry information about non-local quantum coherence for which the cQPA scheme can be used to study many out-of-equilibrium quantum systems.

This talk is therefore focused on describing how the standard neutrino density matrix equations can be derived from more fundamental grounds than has been done before. The derived equations of motion include incoherent collisions, neutrino flavor mixing and all particle-antiparticle coherence effects without assuming any symmetry from the system, such as homogeneity and isotropy. We develop also a systematic way to compute collision terms while including flavor coherence and all particle-antiparticle coherence effects. Thus, the derived equations can be used for example to study the significance of particle-antiparticle coherence for light and heavy neutrinos in various scenarios.

References

[1] H. Jukkala, K. Kainulainen, H. Parkkinen, "Neutrino density matrix formalism derived from Kadanoff-Baym equations". In preparation.

[*]Corresponding author: henri.a.jukkala@student.jyu.fi
[†]Corresponding author: kimmo.kainulainen@jyu.fi
[‡]Corresponding author: harri.h.parkkinen@jyu.fi

Superconducting quantum light-emitting diodes using two-dimensional material superlattices

Yuvraj Chaudhry[†1,2], LD Varma Sangani[1], Marios Matheou[1], Ethan Minot[1,3], Zhipei Sun[4], Pertti Hakonen[1,2]
[1] QTF Centre of Excellence, Department of Applied Physics, Aalto University, Po Box 15100, FI-0076 AALTO, Finland
[2] InstituteQ – The Finnish Quantum Institute, Aalto University Foundation, Otakaari 1, FI-02150 Espoo, Finland
[3] Department of Physics, Oregon State University, U.S.A.
[4] QTF Centre of Excellence, Department of Electronics and Nanoengineering, Aalto University, Finland

There is a great demand for efficient sources of entangled photons, but current methods of creating them are highly inefficient, bulky and non-deterministic. Highly efficient electrically pumped entangled light sources have the potential to unlock, e.g., distributed large scale quantum computing distribution and facilitate quantum photonic applications such as communication, sensing and imaging [1]. Our approach is based upon the conversion of Cooper pairs into photon pairs [2] wherein Cooper pairs are injected into a semiconductor diode and recombination in the active layer results in production of entangled photons. Such devices, called Superconducting Quantum Light Emitting Diodes (SQ-LED) may provide the awaited technological solution.

For now, high electron transmission via superconductor-semiconductor interfaces and appropriate band alignment for optimal SQ-LED design are being studied, and van der Waals stacking schemes have been developed to avoid unintentional doping and Fermi level pinning [3]. We have tested a device (Fig. 1) with a WSe_2 monolayer which is shown to enhance electroluminescence [4]. So far, we have observed photoluminescence from it at 750nm from active layer formed by a single layer WSe_2. Electroluminescence will be measured at low temperature from it using a dilution refrigerator. Integration of a superconducting $NbSe_2$ layer is expected to inject Cooper pairs into the active region via proximity effect [5] and enhance the carrier recombination rate.

Different device concepts will be explored to increase the efficiency of Cooper-pair injection into the light-emitting semiconductors. These superconductor-semiconductor interfaces and Cooper-pair injection performance will be characterised by current-voltage measurements. Heterostructure superlattices built upon single- or few-layer semiconducting TMDCs sandwiched between h-BN tunnelling barriers and superconducting electrodes (classic or 2D) will be tested for different performance parameters like carrier injection, luminescence efficiency, coherence, etc. Ultimately, the characterization of the fabricated SQ-LEDs will be performed using low-temperature photon correlation measurements [6]. Our proposed SQ-LEDs promise to produce entangled photon pairs at a rate which is an order of magnitude larger than in the presently available devices. Such highly efficient electrically pumped entangled light sources have a great potential to become the new standard for entanglement generation with huge scientific prospects.

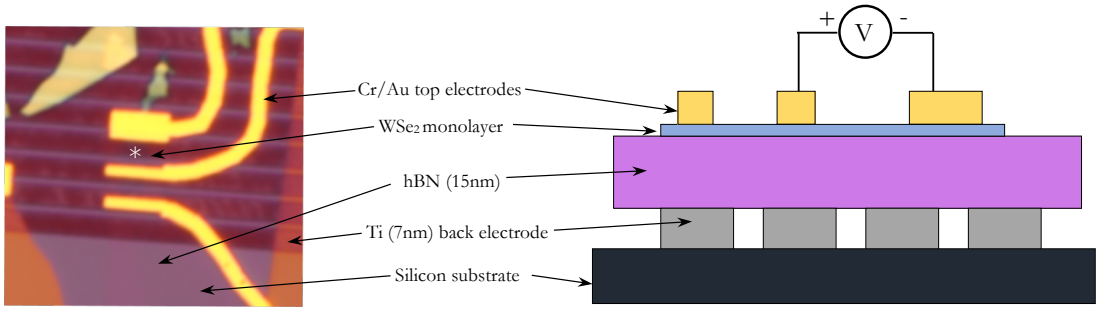

*Figure 1 Fabricated device on a Si(p++)/SiO_2 substrate consisting of (from bottom to up) several Ti (7nm) back electrode, an hBN flake (15nm), a WSe_2 monolayer and Cr/Au top electrodes. The gap between the Ti electrodes is 500 nm. Luminescence is observed from the point labelled *.*

References

[1] "Quantum Manifesto: A New Era of Technology," (2016). https://qt.eu/engage/resources/
[2] I. Suemune, T. Akazaki, K. Tanaka, M. Jo, K. Uesugi, M. Endo, H. Kumano, E. Hanamura, H. Takayanagi, M. Yamanishi, and H. Kan, Japanese Journal of Applied Physics **45**, 9264 (2006).
[3] Y. Liu, J. Guo, E. Zhu, L. Liao, S.-J. Lee, M. Ding, I. Shakir, V. Gambin, Y. Huang, and X. Duan, Nature **557**, 696 (2018).
[4] J. S. Ross, P. Klement, A. M. Jones, N. J. Ghimire, J. Yan, D. G. Mandrus, T. Taniguchi, K. Watanabe, K. Kitamura, W. Yao, D. H. Cobden, and X. Xu, Nature Nanotechnology **9**, 268 (2014).
[5] H. Sasakura, S. Kuramitsu, Y. Hayashi, K. Tanaka, T. Akazaki, E. Hanamura, R. Inoue, H. Takayanagi, Y. Asano, C. Hermannstädter, H. Kumano, and I. Suemune, Physical Review Letters **107**, (2011).
[6] Y. Hayashi, K. Tanaka, T. Akazaki, M. Jo, H. Kumano, and I. Suemune, Applied Physics Express **1**, 011701 (2008).

[†]Corresponding author: yuvraj.chaudhry@aalto.fi

Ion irradiation as a wafer-scale method for amorphizing superconducting thin films

Katja Kohopää[*,1], Alberto Ronzani[1], Robab Najafi Jabdaraghi[1], Arijit Bera[1], Mario Ribeiro[1], Dibyendu Hazra[1], Emma Mykkänen[1], Jorden Senior[1], Mika Prunnila[1], Joonas Govenius[1], Janne Lehtinen[1], Antti Kemppinen[1]
[1] VTT Technical Research Centre of Finland Ltd, 02150 Espoo, Finland

Nanoscale superconducting structures, such as nanowires, have several promising applications in quantum technology. Typical superconducting devices are fabricated from polycrystalline materials. The nanostructures can become irreproducible when their dimensions are comparable with the grain sizes of the material. One possible solution is to use amorphous materials, i.e., reducing the grain size ultimately to an atomic level. We demonstrate ion irradiation as a wafer-scale method for the fabrication of amorphous superconducting thin films [1], in contrast to previous work on local increase of disorder [2].

We study the ion irradiation treatment using argon or gallium ions on single-element and compound materials. We characterize the structural and superconducting properties of the films with transmission electron microscopy imaging and electrical transport measurements, respectively. Our results indicate that gallium and argon ions increase disorder in the thin films in qualitatively similar manner - they destroy the grain structure, increase the resistivity, and alter the superconducting transition temperature. However, our results show that argon tends to form gas pockets that can be detrimental for certain applications, whereas gallium ion irradiation allows to produce a thin, uniform, and amorphous film that is promising, e.g., for superconducting nanowire single-photon detectors.

References

[1] K. Kohopää, A. Ronzani, R. N. Jabdaraghi, A. Bera, M. Ribeiro, D. Hazra, E. Mykkänen, J. Senior, M. Prunnila, J. Govenius, J. Lehtinen, A. Kemppinen, in preparation (2023)
[2] E. Mykkänen, A. Bera, J. S. Lehtinen, A. Ronzani, K. Kohopää, T. Hönigl-Decrinis, R. Shaikhaidarov, S. E. de Graaf, J. Govenius, M. Prunnila, Nanomaterials, 10(5), 950 (2020)

[*]Corresponding author: katja.kohopaa@vtt.fi

Tensor-Network Simulations of Noisy Quantum Computers

Marcel Niedermeier[*,1], **Christian Flindt**[1], **and Jose Lado**[1]
[1] Department of Applied Physics, Aalto University, 02150 Espoo, Finland.

In the analysis and development of quantum algorithms, especially for NISQ hardware, it is crucial to understand how the entanglement requirements and noise resilience of a given quantum algorithm scale with the system size. However, the classical resources required for exact simulations of quantum algorithms grow exponentially with the number of simulated qubits. In contrast, for noisy quantum computers, faithful simulations based on tensor-networks and matrix product states could be performed with computational resources scaling only linearly with the system size [2]. In those cases, the computational costs are kept low by working with a finite bond dimension of the matrix product states, which limits the amount of entanglement they can describe mimicking the loss of entanglement incurred in a noisy quantum computer. Here, we simulate the execution of three well-known quantum algorithms on noisy quantum computers: the quantum Fourier transform, Grover's search algorithm, and the quantum counting algorithm, an application of the more general quantum phase estimation. In particular, the quantum Fourier transform has recently been better understood and successfully classified as a low-entanglement quantum routine [3]. We analyse suitable measures of fidelity of these algorithms as functions of the total system size, the parameters of the algorithms, and, most importantly, the level of noise as modelled by the matrix product state approach. In particular, we find the Grover- and quantum phase estimation-type algorithms can be executed with high fidelity at comparatively low bond dimensions. Overall, we have shown that these quantum algorithms based on quantum circuits with up to 34 qubits can be efficiently simulated on a single-core computer. Our study shows the potential of approximate classical simulations of quantum circuits for emulating results obtained with noisy intermediate-scale quantum computers.

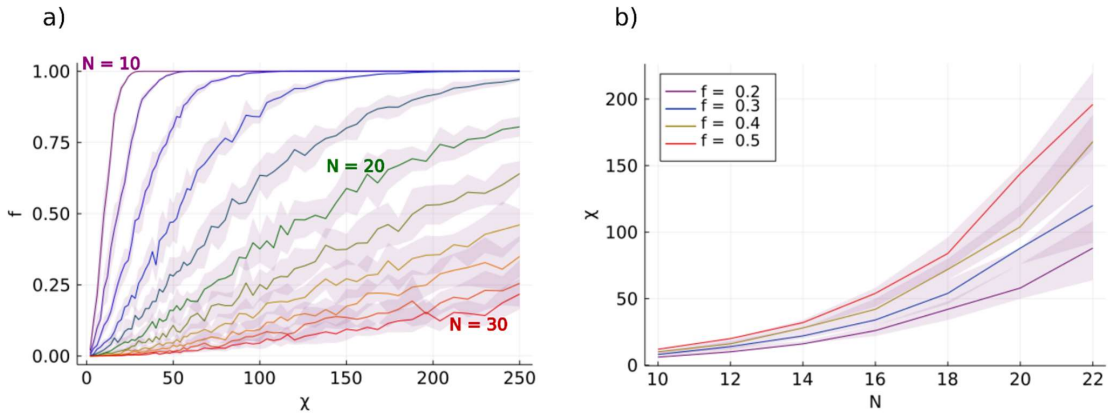

Figure 1. Panel (a): fidelity $f = |\langle\psi_0'|\psi_0\rangle|^2$ of the quantum Fourier transform. The initial state $|\psi_0\rangle$ is created by a random quantum circuit and is then projected onto the state $U_{QFT}^{-1}U_{QFT}|\psi_0\rangle$. The results are averaged over 10 different samples, with the mean plotted and the error ribbons corresponding to one standard deviation. For smaller system sizes N, the fidelity f saturates quickly to 1, whereas for larger system sizes the bond dimension \chi needs to be increased in order to achieve the same fidelity, corresponding to a higher cost in entanglement required for the realisation of the quantum circuit. Panel (b) shows the slope of the curves with constant fidelity actually increases with greater system size. The error bars here correspond to the statistical fluctuations of panel (a).

References

[1] M.Niedermeier, C. Flindt, and J. Lado, in preparation (2023).
[2] Y. Zhou, E. M. Stoudenmire, and X. Waintal, "What limits the simulation of quantum computers?", **Phys. Rev. X 10, 041038 (2020).**
[3] J. Chen, E. M. Stoudenmire, and S. R. White, "The Quantum Fourier Transform Has Small Entanglement", **arXiv:2210.08468 [quant-phys] (2022).**

[*]marcel.niedermeier@aalto.fi

Optomechanical Systems as Quantum Heat Engines

Miika Rasola[*1], **Mikko Möttönen**[1]
1. QCD Labs, Department of Applied Physics, Aalto University, Tietotie 3, Espoo, Finland

From its very beginning, the 20th century was miraculous in providing a new and exciting microscopic world, that of quantum physics. The 21st century may prove to be as marvelous in demonstrating the use of quantum systems, controlled at the level of single excitation quanta, in technological applications, i.e., quantum technologies [1]. While new quantum technologies are being investigated at an accelerating pace, the field of quantum thermodynamics (QTD) [2] is attracting a lot of attention, as researches find themselves wondering, how do these new quantum devices actually interact with heat baths. QTD attempts to answer that question by investigating the relationship between two fundamental theories: quantum mechanics and thermodynamics. From such considerations, a completely new type of device can be enviosioned. A quantum heat engine [2][3] is a device operating at the quantum level, spesifically designed to interact with heat baths and extract work from heat flow. Here we propose to utilize a well-know quantum technology in a novel manner in order to realize such a quantum heat engine.

An optomechanical cavity is an interesting type of quantum system where various quantum phenomena are regularly investigated [4]. In an optomechanical system, two oscillator modes are coupled with a non-linear coupling, described by the following Hamiltonian:

$$\hat{H}_{int} = -\hbar g_0 \hat{a}\hat{a}^\dagger \left(\hat{b} + \hat{b}^\dagger\right). \tag{1}$$

Traditionally, the mode related to the operator $\hat{a}$ is the optical cavity mode and the mode related to $\hat{b}$ is the mechanical mode.

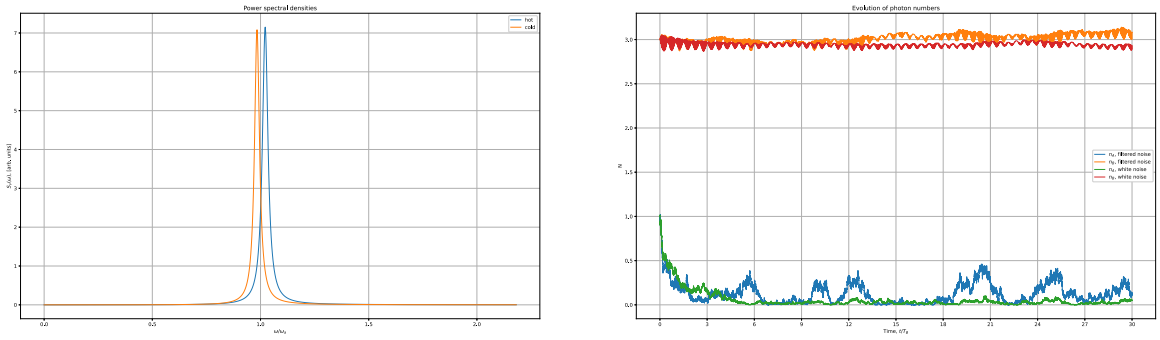

(a) Power spectral densities of the heat baths. *(b) Evolution of photon occupations.*

Fig. 1: This figure shows the power spectral densities of the heat baths (on the left) and the simulated evolution of the occupations in the optical and mechanical modes (on the right). On the right, we compare filtered (orange and blue curves) and white noise (green and red curves).

The optical mode in an optomechanical system is typically driven by a coherent laser. Here, we present a new scheme of utilizing an optomechanical system by coupling the optical mode with two heat baths separated in temperature. The heat baths are given Lorentzian line shapes centered at different frequencies, so that the hot bath has a higher characteristic frequency. As heat flows from the hot to the cold bath through the optical cavity, some of the energy of the photons passing through the optical cavity is transferred to the mechanical mode due to the difference in average photon energies between the baths.

The rather intricate dynamics of this system can be relatively well captured (in a certain parameter regime) by a Heisenberg-Langeving (HL) stochastic equation. Here, we derive and numerically solve the HL equations for a system described above. In figure 1 we present the evolution of expected photon occupations of the optical and mechanical modes with different types of couplings to the environment, as well as the line shapes of the baths.

There are numerous ways of realizing the system envisioned here physically. One candidate is circuit quantum electrodynamics (cQED) [5], where all parameters can be designed and altered relatively easily, and heat baths realized by resistive components. Further, it has been shown that optomechanical coupling can be achieved in cQED [6].

References

[1] Wolfgang P. Schleich et al, Quantum technology: from research to application (2016)
[2] S. Deffner and S. Campbell, Quantum Thermodynamics. 2053-2571. Morgan and Claypool Publishers (2019)
[3] Q. Bouton et al, Nat Commun **12** 2063 (2021)
[4] Markus Aspelmeyer, Tobias J. Kippenberg, and Florian Marquardt, Rev. Mod. Phys. **86** 1391 (2014)
[5] Alexandre Blais, Arne L. Grimsmo, S. M. Girvin, and Andreas Wallraff, Rev. Mod. Phys. **93** 025005 (2021)
[6] J. R. Johansson, G. Johansson, and Franco Nori, Phys. Rev. A **90** 053833 (2014)

*Corresponding author: miika.rasola@aalto.fi

Novel superconducting devices using high quality epitaxial niobium titanium nitride

Aki Ruhtinas[*1], **Manu Lahtinen** [2], **Jaakko Julin** [3], **Timo Sajavaara** [3], **Ilari Maasilta** [1]
1. Nanoscience Center, Department of Physics, University of Jyväskylä, Finland
2. Department of Chemistry, Laboratory of Inorganic and Analytical Chemistry, Finland
3. Accelerator Laboratory, Department of Physics, University of Jyväskylä, Finland

Progress towards superconducting devices with higher operating temperatures while maintaining excellent electrical and microwave characteristics is an ever-ongoing effort. In this work, we demonstrate infrared pulsed laser deposition (PLD) [1],[2] of high quality NbTiN for use in novel superconducting devices. PLD deposited NbTiN films show excellent electrical characteristics with T_c reaching as high as $\sim$16 K. Elemental and structural analyses show that films have low impurity concentrations, and that films grow epitaxially on a MgO substrate.

We use these high quality films for fabricating Josephson junctions with helium ion beam direct writing. This method was first demonstrated in YBCO [3], and here we show that it is possible to use direct writing method for also conventional low temperature superconductors such as NbTiN. In this method, superconductivity is suppressed locally via disorder induced by the focused helium ion beam from helium ion microscope (HIM), thus creating a weak link to serve as a Josephson junction. As the strength of the weak link can be tuned continuously from superconducting to insulating, this method enables exceptionally good control over weak link properties. Transport measurements reveal that Josephson junctions fabricated with the method have excellent DC and microwave characteristics. As an example application, we demonstrate successful fabrication of high quality superconducting quantum interference devices (SQUIDS) using direct writing method.

Direct writing method can be used to fabricate whole devices using only one material, thus reducing required fabrication steps and enabling junction fabrication to complex geometries. When combined to high tunability of junctions, the method could provide a simple, fast and reproducible way to fabricate high quality Josephson junctions for a wide variety of applications.

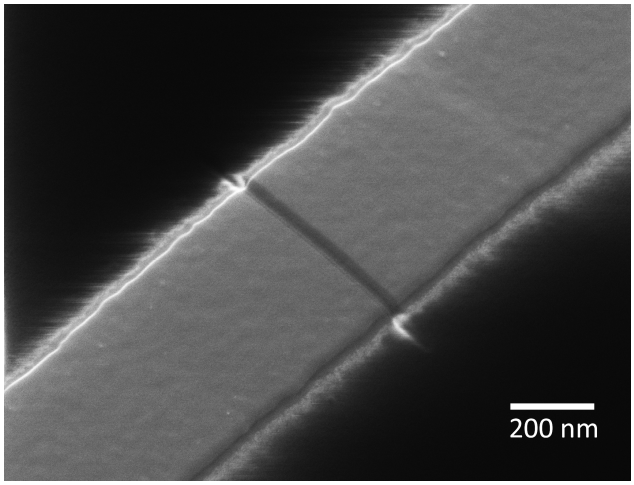

Fig. 1: Helium ion microscope image of weak link fabricated to 35 nm thick and 500 nm wide NbTiN wire using helium ion direct writing.

References

[1] S . Chaudhuri, M. R. Nevala, T. Hakkarainen, T. Niemi and I. J. Maasilta, *IEEE Trans. Appl. Supercond.*, 21(3), 143-146 (2011).
[2] A . Torgovkin, S. Chaudhuri, A. Ruhtinas, M. Lahtinen, T. Sajavaara and I. J. Maasilta, *Supercond. Sci. Technol.*, 10(5), 055017 (2018).
[3] S . Cybart, E. Cho, T. Wong, et al., *Nat. Nanotechnol* 10, 598–602 (2015)

[*]Corresponding author: akperuht@jyu.fi

Fast Qubit Reset with a Quantum-Circuit Refrigerator

Timm F. Mörstedt[*,1], Wallace S. Teixeira[1], Arto Viitanen[1], Vasilii Vadimov[1], Vasilii Sevriuk[2], Mikko Möttönen[1,2]
[1] QCD Labs, Department of Applied Physics, Aalto University, Tietotie 3, 02150 Espoo
[2] IQM Finland

Superconducting qubits have emerged as powerful building blocks for a quantum computer. However, controlling superconducting qubits remains a challenge, particularly resetting the qubit into the ground state on demand. Although a qubit naturally relaxes to its lowest-energy state, this process can be slow for high-coherence qubits and eventually inhibit fast computing. In 2017, Tan et al. have demonstrated an efficient cooling method for superconducting systems: the voltage-tunable quantum circuit refrigerator (QCR) [1]. This device, an electronic microcooler based on single electron tunneling in a normal metal-insulator-superconductor (NIS) junction [2], has proven to be able to reduce the electron temperature locally below the phonon bath temperature. Thus, it is a highly promising candidate for fast, on-demand qubit reset. With an experimentally feasible Dynes-parameter and qubit characteristics it shows fast reset times ($\ll T_1, T_2$) and high reset fidelity [3, 4]. Beyond control with a DC-pulse, the QCR can be combined with other reset protocols, such as f0g1-reset or parametric driving when the QCR and qubit are coupled through a CPW resonator [5]. We present qubit initialization experiments comparing and combining these protocols, including DC and RF control of the QCR [6].

Further studies on the single-junction QCR have simplified the device and offer advanced reset possibilities of a qubit-resonator-QCR system. As a standalone device, it can be added to different superconducting circuits and lends itself very well to the study of open quantum systems [7].

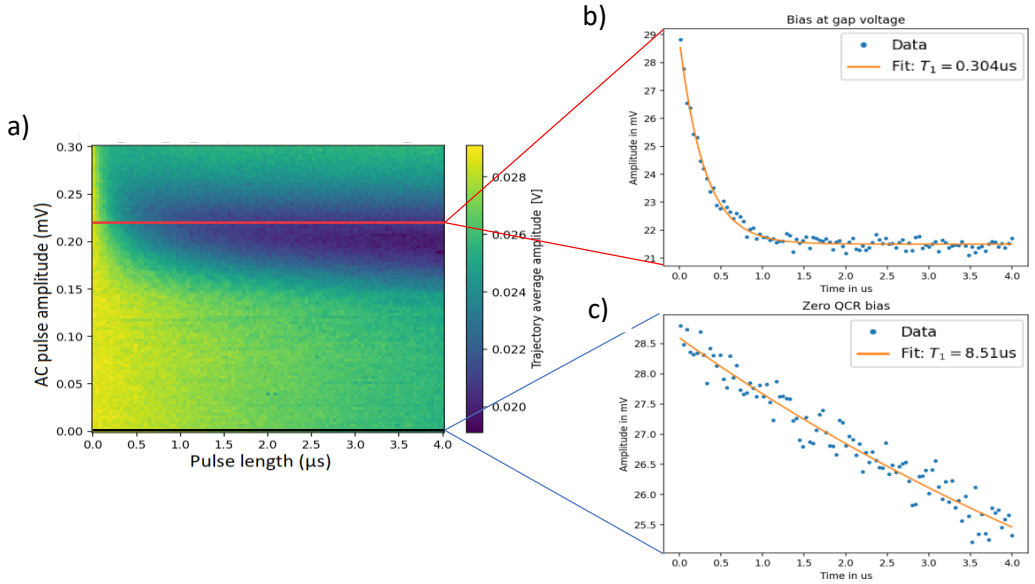

Figure 1. a) Initialization of a Transmon qubit by applying a net-zero voltage pulse of different amplitudes to the QCR. b) With a pulse amplitude of 0.22 mV (red line), which is equal to the superconducting gap of the aluminium junction, accelerated decay to the ground state can be observed. c) Decay experiment with zero pulse amplitude. This corresponds to the QCR off-state and represents the natural decay of the qubit. When comparing the two experiments, active reset is 30 times faster than natural decay. This ratio can be significantly increased with increased coupling or a lower Dynes-parameter.

References

[1] K. Tan et al., Nat. Comm. vol. 8, 15189 (2017)
[2] V. Vadimov et al., AIP Adv. 12, 075005 (2022)
[3] V. Sevriuk et al., Appl. Phys. Lett. 121, 234002 (2022)
[4] H. Hsu et al., Phys. Rev. B101, 235422 (2020)
[5] T. Yoshioka and J.S. Tsai, App. Phys. Lett. 119 124003 (2021)
[6] A. Viitanen et al., Phys. Rev. Research 3, 033126 (2021)
[7] T. Mörstedt et al., Ann. d. Phys. 534, 2100543 (2022)

[*]Corresponding/presenting author: timm.morstedt@aalto.fi

Non-Markovian quantum input-output theory based on hierarchical equation of motion

Vasilii Vadimov*[1], Suman Kundu [1], Eric Hyyppä [2], Meng Xu [3], Jürgen Stockburger [3], Joachim Ankerhold [3], Mikko Möttönen [1,2,4]

1. QCD Labs, QTF Centre of Excellence, Department of Applied Physics, Aalto University, P.O. Box 13500, FIN-00076, Aalto, Finland
2. IQM, Keilaranta 19, 02150 Espoo, Finland
3. Institute for Complex Quantum Systems and IQST, Ulm University - Albert-Einstein-Allee 11, D-89069 Ulm, Germany
4. VTT Technical Research Centre of Finland Ltd. & QTF Centre of Excellence, P.O. Box 1000, 02044 VTT, Espoo, Finland

Hierarchical equation of motion (HEOM) [1] is known as one of the most popular and reliable methods of modelling of open quantum system dynamics. This technique can be straightforwardly applied for a broad class of Gaussian environments with meromorphic noise spectral functions. However, free-pole expansion [2] allows to extend this method for environments with more singular spectral densities and drastically enhance its performance even in low temperature limit.

HEOM represents a first order in time differential equation for the reduced density operator of the system and so-called auxiliary density operators which contain information about system–environment correlations. The latter are usually disregarded in the end since it is thought that all the system–related observables can be calculated using just reduced density operator. However, for a typical example of open quantum systems, namely superconducting circuits coupled to transmission lines, the only quantities accessible to experimentalists, are output fields in these lines, which are observables of environment rather than of system. For systems in Markovian environments the solution to this problem is given by input–output theory [3][4] which relates system observables to the output fields. For linear circuits the scattering problem can be solved using just classical approach.

In our work we show that the HEOM can serve as a basis for construction of both non-Markovian and nonlinear input–output theory. Auxiliary density operators play a key role in this theory, since they contain all the necessary information about system–environment correlations. We illustrate our theory on the standard transmon dispersive readout setup and the readout of a recently developed superconducting qubit called unimon [5].

References

[1] Y. Tanimura, and R. Kubo, Journal of Physical Society of Japan **58.1** 101–114 (1989)
[2] M. Xu, Y. Yan, Q. Shi, J. Ankerhold, and J. T. Stockburger, Phys. Rev. Lett. **129** 230601 (2022)
[3] C. W. Gardiner, Phys. Rev. Lett. **70** 2269 (1993)
[4] H. J. Carmichael, Phys. Rev. Lett. **70** 2273 (1993)
[5] E. Hyyppä, S. Kundu, C. F. Chan, A. Gunyhó, J. Hotari, D. Janzso, K. Juliusson, O. Kiuru, J. Kotilahti, A. Landra, W. Liu, F. Marxer, A. Mäkinen, J.-L. Orgiazzi, M. Palma, M. Savytskyi, F. Tosto, J. Tuorila, V. Vadimov, T. Li, C. Ockeloen-Korppi, J. Heinsoo, K. Y. Tan, J. Hassel, M. Möttönen, Nature Communications **13** 6895 (2022)

*Corresponding author: vasilii.1.vadimov@aalto.fi